ELECTRICAL RESISTIVITY IMAGING FOR UNKNOWN BRIDGE FOUNDATION DEPTH DETERMINATION

A Dissertation

by

RUNGROJ ARJWECH

Submitted to the Office of Graduate Studies of
Texas A&M University
in partial fulfillment of the requirements for the degree of

DOCTOR OF PHILOSOPHY

December 2011

Major Subject: Geophysics

Electrical Resistivity Imaging for Unknown Bridge Foundation Depth Determination

ELECTRICAL RESISTIVITY IMAGING FOR UNKNOWN BRIDGE FOUNDATION DEPTH DETERMINATION

A Dissertation

by

RUNGROJ ARJWECH

Submitted to the Office of Graduate Studies of
Texas A&M University
in partial fulfillment of the requirements for the degree of

DOCTOR OF PHILOSOPHY

Approved by:

Chair of Committee,	Mark E. Everett
Committee Members,	Jean-Louis Briaud
	Richard L. Carlson
	Benchun Duan
	Andreas K. Kronenberg
Head of Department,	Rick Giardino

December 2011

Major Subject: Geophysics

ABSTRACT

Electrical Resistivity Imaging for Unknown Bridge Foundation

Depth Determination. (December 2011)

Rungroj Arjwech, B.A., Khon Kaen University;

M.S., Khon Kaen University

Chair of Advisory Committee: Dr. Mark E. Everett

Unknown bridge foundations pose a significant safety risk due to stream scour and erosion. Records from older structures may be non-existent, incomplete, or incorrect. Nondestructive and inexpensive geophysical methods have been identified as suitable to investigate unknown bridge foundations. The objective of the present study is to apply advanced 2D electrical resistivity imaging (ERI) in order to identify depth of unknown bridge foundations.

A survey procedure is carried out in mixed terrain water and land environments with rough topography. A conventional resistivity survey procedure is used with the electrodes installed on the stream banks. However, some electrodes must be adapted for underwater use. Tests were conducted in one laboratory experimentation and at five field experimentations located at three roadway bridges, a geotechnical test site, and a railway bridge. The first experimentation was at the bridges with the smallest foundations, later working up in size to larger drilled shafts and spread footings. Both known to unknown foundations were investigated. The geotechnical test site is used as an experimental site for 2D and 3D ERI. The data acquisition is carried out along 2D profile with a linear array in the dipole-dipole configuration. The data collections have been carried out using electrodes deployed directly across smaller foundations. Electrodes are deployed in proximity to larger foundations to image them from the side. The 2D ERI can detect the presence of a bridge foundation but is unable to resolve its precise shape and depth.

Increasing the spatial extent of the foundation permits better image of its shape and depth. Using electrode < 1 m to detect a slender foundation < 1 m in diameter is not feasible.

The 2D ERI method that has been widely used for land surface surveys presently can be adapted effectively in water-covered environments. The method is the most appropriate geophysical method for determination of unknown bridge foundations. Fully 3D ERI method at bridge sites is labor intensive, time consuming, and does not add enough value over 2D ERI to make it worthwhile.

ACKNOWLEDGEMENTS

I would like to express my deepest gratitude to my committee chair Dr. Everett for his guidance, supervision, patience, and mentorship throughout my education period. In addition I am very thankful to my committee members, Dr. Kronenberg, Dr. Carlson, Dr. Duan, and Dr. Briaud, for their strategic and knowledgeable supports through out the course of this research.

Sincere thanks are also expressed to all of professors and staffs at Department of Geology & Geophysics, Texas A&M University and Thai students for field and laboratory support.

I would like to thank the Ministry of Science and Technology, Royal Thai Government for financial support through out my study at Texas A&M University as well as Texas Department of Transportation (TxDOT) for financial support for this project. Without this funding, I could not have completed my study.

In particular, I am very grateful and proud to be born and raised in the Arjwech family. I would like to express my deepest appreciation to my parents. They provide valuable encouragement through my life.

Finally, I would like to dedicate this dissertation to my homeland for the first philosophy doctor of the community who graduated abroad with a prestigious state scholarship.

TABLE OF CONTENTS

LIST OF FIGURES

FIGURE Page

FIGURE Page

FIGURE Page

FIGURE Page

LIST OF TABLES

CHAPTER I

INTRODUCTION

UNKNOWN BRIDGE FOUNDATION

Approximately 83% of the 583,000 roadway bridges in the United States are built over waterways (Lagasse et al., 2007). For many of these structures, designed or as-built bridge information is not available for the type, depth, geometry, or materials incorporated in the foundations. Consequently, over 80,000 of these bridges have been identified as having unknown foundations according to the National Bridge Inventory (FHWA, 2006). The state of Texas has the largest number of bridges with unknown foundations (Stein and Sedmera, 2006). There are approximately 43,000 bridges over waterways in Texas and more than 8,000 of these have been identified as ones with unknown foundations (Delphia, 2010).

Unknown bridge foundations present a significant problem to the State Departments of Transportation due to concerns of scour vulnerability (Olson et al., 1998). The undermining of bridge foundations is a public safety hazard (INDOT, 2010). Moreover, unavailable foundation information exposes the public to unnecessary risk, congestion, and cost as relatively uninformed decisions are made to prioritize and plan bridge repairs, upgrades, or replacements (FHWA, 2006). The foundation depth is considered to be the foremost parameter of interest in a scour (refer to section 1.3) evaluation followed by foundation type, geometry, and subsurface conditions (Olson et al., 1996; Breen et al., 2010). Therefore, foundation depth information is necessary to evaluate the risk of severe scour at each bridge location. Information on foundation type, geometry, materials, and subsurface conditions is also desired for a designing repair work (FHWA, 2004).

This dissertation follows the style of Geophysics.

In 1989, the Federal Highway Administration (FHWA) requested all states to establish a scour evaluation program (Beard, 2009). The State Departments of Transportation would begin by identifying and evaluating all bridges over rivers or streams to determine their vulnerability to scour (Harrigan and Reynaud, 2008). Determining the type, size, depth, configuration, materials, and condition of unknown foundations is essential for scour hazard assessments, structural upgrades, and seismic retrofitting. Identifying the type and condition of existing foundations is essential for determining structure repair or upgrade strategies. Furthermore because the number of bridges with unknown foundations is so large, developing effective strategies for managing and characterizing unknown foundations using a practical, economical, and nondestructive approach is critical for realizing these benefits (FHWA, 2006).

Assessing and characterizing geotechnical conditions at existing roadway bridges can become complex and costly if there are obstacles such as difficult access, difficult ground conditions, or regulatory constraints that limit traditional exploratory methods. When traditional methods can be applied, results based on penetration testing or recovered samples may be of limited utility. When the ground surface is accessible during non-flood seasons, surface geophysical techniques can provide methods for subsurface characterization. Surface geophysics can provide information regarding the subsurface distribution of relevant material properties (Rucker, 2006). Though geophysics is not a substitute for geotechnical boring or testing, it is often a very cost-effective and efficient means of imaging subsurface profiles and for determining the in-situ bulk properties (Anderson et al., 2008).

Geophysics is the use of non-invasive survey techniques to determine subsurface anomalies without having to engage in destructive excavation (Barker, 1993). Non-destructive testing (NDT) is the use of analysis techniques to evaluate the properties of a material, component or system without causing damage (Louis, 1995). In the last few decades, geophysical NDT methods have been developed to evaluate the type, size, depth, configuration, and condition of unknown foundations. The geophysical NDT capabilities have been increasingly applied for solving specific engineering problems

throughout state and federal highway departments. Transportation personnel have used geophysical NDT methods in assisting geotechnical site investigation, construction, and maintenance of highways (Dahlin, 2001; Wightman and Jalinoos, 2003). In many instances, geophysical NDT methods enhance the reliability, speed of geotechnical investigations, and effectively reduce the cost of the investigation (Anderson et al., 2008).

The Electrical Resistivity Imaging (ERI) method is one of the geophysical methods of primary interest for engineering applications. The method has been widely used for mapping subsurface electrical properties in two and three dimensions (Dahlin, 2001). The ERI technique has been used for geotechnical site investigations of civil infrastructure such as bridges, highways, dams, tunnels, and underground sewage or waste disposal systems. The ERI method is applicable at bridges if there is a resistivity contrast between the concrete foundation and the riverbed sediments. The application of ERI surveys for determining the depth of buried infrastructure and particularly bridge foundations remains an area of active research interest.

BRIDGE FOUNDATION

The parts of a bridge can be categorized as superstructure and substructure. A bridge superstructure refers to all structures above the bridge bearing elevation that distribute loads to the substructure units. We are not interested here in superstructure. A bridge substructure includes all structures that support the superstructure. Therefore, the bridge substructure incorporates all foundation elements such as abutments, piers, columns footings, and piles (Olson and Aouad, 1998; Breen et al., 2010). Figure 1.1 shows a cross sectional view of the parts and types of a bridge foundation.

A bridge foundation is the part of the bridge substructure that connects a bridge structure with the ground. Foundations are constructed above or within existing geologic materials (Chen and Duan, 2000). The purpose of a bridge foundation is to support loads from the bridge superstructure by: (1) spreading concentrated loads over a sufficient area to provide adequate bearing capacity and to limit settlement under the imposed load, or;

(2) transferring loads or energy between the bridge structure and the ground (MDOT, 2008). Bridge foundations are critical because they support the entire load of the superstructure plus the traffic loads that it will carry (ODOT, 2011).

Bridge foundations are generally categorized into two types, shallow and deep, depending on how they are embedded into the ground. Shallow foundations provide the simplest form of load transfer from a structure to the near-surface soils. They are placed to shallow depth beneath the soil surface and typically constructed with generally small excavations into the ground. The most common of these types of foundations are spread footings.

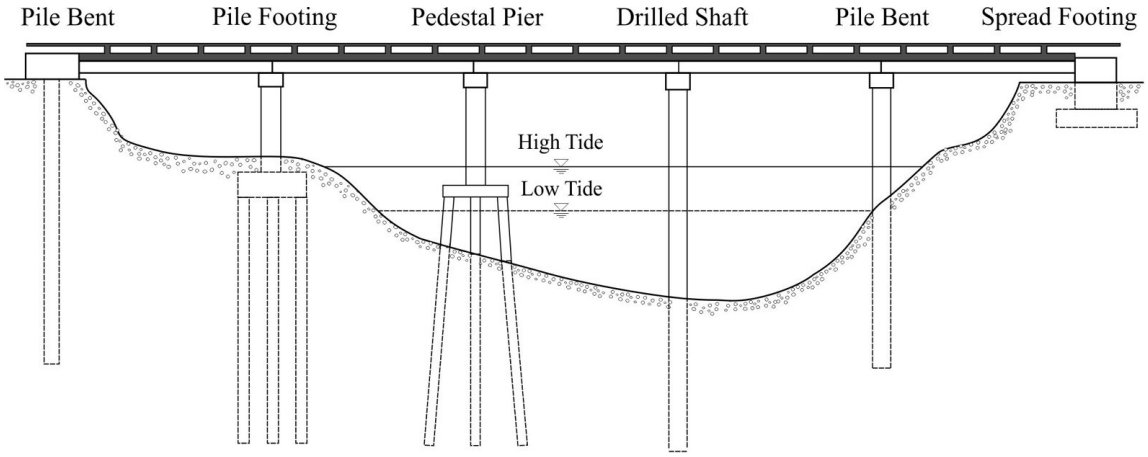

Figure 1.1 Type of bridge foundation (Chen and Duan, 2000)

Deep foundations are structural assemblies that transfer load down through low-strength soil strata into deeper and stronger zones to minimize the settlement of a structure. These deep foundations can be driven, drilled, cast-in-place, or alternatively grouted-in-place. The most common of these types of foundations are piles and drilled shafts. Bridges are frequently supported on deep foundations (Kimmerling, 2002; Ostrom et al., 2000; SCDOT, 2010). A shallow foundation is a type of foundation for which generally its depth is less than its width. The depth may range from the topsoil

surface to about 3 m but this is not a strict rule. A deep foundation is a type of foundation where its embedment is greater than its maximum plane dimension. The depth is generally > 3 m. The type of foundation utilized depends on the geologic materials at the site. The soil or rock near the ground surface must be competent enough to support the design loads (Chen and Duan, 2000).

The advantage of a deep foundation is that large loads can be supported if there is a poor soil at shallow depth. Deep foundations can usually support greater loads than shallow foundations that occupy the same area of the ground surface. Deep foundations can reach underlying competent layers of bearing soil or rock and can also support large uplift and lateral loads (Chen and Duan, 2000). Bridge foundations at a particular site can be individual, grouped, or form a combination. For small bridges, small-scale foundations such as individual footings or drilled shaft foundations, or a small group of driven piles, may be sufficient. For larger bridges, large-scale foundations such as shaft foundations, grouped foundations, caissons, or combination foundations may be required (Chen and Duan, 2000).

BRIDGE FOUNDATION SCOUR

Scour is the result of the erosive action of flowing water which excavates and carries away sediments from the bed and banks of stream and from around the piers and abutments of bridges. It is the primary cause of bridge failures (Zevenbergen, 2004). Failure of bridges due to scour at their foundations is a common occurrence (Khwairakpam1 and Mazumdar, 2009). Bridge scour is responsible for 95% of all severely damaged and failed highway bridges constructed over waterways in the United States. The greatest loss of sediment to scour occurs at high water velocities during heavy storms and floods. These events can expose the bridge footing and lower its factor of safety (Leftor, 1993). A high velocity and complicated flow pattern typically consists of downward flow and vortices around and near bridge foundations. The fluid motions excavate scour holes and carry away material from the bed and banks of streams and from around bridge foundations (Barkdoll et al., 2007). As the scour continuously

progresses at a site, it can undermine the piers and abutments resulting in loss of structural support for the bridge deck and ultimately results in structural collapse (Melville and Coleman, 2000).

Warren (1993) defines scour as the hole left behind when sediments are washed away from the bottom of a river. Although scour may occur at any time, scour action is especially strong during floods. Swiftly flowing water has more energy than calm water to lift and carry sediment down river. Bridge scour may be classified into various components at a site illustrated in Figure 1.2 that are considered independent and additive. The most common components include: (1) degradational scour which is the general removal of sediment from the river bottom by the flow of the river and may cause removal of large amounts of sediment over time at the bridge site; (2) contraction scour, which is the erosion of sediment or material from the bottom and bank of a river channel resulting from the contraction of the flow area; (3) local scour, which is the removal of bed sediment from around a flow obstruction caused by the local flow field induced by a pier or abutment. Local scour is the most significant cause of bridge scour (Richardson and Davies, 1995).

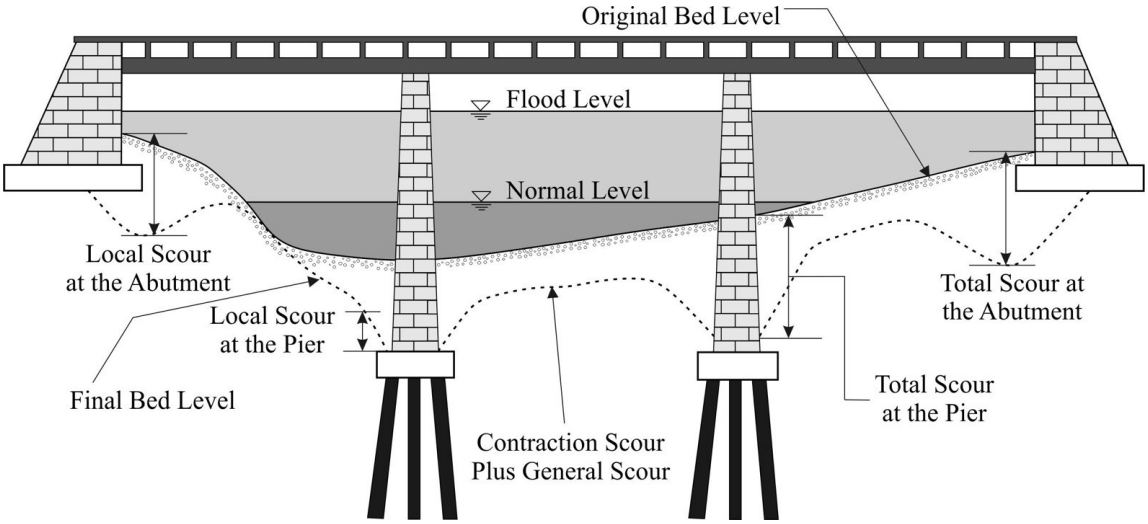

Figure 1.2 The types of scour that can occur at a bridge (Melville and Coleman, 2000).

The basic mechanism of scour at a bridge pier is the formations of vortices at the base as shown in Figure 1.3 (Garcia, 2007). A horseshoe vortex results from the interaction of the water flow field on the upstream surface of the abutment and subsequent acceleration of the flow around the base of the pier. The action of the vortex removes riverbed material from around the base of the pier. The horseshoe vortex has high lift and shear stress and triggers the onset of sediment scour. Besides the horseshoe vortex in the vicinity of the pier base, there are also vertical vortices downstream of the pier referred to as wake vortices. The wake vortices result due to the separated flow at the pier corners. These wake vortices are not stable and shed alternately from one side of the pier and then the other. They lift up riverbed sediment and create a large scour hole behind the pier. Consequently, both horseshoe and wake vertices combine to develop a larger scour hole. The intensity of the wake vortices is greatly reduced with distance downstream (Richardson and Davies, 1995).

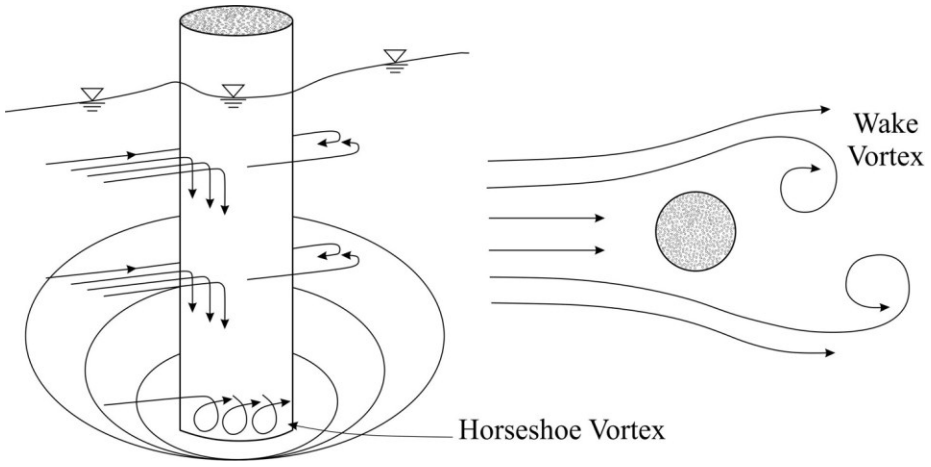

Figure 1.3 Schematic representation of scour at a cylindrical pier (Garcia, 2007).

Factors that affect the magnitude of scour depth at a pier include: (1) width of the pier; (2) length of the pier if skewed to flow; (3) depth of flow; (4) velocity of the approach flow; (5) size and gradation of bed material; (6) angle of attack of the approach

flow to the pier; (7) shape of the pier; (8) bed landform (Garcia, 2007).

EXISTING METHODS TO DETERMINE UNKNOWN FOUNDATION

There exist several methods of characterizing bridge foundations. Methods that are useful to delineate a bridge foundation must consider the range of substructure, geological, and hydraulic conditions at a particular bridge site. The foundation material may be steel, wood, concrete, or masonry. The bridge foundation shape may be footing, pile, or a combination of both. The subsurface environment around the bridge foundation is typically composed of a mixture of air, water, riprap materials, soils, and/or rock. The difference of geological material types and geometries of foundations are the two most important factors that have been considered in methods to determine bridge foundations (Olson et al., 1998).

The investigation and evaluation of unknown foundations can be performed either by conventional methods, such as physically disruptive excavation, coring, or boring methods, or by nondestructive methods including surface geophysics. The conventional methods are typically considered to be expensive, destructive, and limited in their application. Recently the NDT methods have been grown in popularity because they are inexpensive and reliable. Moreover the data are obtained without interruption of integrity in the investigated objects (Breen et al., 2010).

The NDT methods described by Olson and Aouad (1998) and Breen et al (2010) that are applicable for unknown bridge foundation depth determination can be divided into two categories: surface methods and borehole methods. The surface methods are generally less invasive since they do not require soil disruption, although they often require access to the exposed parts of bridge substructures. The borehole methods require access through a nearby borehole, inflicting soil damage. The surface methods include ultraseismic, sonic echo/impulse response, spectral analysis of surface waves and bending waves tests. These are shown in Figure 1.4. The borehole methods include the parallel seismic test, induction field method, and borehole radar method. These are shown in Figure 1.5.

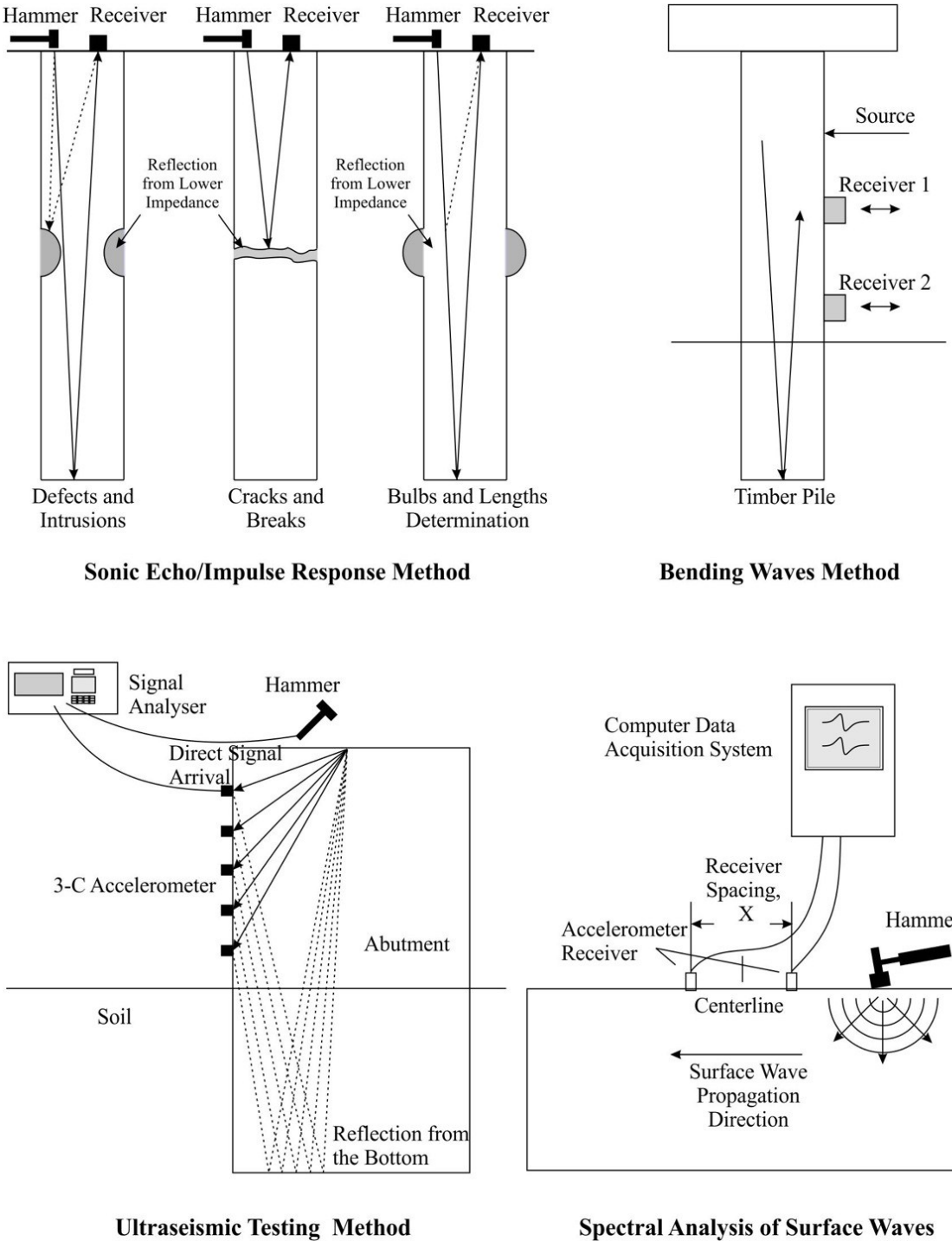

Figure 1.4 Schematics of surface-based NDT methods (Olson, 2003).

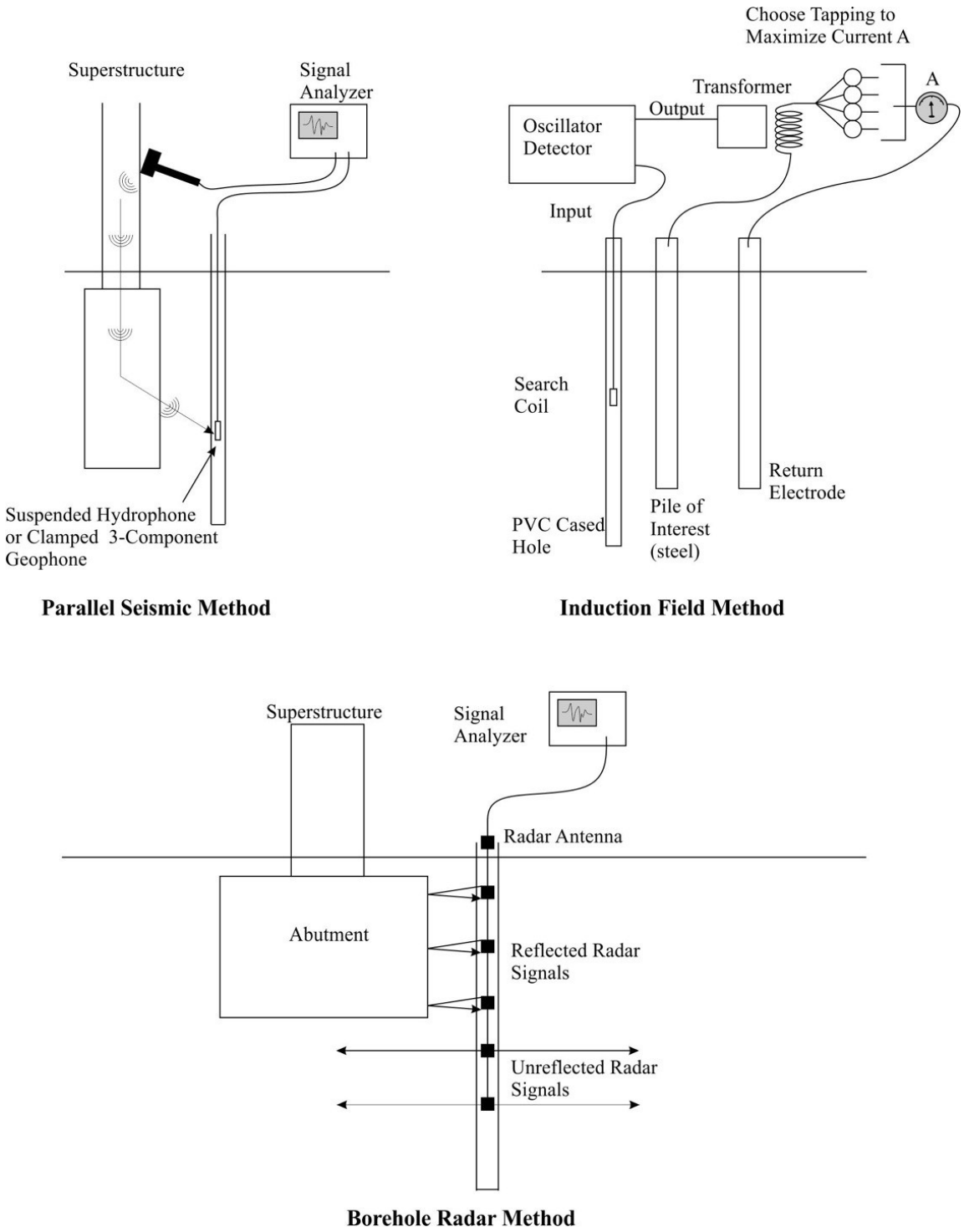

Figure 1.5 Schematics of borehole-based NDT methods (Olson, 2003).

Many studies of geophysical methods have been carried out in attempt to determine unknown foundation. Olson et al (1996), Olson and Aouad (1998), and Olson (2002) tested the capabilities of surface and borehole of NDT methods to indicate the depth of unknown bridge foundation. They found two methods to be the most accurate and applicable. The parallel seismic test has the broadest applications of the borehole methods. The ultraseismic test has the broadest application of surface methods but provides no information on piles below larger substructure (i.e. pile caps). Other NDT methods had more limited application.

PURPOSE OF RESEARCH

Geophysical methods can be used to improve geotechnical site characterization. Many practical approaches including almost all conventional geophysical methods have been developed to provide NDT solutions to a variety of specific engineering problems. The research described in this dissertation is focused on a NDT method of geophysics (ERI, electrical resistivity imaging) that can inexpensively and reliably determine foundation properties such as depth condition.

A major goal of this study is to investigate applicable ERI techniques for foundation determination. ERI offers an improvement over the conventional methods for bridge foundation investigation. Questions arise as to whether ERI techniques can be employed effectively to image bridge foundations. The ERI survey will be applied in mixed land and water covered-environments beneath bridges. This means there is a special requirement for underwater electrodes.

Different sizes, shapes, and types of foundations yield different anomalies on an ERI image. In particular, exposed and buried rebars affect and distort the resistivity image of a concrete foundation. The condition of the foundation can be inspected at the surface. We then design a suitable electrode spacing and array configuration to gain high spatial resolution. Furthermore, the bulk resistivity of the host geological medium can be measured by a portable resistivity meter to constrain the foundation image. It is sufficient in many cases to image only the upper portion of a deep, slender foundation to

assess bridge safety from scour hazard. Since scour is generally critical to only a few meters deep, imaging a long, slender foundations to its full depth extent, which is very challenging, may not be necessary for adequate scour hazard assessment.

ORGANIZATION OF RESEARCH

There are several methods that have been used effectively in engineering applications. Those methods are often limited to one-dimensional interpretation (depth profiles) and do not provide subsurface information over wide areas. Although the ERI technique is less frequently used for engineering applications, it has proven to be successful and effective for imaging foundations and surrounding materials in many subsurface geological conditions. Moreover the ERI technology works effectively in a water-covered environment. The ERI method is widely viewed as the most promising geophysical method for addressing the problem of unknown bridge foundation determination. The methodology comprises data acquisition, data analysis, interpretation, and accuracy verification.

Forward Synthetic Model

One major challenge to acquiring diagnostic ERI information on foundation depth is that the bridge foundation has a finite cylindrical geometry. This subsurface geometry is different from vertical and elongated features of geological interest such as faults, fractures, or the igneous dyke shown in Figure 1.6. If the survey is conducted across the strike of a 2D dyke or fracture, the 2D ERI method can provide reliable images. The question has risen as to whether the 2D ERI technique can also provide reliable imaging results in support of bridge foundation efforts. We carry out 2D and 3D synthetic modeling to investigate the reliability of ERI imaging. We demonstrate that 2D ERI methods to image bridge foundation can be effective instead of using a complicated 3D ERI method. Forward modeling can be used to quantify the effects of foundations in ERI images.

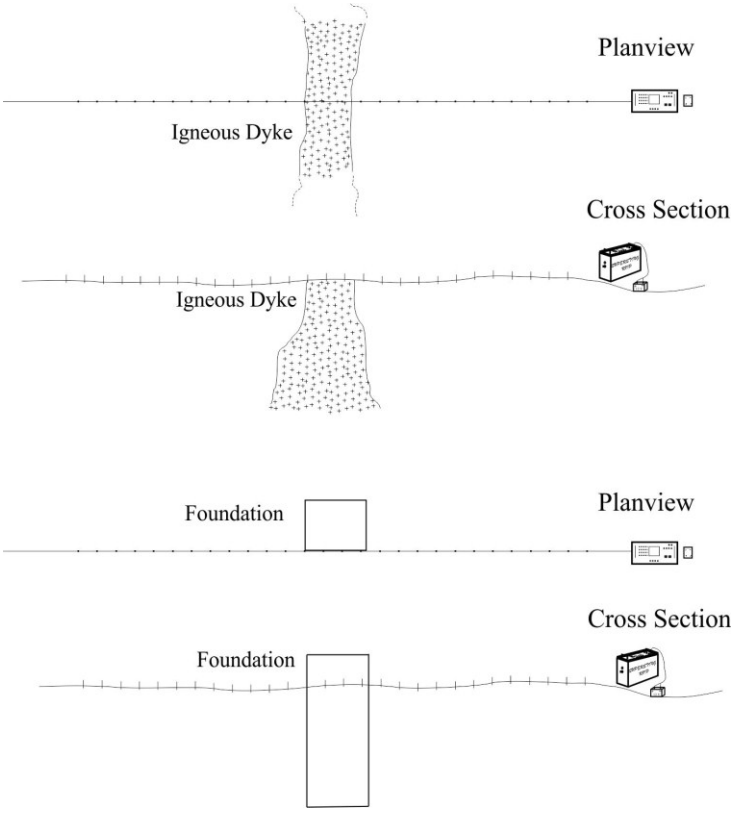

Figure 1.6 Schematic views of 2D ERI surveys across elongated and vertical geometry of an igneous dyke and a bridge foundation.

2D and 3D synthetic models were generated using the public domain RES2DMOD (Loke, 2002) and RES3DMOD (Loke, 2001) forward modeling programs, respectively. A 2D model refers to two-dimensional image in horizontal and vertical axes (i.e. *x* and *z* axes). The 3D model is three-dimensional incorporating the second horizontal axis (i.e. *y* axis). Starting model is based on measurement on soil resistivity made by a portable meter and various resistivity values of concrete foundation. 3D synthetic model is generated and a 2D apparent resistivity profile is extracted and processed inversion. These forward models are used for survey planning and evaluating the reliability of the 2D ERI method.

Experimentation and Data Acquisition

Experimentation and data acquisition were conducted during November 2009 to May 2011. The effort is divided into one laboratory experimentation and five field experimentations located at three roadway bridges, a geotechnical test site, and a railway bridge. The first experimentation was at the bridges with the smallest foundations, later working up in size to the drilled shafts and spread footing and from known to unknown foundations. The geotechnical test site is used as an experimental site for the 2D and 3D ERI, with lessons learned to be applied in practice at actual bridges. The data acquisition is carried out using the 2D method with a linear array of electrodes in the dipole-dipole configuration.

The data collections have been carried out using two methods of electrode deployments: (1) electrodes deployed across smaller foundations using equal electrode spacing, mainly conducted at drilled shaft and concrete pile foundations; (2) electrodes deployed in proximity to larger foundations to image them from the side such as spread footings. In mixed terrain underwater environment, waterproof electrodes are constructed and planted on the riverbed. On land surface, regular stainless steel electrodes are used. Data acquisitions are conducted to image foundation with electrodes aligned parallel to and across the river.

Data Analysis

The data analyses have been performed using the RES2DINV (Loke, 2004a) and RES3DINV (Loke, 2004b) commercial programs for 2D and 3D pseudo-section plotting, data editing, and inversion. The RES2DINV and RES3DINV inversion programs are based on the Windows 32-bit computational platform and the inversion algorithm is described by Loke and Barker (1996) and Yang (1999). Since the foundations are embedded vertically into the ground and exhibit a relatively sharp boundary and large contrast in resistivity with the surrounding earth materials, the inversion algorithm is best carried out using a robust inversion optimization method. A 2D data analysis is carried out profile by profile. A 3D data analysis is carried out by

combining parallel 2D profiles.

Interpretation and Accuracy Verification

2D ERI for unknown bridge foundation determination is geophysical NDT method that might be conducted without a related destructive method or without other relevant subsurface information such as geological and geotechnical information. The ERI by itself however lacks sufficient reliability. In this study therefore we begin working on the 2D ERI experimental design with known foundations to prove the capability for subsurface imaging of the 2D ERI technique. The 2D ERI method is also verified for accuracy of each inversion by a comparison of inversion results with actual foundation plans. For unknown foundations, a number of surveyed profiles are conducted using different profile orientations to increase the reliability. The inversion results are compared to profile data produced by synthetic forward modeling.

The dissertation is composed of five main chapters. An introduction to the subject matter and statement of purpose is addressed in Chapter I. Detailed review of literature concerning the electrical resistivity methods used in this research is described in the Chapter II. This chapter also presents literature reviews of resistivity of materials and successful previous ERI studies to determine unknown bridge foundation. Chapter III discusses forward modeling procedures, field data acquisition, and data analyses. Details of the individual study sites are described and the objectives of study are discussed. A comprehensive analysis and data interpretation of all test results are presented in Chapter IV. Finally, a summary of accomplished work and additional discussion are provided in Chapter V.

CHAPTER II

LITERATURE REVIEW

In this chapter, the fundamental electrical resistivity principles, different methods of electrical resistivity surveys, forward modeling, inversion, and the electrical resistivity of geological materials and bridge foundations are described. Previous studies of unknown bridge foundations by the ERI geophysical technique are described at the end of this chapter.

FUNDAMENTALS OF ELECTRICAL RESISTIVITY SURVEY

Electrical resistivity is the bulk physical property describes how well that a given material allows steady electric currents to flow through it. The electrical resistivity ρ (Ωm) of a substance depends on the resistance R (Ω) of an ideal cylindrical shaped body with uniform composition of length L (m) and cross-sectional area A (m^2). The formula is $\rho = RA/L$. The electrical resistance of the cylindrical body R (Ω), is defined as $R=V/I$, where V (volt, V) is the potential difference across the long axis of the cylinder and I (amperes, A) is the current flowing through the cylinder.

A fundamental governing equation is Ohm's law that describes the relation between the flow of current density and the electric field. Ohm's law in an isotropic homogeneous medium is given by

$$\boldsymbol{J} = \sigma \boldsymbol{E}, \tag{1}$$

where $\boldsymbol{J}$ is the current density vector measured in (A/m^2), $\boldsymbol{E}$ is the electric field vector measured in volts per meter (V/m), and σ is the conductivity measured in siemens per meter (S/m). Conductivity is the reciprocal of resistivity, $\sigma=1/\rho$. The relationship between the electric potential V and the field intensity $\boldsymbol{E}$ is given by

$$\boldsymbol{E} = -\nabla V \tag{2}$$

Combining equations (1) and (2), we get

$$\boldsymbol{J} = -\sigma \nabla V. \tag{3}$$

Figure 2.1 shows the distribution of electric current **I** within a homogeneous isotropic half space due to injection from a single point source electrode C_1 on the ground surface. The current distributes radially outward from the point source through a hemispherical shell with the area of $2\pi r^2$. The potential varies inversely with distance from the current source. The current flow is perpendicular to the equipotential surfaces (i.e. lines of constant V). The current density for one electrode has the simple form

$$\boldsymbol{J} = \frac{I\hat{r}}{2\pi r^2}. \tag{4}$$

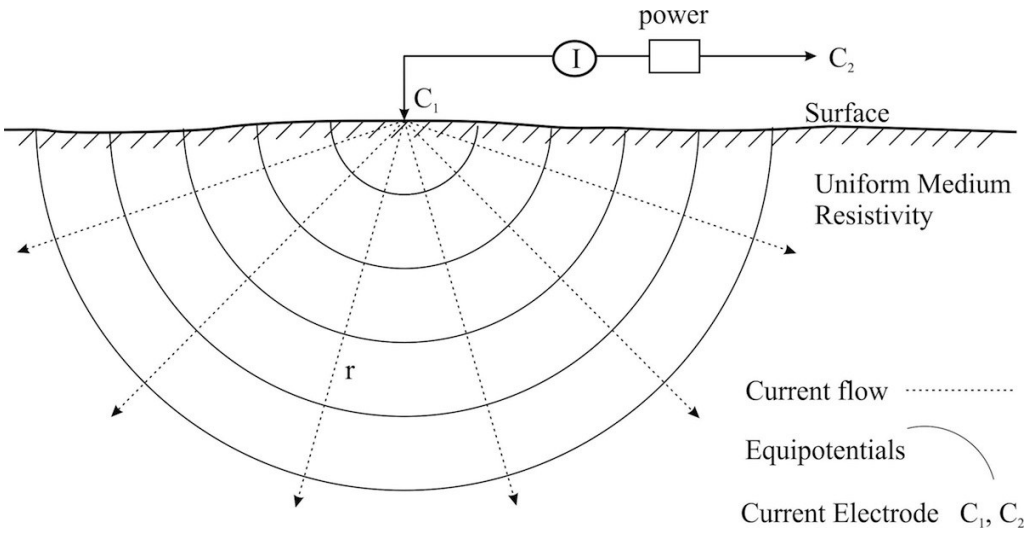

Figure 2.1 Point source of current at the surface of a homogeneous medium (Telford et al., 1990).

By convention, the resistivity is more commonly used than the conductivity σ. Then equations (3) and (4) can be written as

$$\frac{\partial V}{\partial r} = \frac{\rho I}{2\pi r^2}. \tag{5}$$

Integrating the above equation and setting a potential electrode at infinity to zero, the electric potential V at a distance r from the source is then obtained by

$$V = \int_{r}^{\infty} \left(\frac{\rho I}{2\pi r^2}\right) dr = \frac{\rho I}{2\pi r}. \tag{6}$$

The above equation has been derived based on a single current source. In practice, measurement of electrical resistivity usually requires four electrodes as shown in Figure 2.2. The electrical current is injected at C_1 and withdrawn at C_2 and two other electrodes P_1 and P_2 are used to record a potential difference. The potential measurement at electrode P_1 is written in terms of the current sources as

$$V_{P1} = \frac{I\rho}{2\pi}\left(\frac{1}{r_1} - \frac{1}{r_2}\right), \tag{7}$$

where r_1 and r_2 are distances of the potential electrode P_1 from the current electrodes C_1 and C_2 respectively.

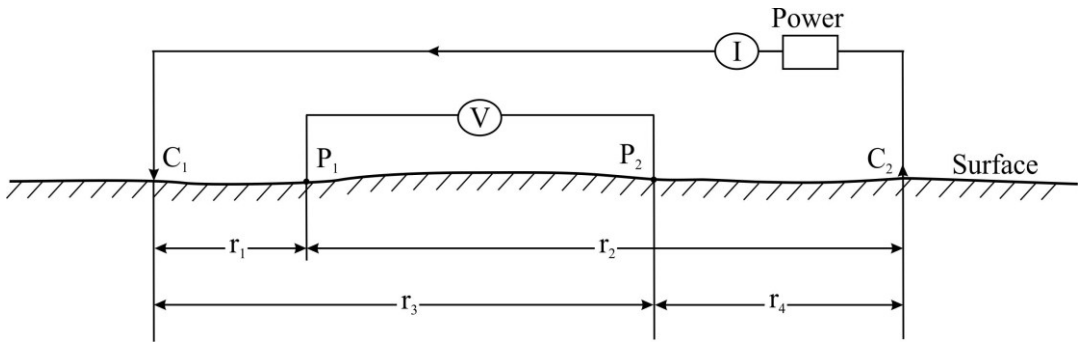

Figure 2.2 Two current and two potential electrodes on the surface of a homogeneous isotropic half space showing two general configuration of the four surface electrodes (Telford et al., 1990).

In practice, a measurement is made of the potential difference between two locations on the surface. The potential difference $\Delta V = V_{P1} - V_{P2}$ between the two potential electrodes P_1 and P_2 on the surface of the homogeneous half space is

$$\nabla V = \frac{I\rho}{2\pi}\left\{\left(\frac{1}{r_1} - \frac{1}{r_2}\right) - \left(\frac{1}{r_3} - \frac{1}{r_4}\right)\right\}, \tag{8}$$

where r_3 and r_4 are distances of the potential electrode P_2 from the current electrodes C_1 and C_2, respectively.

The resistivity of the homogeneous half space can be found by re-arranging equation (8),

$$\rho = \frac{k\Delta V}{I}, \tag{9}$$

where k is a geometric factor dependent on the electrode spacings,

$$k = \frac{2\pi}{\left\{\left(\frac{1}{r_1} - \frac{1}{r_2}\right) - \left(\frac{1}{r_3} - \frac{1}{r_4}\right)\right\}}. \tag{10}$$

The resistivity in equation (9) yields a constant value regardless of where the electrodes are placed over a homogeneous medium. In practice, resistivity surveys are performed over a heterogeneous subsurface and consequently the resistivity value is not constant at every measurement point. The resistivity measured in the field is therefore known as an "apparent" resistivity ρ_a defined by,

$$\rho_a = \frac{k\Delta V}{I}. \tag{11}$$

The measured apparent resistivity depends on the geometry of the electrode configuration. In order to obtain a high resolution and reliable image, the electrode configuration used should provide data that are sensitive to the prospective anomaly, provide reasonable subsurface coverage, and offer a high signal to noise ratio. The best configuration for a field survey depends on the features of structure to be mapped, the sensitivity of the resistivity meter, and the background noise level. Practically, the configurations used for 2D ERI surveys are classified according to the array type. The standard array types are Wenner, dipole-dipole, Wenner-Schlumberger, pole-pole, pole-dipole, and equatorial dipole-dipole. Figure 2.3 shows these common electrode configurations together with their geometric factors (Telford et al., 1990; Loke, 2000; Kearey and Brooks, 2002; Dahlin and Zhou, 2004; Loke and Lane, 2004; Loke, 2010). For each configuration, electrodes are spaced at particular distances defined by the electrode spacing a and dipole factor n. Each configuration has specific advantages and

limitations. Table 2.1 summarizes different 2D electrode configurations and compares key characteristics (Griffiths and Barker, 1993; Loke, 2010).

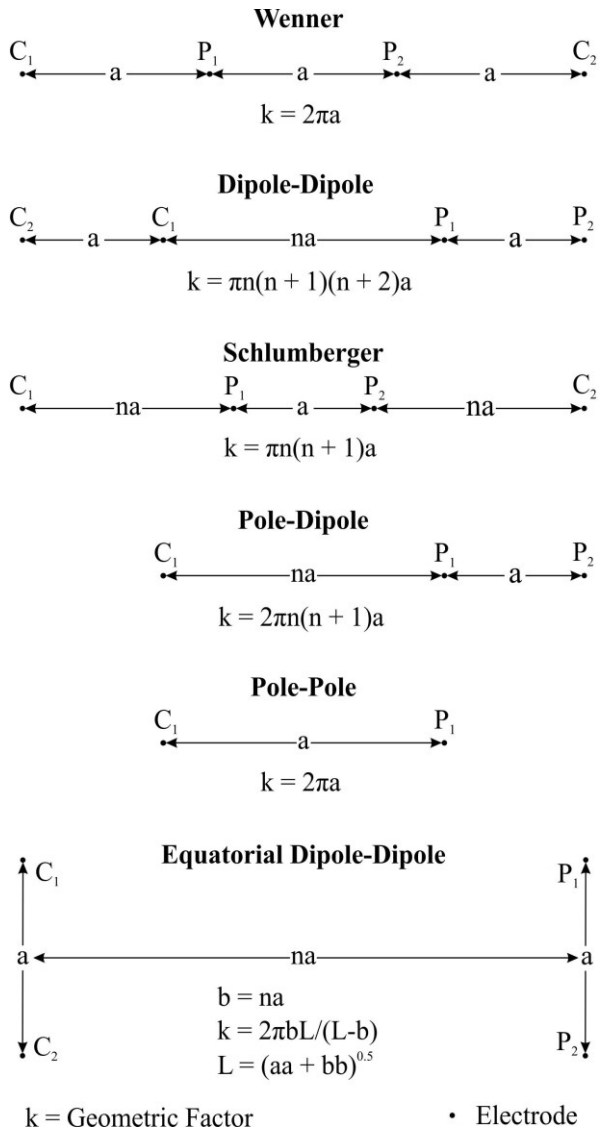

Figure 2.3 Common configurations used in resistivity surveys and their geometric factors. Note that the Schlumberger, dipole-dipole and pole-dipole configurations have two parameters, the dipole length *a* and the dipole separation factor *n*. Equatorial dipole-dipole has 3 parameters that includes L. While the *n* factor is commonly an integer value, noninteger values can also be used (Loke, 2000).

ELECTRICAL RESISTIVITY FIELD SURVEY

Electrical resistivity surveying is one of the most widely used near-surface geophysical survey methods. The technique is based on the assumption that subsurface geological materials have a wide variability of resistivity and that different geological materials can be identified based on measurements of their resistivity. If a target of interest has a sufficiently different electrical rsesistivity property than that of the surrounding material, a change in resistivity contrast will be detected by voltage measurements made at the surface (Barker, 1993).

Table 2.1 Characteristics of 2D configuration types (Samouëlian et al., 2005)

	Wenner	**Wenner-Schl***	**Dipole-Dipole**	**Pole-Pole**	**Pole-Dipole**
Sensitivity to horizontal structures	****	**	*	**	**
Sensitivity to vertical structures	*	**	****	**	*
Depth to investigation	*	**	***	****	***
Horizontal data coverage	*	**	***	****	***
Signal strength	****	***	*	*	**

*Wenner-Schl refers to Wenner-Schlumberger (i.e. the combination of Wenner and Schlumberger configurations). The labels are classified from equivalent poor sensitivity (*) to high sensitivity (****).

The purpose of a resistivity survey is to determine the distribution of underground resistivity from measurements of potential difference made on the ground surface. The electric current pathways within the ground following injection of current are modified by the presence of an electrical resistivity anomaly, which is a zone of different resistivity from that of the background medium. The information provided in resistivity images can be useful for locating subsurface geologic structures and environmental hazards (Loke, 2000; Loke et al., 2003; Loke, 2010). The technique has been used for identifying subsurface bedrock structures (Hsu et al., 2010), subsurface

pollution and hydrogeology (Buselli and Lu, 2001; Amidu and Olayinka, 2006), subsurface cavities or sinkholes (Schoor, 2002), geotechnical and mining targets (Verma and Bhuin, 1979; Aristodemou and Thomas, 2000), and slope stability (Bichler et al., 2004; Udphauy, 2008). The resistivity method recently has been extended to civil engineering and environmental problems (Castilho and Maia, 2008).

Traditional Four Electrode Systems

The resistivity method is one of the oldest geophysical methods, having been established in the 1920's due to the work of the Schlumberger brothers (Loke, 2000). The traditional system consists of a power source, current meter, voltage meter, and four electrodes. Commonly used methods for four electrodes are vertical resistivity sounding and electrical resistivity profiling (Telford et al., 1990).

A vertical resistivity sounding or Schlumberger sounding is used to determine changes in resistivity with depth. The four electrodes are placed in the ground on one line symmetrically around a measurement point. A current is injected and withdrawn through the outer electrodes and the potential difference between the inner electrodes is measured simultaneously. The measurement and the distances between the electrodes are used to calculate the apparent resistivity. The current electrode distances are gradually increased, as the potential electrodes remain in a fixed location. As the current electrode spacing is successively increased, deeper resistivites within the subsurface section are probed. The measured apparent resistivity values as a function of current electrode spacing are normally plotted on a log-log graph. The data from a sounding survey is typically interpreted by comparing the measured results to calculations using a one-dimensional model of a layered subsurface. In this case, the subsurface resistivity changes only with depth, but does not change in the horizontal direction. This method has given useful results in many geological situations and is still used for mapping the depth of the water table.

An electrical resistivity profile or Wenner profiling can also image lateral variations in subsurface resistivity at a given depth. The basic difference between

sounding and profile measurements is that, in profiling, measurements are taken at various stations along the horizontal profile. The four electrodes are placed on the ground with spacing between electrodes fixed. The configuration is moved along the profile horizontally between measurements. It is useful to perform repeated surveys along the same line for several values of electrode spacing, the smaller electrode spacing provides information about the near-surface section while the larger electrode spacing explores the deeper subsurface. Results from measurements can be used to locate lateral changes in the subsurface resistivity distribution along the measurement line. Interpretation of data involves a simple plot of a function of resistivity against distance corresponding to the stations along the line so that anomalous readings can be identified (Loke, 2000; Kearey and Brooks, 2002; Hiltunen and Roth, 2003; AGI, 2010).

Multi-Electrode Systems

The development of direct current resistivity techniques in the last decade has been rapid in both instrumentation and software (Dahlin, 2001). The evolution of computer processing has led to the development of advanced field resistivity equipment, which now includes a large number of electrodes and automatic switching of these electrodes to acquire profiling data. This technique is called Electrical Resistivity Imaging (ERI) or Electrical Resistivity Tomography (ERT) (Bernard et al., 2005). The multi-electrode techniques have tremendously improved investigation capabilities. Instead of making several measurements with different spacing and moving equipment between data points, the multi-electrode technique is able to rapidly collect thousands of measurements with stationary equipment. This new technique greatly reduces the required labor (Hiltunen and Roth, 2003). Recently, one of the most significant developments in the resistivity survey method is the use of 2D and 3D ERI acquisition, modeling, and inversion. This method has been successfully used in complex geology where traditional vertical electrical sounding and electrical resistivity profiling surveys are not able to resolve structures adequately (Loke et al., 2010).

2D electrical Resistivity Surveys

A 2D multi electrode ERI survey is carried out using a number of electrodes connected to a multi-core cable. The electrode cable is divided into sections, which are connected end-to-end. Electrodes are inserted into the ground at a specified inter-electrode spacing along a survey line. A resistivity meter and electronic switching unit are used to automatically select the combination of four electrodes for each measurement. The acquisition of many readings is achieved by measuring several voltages simultaneously across multiple pairs of electrodes for a single injection of electrical current (Loke, 2000; Bernard, 2003; Hiltunen and Roth, 2003; Loke, 2010). Figure 2.4 shows an example of the electrode arrangement and measurement sequence for a 2D ERI survey.

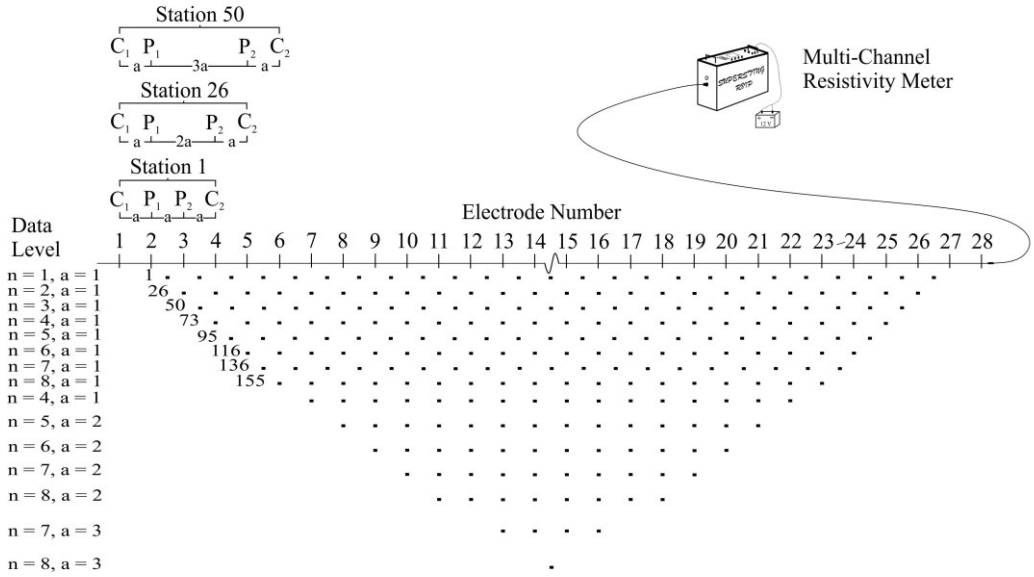

Figure 2.4 The arrangement of electrodes for a 2D electrical survey and the sequence of measurements used to build up a pseudo-section (Loke, 2000).

Often the survey line is longer than the available electrode spread. After the original data have been acquired, the survey line can be extended or “rolled” by moving

the first electrode cable section and electrodes to the end of the last cable. Data for each roll are then recorded and added to the previous data as one complete data file. This type of survey is called a roll-along technique. The technique is useful particularly for a resistivity system with a limited number of cables and electrodes. By using this technique a survey line in principle can be extended indefinitely (AGI, 2006).

The resulting data set from a 2D ERI survey consists of various configurations of transmitting C_1 and C_2 and receiving P_1 and P_2 electrode pairs that comprise a mixed sounding and profiling of the subsurface section (Bernard et al., 2005). The depth of investigation depends on the largest dipole separation during the survey but not on the total length of a survey line. The roll-along technique cannot increase the depth of investigation. The actual depth of penetration also depends on subsurface resistivity distribution (AGI, 2006). In general, a larger spacing a and larger value of n give relatively deeper information about the subsurface structure, while a small spacing a and small n offer relatively good horizontal resolution for the shallower sections of the ground (Dahlin and Zhou, 2004). The 2D electrical resistivity images obtained with the multi-electrode technique are usually used for studying shallow structures located a few tens of meters down to ~ 100 m whereas the traditional vertical electrical sounding technique mainly aims at determining the depths of horizontal 1-D structures down to several hundreds meters (Bernard et al., 2005).

3D Electrical Resistivity Surveys

Since all geological structures are 3D in nature, an ERI survey using a 3D interpretation model should give a more accurate and reliable picture of the subsurface (Loke, 2000) than its 2D counterpart. Two methods of 3D electrical resistivity acquisition are often used. The first method is to build a 3D electrical model by combining data from 2D lines (Samouëlian et al., 2005). Multiple 2D data sets collected along parallel lines are combined into a single 3D data set for inversion (AGI, 2010). Ideally, in order to obtain accurate 3D information on the subsurface, there should be a set of survey lines with measurements in the x direction followed by another series of

lines in the *y* direction (Loke, 2010). If electrical anomalies are preferentially oriented and if the in-line measurement electrodes are perpendicular to the orientation of the anomalies, a 3D electrical picture is thus recorded more accurately (Samouëlian et al., 2005). Orthogonal and arbitrary 2D survey lines have been increasingly used, in which 2D data files are combined into a 3D file for inversion (Gharibi and Bentley, 2005; Günther et al, 2006). However, the best 3D coverage is one in which current electrodes and potential measurements are made over a large range of azimuths.

The second method is the rectangular grid method. Figure 2.5 shows the electrode arrangement for a 3D survey using a multi-electrode system with 56 electrodes. The data set is collected with electrodes arranged in square or rectangular grids with constant electrode spacing in both *x* and *y* directions (AGI, 2010; Loke, 2010). A large-scale 3D resistivity survey involves grids and requires large numbers of electrodes, often more than are available. The roll-along technique has been used to overcome this limitation and to enable coverage of a large area (Dahlin and Bernstone, 1997). The technique is to extend the cable back and forth in the *y* direction, and the measurements are carried out until the entire grid area is covered (Loke and Barker, 1996). The process however can be tedious and cumbersome. The pole-pole array therefore has been commonly used because it has the highest number of possible independent measurements and the widest horizontal coverage (Dahlin and Bernstone, 1997). The cross diagonal technique of pole-pole is used to efficiently make the potential measurements. The potential measurements are made along the *x* direction, the *y* direction, and 45° diagonal rows passing through the current electrode. This technique reduces the number of measurements required without seriously degrading the quality of the model obtained (Loke and Barker, 1996).

ERI Survey in Water Covered-Area

The ERI method is widely used for ground surface surveys. Recently it has been adapted for water-covered environments in Kim et al (2002), Loke and Lane (2004), Kwon et al (2005), and Castilho and Maia (2008). The use of the electrical resistivity

technique to image subsurface structures in water-covered areas is increasing due to frequent construction activities on and under riverbeds, such as bridges and tunnels. However, since the water layer is an important barrier that prevents routine surface geophysical surveys, it is rather difficult to image beneath a river bottom (Kwon et al., 2005). ERI carried out in underwater environments has low signal levels compared to ground surface surveys the due to high resistivity ratio of the true media (i.e. water and earth) (Chung et al., 2001).

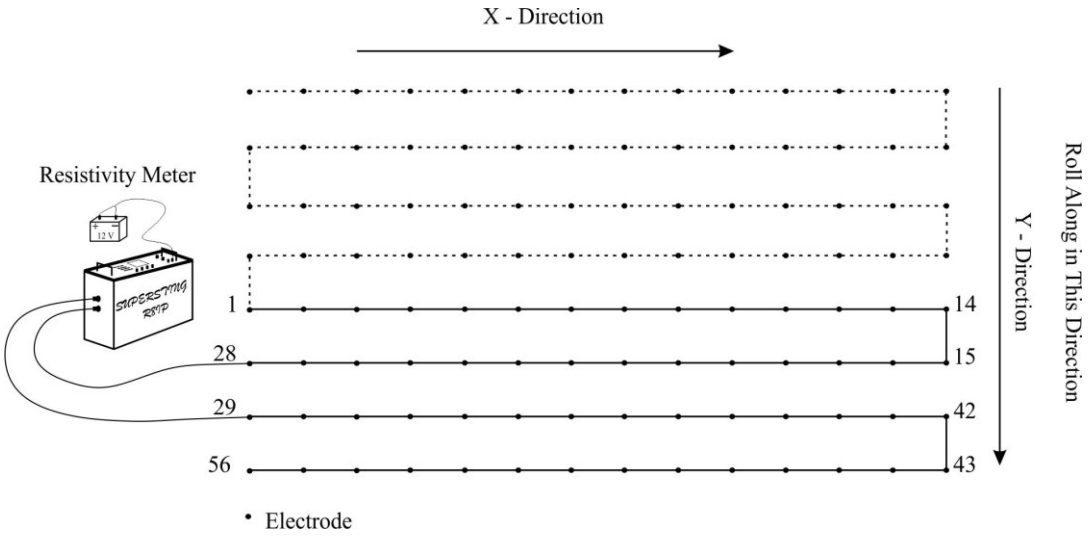

Figure 2.5 The arrangement of 56 electrodes and roll along method for a 3D survey with a multi-electrode system (modified from AGI, 2006).

There are three scenarios for resistivity surveys in water-covered areas: (1) mixed terrain underwater environment, in which some of electrodes are under the water surface while other electrodes are on the ground surface. The mixed terrain underwater case is used when the survey line runs across a creek, a narrow stream, or an open-ended water segment; (2) underwater environment, in which all electrodes are under the water surface and on uneven bottom. The electrode arrangements (1 and 2) are as in a standard resistivity survey system where cables and electrodes are fixed; (3 and 4) mobile surveys

with floating electrodes on the water surface and towed electrodes along the riverbed. The entire measurement array is moved for each series of measurements. Special electrodes are designed to be towed behind a boat on the water surface or on the river bottom. However, aquatic plants growing at the water surface and on the river bottom can be an obstacle for electrode deployments. Floating electrodes can avoid underwater obstacles such as a rough riverbed and aquatic plants growing at the bottom. Towing electrodes at the bottom gives higher resolution provided the bottom does not contain obstacles. Towed-electrode methods easily generate long survey lines, for which the length of the survey line is much greater than the maximum depth of investigation (Loke and Lane, 2004; AGI, 2006). Figure 2.6 illustrates these three electrode scenarios for 2D ERI in water-covered environments.

Each electrode arrangement has advantages and limitations depending on the environment (Castilho and Maia, 2008). Direct contact of electrodes to the earth increases the current injected into the earth, and the resulting sensitivity to the subsurface anomaly is much greater than with floating electrodes, but it requires effort to install electrodes on the water bottom. In practical field surveys, the floating and towed electrode methods are often easier and more convenient (Kwon et al., 2005) but not always, since a boat is required. In my study of bridge foundations, ERI surveys fall in the case of a mixed terrain underwater environment. Special electrodes were made for planting in the riverbed. They were designed leaving only the pointed end of stainless steel stakes exposed. Electrodes were planted into the riverbed leaving the waterproof section partly in water and partly above the water surface; the details are described in Chapter III.

Castilho and Maia (2008) conducted a mixed land-underwater 3D resistivity survey in an extremely challenging environment in the heavy jungles of Amazon. The target was a ruptured crude oil pipeline crossing a river. Data acquisition was conducted with different electrodes arrangements in each of several subareas. In some subareas, there was almost no water and only a half-meter of a mud layer. Electrodes in this case were planted on the ground. In other subareas, the water level was two meters deep with

over two meters of mud without any kind of aquatic plants below and above the water level. Cables in this case could be laid out on the river bottom. In the subareas with heavy aquatic vegetation over mud and water, long underwater electrodes were designed. The electrodes were planted through the vegetation and the mud of the river bottom. The resistivity images have shown that conductive anomalies were detected and they reveal contamination in some regions.

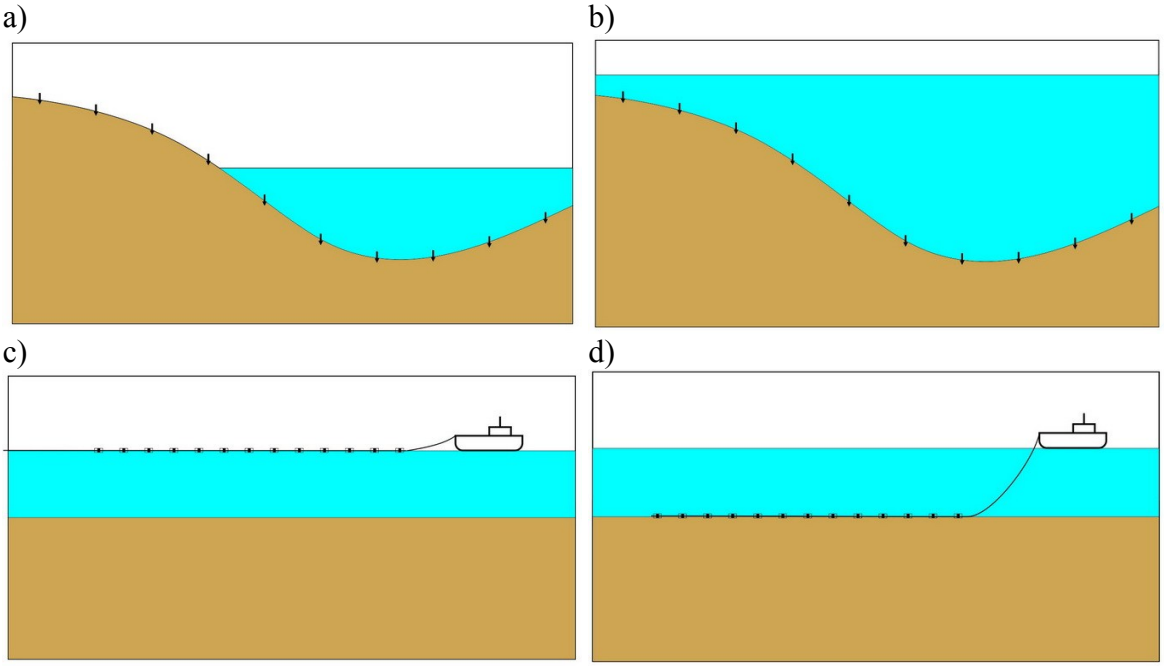

Figure 2.6 Three possible scenarios for ERI surveys of in water-covered area: (a) mixed terrain underwater environment with some electrodes under water and some electrodes on ground surface; (b) underwater environment, all electrodes under water; (c and d) floating electrodes behind a boat on the water surface or towing electrodes on the river bottom (Loke and Lane, 2004; AGI, 2007).

Kim et al (2002) and Kwon et al (2005) conducted a survey to delineate faults or weak zones beneath a water layer for site characterization of planned tunnel construction beneath the Han River in Seoul, Korea. Two electrode installation methods were carried out: (1) electrodes on the water bottom; (2) floating electrodes on the water surface. The

dipole-dipole and pole-pole arrays were modified to enhance the signal-to-noise ratio in the field measurement and the resolution of the inverted image. The result shows that in water-covered areas, the method of installing electrodes on the water bottom is suitable for detailed surveys because the resolution of subsurface images is higher; however, it is time consuming to achieve the electrode installation. The floating electrode method might be preferred in some cases because of better efficiency and lower cost of fieldwork. In particular the streamer resistivity survey is a powerful tool to produce a continuous subsurface resistivity image of a water-covered area with a high speed of fieldwork.

ELECTRICAL RESISTIVITY FORWARD MODELLING

Forward modeling is an essential procedure to provide theoretical values of apparent resistivity for any given subsurface resistivity distribution. The techniques that are most often used to calculate theoretical apparent resistivity values for a defined model are the finite-difference and finite-element techniques (Loke, 1994). In this research the RES2DMOD (Loke, 2001) and RES3DMOD program (Loke, 2002) are used for forward modeling.

The RES2DMOD and RES3DMOD forward modeling consists of producing a set of computed apparent resistivity values based on Poisson's equation,

$$-\vec{\nabla}\cdot\left[\sigma(x,z)\nabla V(x,y,z)\right]=\frac{\partial\rho}{\partial t}\delta(x)\delta(y)\delta(z) \qquad (12)$$

here

$$\vec{\nabla}=\hat{x}\frac{\partial}{\partial x}+\hat{y}\frac{\partial}{\partial y}+\hat{z}\frac{\partial}{\partial z}$$

$$I=\frac{\partial\rho}{\partial t}$$

where V is the scalar electrical potential, ρ is resistivity, t is time and σ is electrical conductivity as a function of x and z, I is the current injection point.

The first term contains $\sigma(x,z)$ since it is assumed that there is no change in conductivity in the y direction. The governing 3D partial differential equation (12) is

Fourier transformed into a 2D equation in the *x, z* plane. The solution is carried out for a set of wavenumbers λ in Fourier space and an inverse Fourier transform is employed to return to return *V(x,y,z)* from the set of transformed potentials χ (*x*,λ,*z*).

In the Fourier domain,

$$-\nabla\cdot\left[\sigma(x,z)\nabla\chi(x,\lambda,z)\right]+\lambda^2\sigma(x,z)\chi(x,\lambda,z)=Q\delta(x)\delta(z) \tag{13}$$

where

$$\overset{\vee}{\nabla}=\hat{x}\frac{\partial}{\partial x}+\hat{z}\frac{\partial}{\partial z}$$

and λ is wavenumber in the transform direction, and Q is the steady state current density that is related to the current I injected by

$$Q=\frac{I}{2\Delta A}, \tag{14}$$

where A is a small area about the injection point.

To solve the above equations the lower (*x,z*) halfspace is discretized using a nonuniform but rectangular grid or mesh. The ∇ operator is discretized using a finite different of first order. This leads to a set of linear equations on the interior mesh nodes. Taking into consideration boundary conditions, simplified equations are found for nodes on the edges of the mesh. The set of equations for all nodes on the mesh may then be expressed in matrix form

$$[C]\cdot[\chi]=[S] \tag{15}$$

$$\left(LL^T\right)\chi=S$$

$$\left(L^{-1}L\right)L^T\chi=L^{-1}S$$

$$L^T\chi=L^{-1}S$$

where C is the coupling matrix between the nodes.

The above equations can be solved as

$$L^T\chi=X \tag{16}$$

where L is a real lower triangular matrix.

An inverse Fourier transform then returns V from χ. The apparent resistivity

response is calculated using

$$\rho_{a=}\frac{G\Delta V}{I} \tag{17}$$

where G is a geometric factor dependent on positions of the current and potential electrodes.

The forward formulation is also applied to predict changes in ρ_a with small changes in σ during the inverse stage of the imaging (Smith and Vozoff, 1984).

A synthetic model of subsurface resistivity is particularly used in the planning of surveys. The systematic model predicts the system response based on known, assumed, or hypothetical geological information. The system parameters are the true resistivity of structure that is input into the forward model while the model output is the apparent resistivity of subsurface (Day-Lewis et al., 2006; Loke, 2010).

Forward modeling is also carried out for survey planning to determine as much information as possible before the field survey. A survey design procedure tests the effectiveness of the resistivity technique with different factors such as electrode arrays, subsurface medium, or features of interest, before carrying out the actual field survey (Yang and Lagmanson, 2003). The user can determine an appropriate array for different geological situations or surveys (Loke, 1999). The synthetic apparent resistivity values from forward modeling are inverted to reconstruct the subsurface resistivity distribution. The forward models may be refined by adjusting model parameters until the synthetic resistivity data and the measured resistivity data approximately match. The final forward model is then used as a geological interpretation of subsurface structures (Kress and Teeple, 2005).

ELECTRICAL RESISTIVITY INVERSION

Theory of Electrical Resistivity Inversion

Methods of geophysical inversion try to determine a subsurface model whose forward response agrees with the measured data subject to certain restrictions. A commonly used technique for 2D and 3D resistivity inversion is the regularized least-

squares optimization method (Loke and Barker, 1996). A 2D forward algorithm using the finite-difference or finite-element method divides the subsurface into a number of rectangular blocks beneath the locations of the observed data. The interior blocks within each layer are of the same size and their positions are fixed in order to efficiently resolve structures with an arbitrary resistivity distribution. Figure 2.7 shows a field arrangement for 2D ERI surveys and the rectangular blocks used for RES2DINV resistivity inversion.

In this research the RES2DINV (Loke, 2004a) program is used for inversion. The model consists of a set of parameters that is estimated from the measured data. The inverse algorithm calculates a model response for a given set of model parameters. At each of several iterations, the Gauss-Newton (GN) optimization method is used to determine the change in the model parameters. The GN equation is,

$$J^T J \Delta q_i = J^T g_i \tag{18}$$

where Δq is the model parameter update vector, J is the Jacobian matrix of partial derivatives, and g_i is the data misfit vector containing the difference between the logarithms of the measured and calculated apparent resistivity.

The Jacobian or sensitivity matrix describes the change of the ith model response f_i due to a small change in the jth model parameter q_i. The elements of the Jacobian matrix are therefore given by,

$$J_{ij} = \frac{\partial f_i}{\partial q_j}. \tag{19}$$

Once the parameter update vector Δq from above equation (18) is calculated, the updated model is obtained by

$$q_{k+1} = q_k + \Delta q_k \tag{20}$$

for k=1,...,M where M is the number of model parameters.

Problems can arise with calculations using the above equations. Parameter update vector often gives excessively large components so that the updated resistivity values might not be realistic. The Gauss-Newton equation is modified to avoid this problem,

$$(J^T J + \lambda I)\Delta q_k = J^T g_i \tag{21}$$

a)

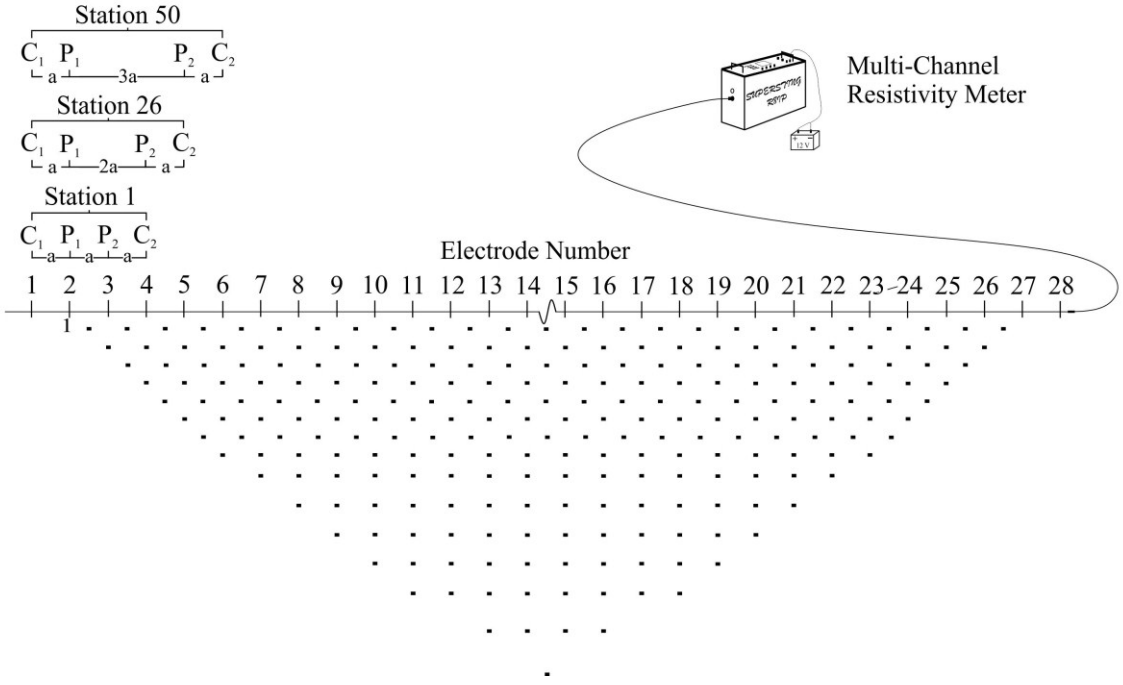

b)

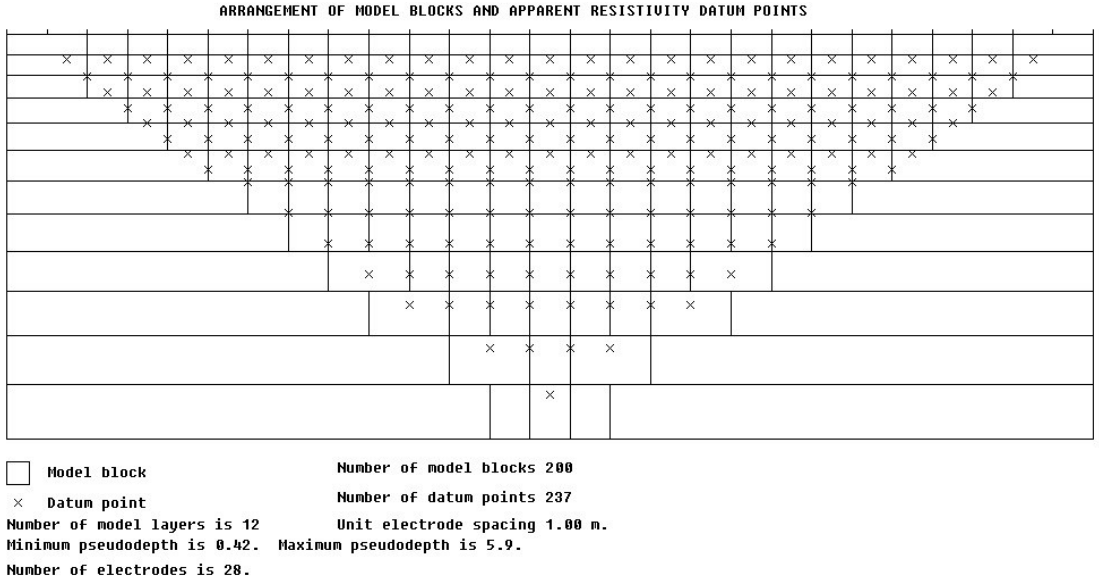

Figure 2.7 (a) A typical field arrangement for 2D ERI surveys with 28 electrodes and (b) arrangement of the model blocks used in a 2D inversion (Loke et al., 2003).

where I is the identity matrix. The factor λ is a damping factor. The damping factor λ determines the relative importance given to minimizing the model roughness. Note that λ is not the same as the Fourier wavenumber described earlier.

This method is used for inverting resistivity soundings that contain a small number of layers. However, when the number of model parameters is large, as in practically important 2D and 3D inversions, the Gauss-Newton least-squares equation should be modified to minimize the spatial variation in model parameters. The model resistivity values could be required to change in a spatially smooth or gradational manner, for example

The method of optimization uses an iterative method so that between calculated apparent resistivity values move closer to the measured values. The distribution of electrical resistivity is adjusted in each iteration so the error between the model and measured apparent resistivities is reduced. The smoothness-constrained inversion method is commonly used. This method minimizes the sum of square of the spatial changes of the model resistivity values. This typically leads to inversion results with smooth spatial variations in resistivity (Loke et al., 2003; Loke, 2010). It is a good optimization choice when gradual geological changes are expected, such as the diffuse boundary of a chemical plume (Barker, 1996). The model update equation for smooth inversion has the following mathematical form:

$$(J^T J + \lambda F)\Delta q_k = J^T g - \lambda F q_k, \tag{22}$$

where

$$F = \alpha_x C_x^T C_x + \alpha_y C_y^T C_y + \alpha_z C_z^T C_z$$

and C_x, C_y and C_z are the smoothing matrices in the x, y, and z directions. The parameters α_x, α_y, and α_z are relative weights given to the smoothness term in the x, y, and z directions, respectively.

However, in cases that a sharp boundary in subsurface structures is expected, such as a bridge foundation, the smoothness-constrained optimization method is not preferred since it tends to smear out sharp resistivity boundaries. An alternative method is the blocky optimization method that tends to produce models containing distinct

regions with sharp resistivity contrasts. The blocky inversion method minimizes the sum of the absolute values of the data misfit. This method produces models with regions of sharper variation in resistivity than smoothness constrained methods (Ellis and Oldenburg, 1994; Dahlin and Zhou, 2004). The blocky optimization equation is modified from the Gauss-Newton formula as follows,

$$(J^T J + \lambda F_R)\Delta q_k = J^T R_d g - \lambda F_R q_k, \tag{23}$$

with

$$F_R = \alpha_x C_x^T R_m C_x + \alpha_y C_y^T R_m C_y + \alpha_z C_z^T R_m C_z, \tag{24}$$

where R_d and R_m are weighting matrices introduced so that different elements of the data misfit and model roughness vectors are given approximately equal weights in the inversion process.

The inversion routine used in this study is based on the blocky optimization method to reveal the sharp boundaries of bridge foundations.

Method of Inversion

Electrical resistivity data for this dissertation were inverted using the programs RES2DINV (Loke, 2004a) and RES3DINV (Loke, 2004b). The inversion uses the non-linear least squares optimization described in the previous section. The 2D algorithm divides the subsurface into a number of rectangular blocks as shown in Figure 2.7. The objective is to determine the resistivity of the rectangular blocks that will produce an apparent resistivity pseudo-section that agrees as far as possible with the actual measurements (Loke et al., 2003; Loke, 2004a).

The data set is in the form of apparent resistivity values, which represent spatial averaged resistivities over a certain volume of the subsurface structure. From these values, the thicknesses and resistivities of subsurface bodies are found. These calculated resistivities are hopefully close to the true resistivities of the actual geological bodies. The inversion starts from a model based on the measured apparent resistivity data. The resistivity values are then modified in an iterative way to reduce the difference between the measured and calculated data (Loke and Barker, 1996). Figure 2.8 illustrates a

generalized flow chart of a resistivity inversion process.

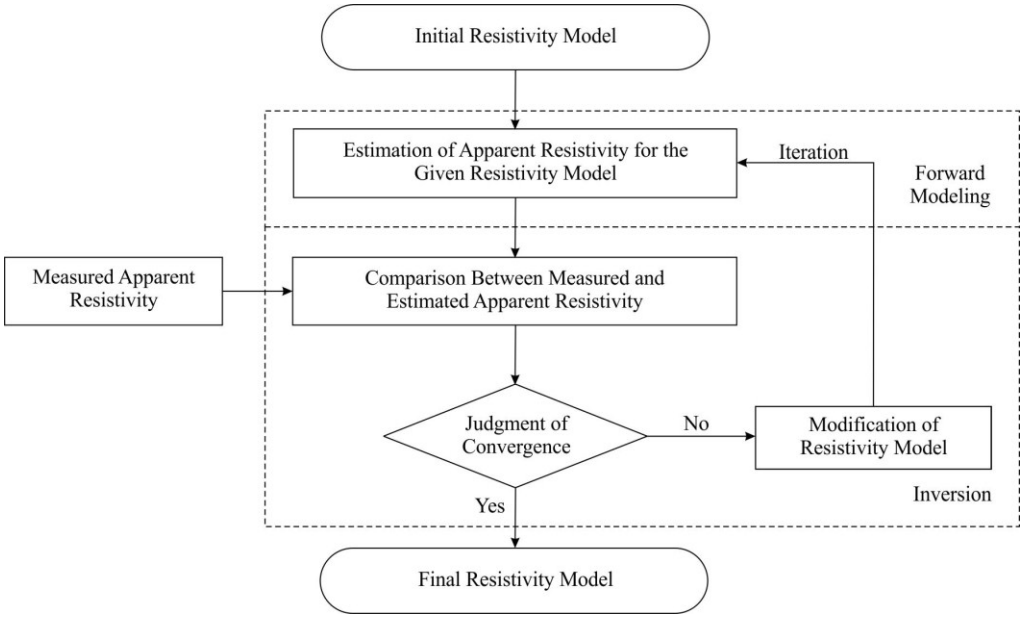

Figure 2.8 Flow chart of resistivity inversion processing (Gakkai, 2004).

The primary objective of inversion is to reduce the data misfit between measured and calculated data. A measure of the fit between the input apparent resistivity data and modeled apparent resistivity values is the RMS error in percent (%) defined below,

$$RMS = \sqrt{\frac{\sum_{i=1}^{N}\left(\frac{d_i^{Cal} - d_i^{Meas}}{d_i^{Meas}}\right)^2}{N}} x100\% \qquad (25)$$

where N is the total number of measurements, d^{Cal} is the calculated data and d^{Meas} is the measured data (AGI, 2006).

The inversion process often yields a high RMS value at the first iteration. As the inversion process refines the degree of the difference of resistivity, ideally the RMS decreases for each following iteration. A model which yields low RMS is identified a good fit between the calculated and measured apparent resistivity values. Eventually the

inversion will attain a pre-defined stopping criterion. A clean data set often converges to a few percent of RMS error in 3-5 iterations. However, the model with the lowest attained RMS error might not be the preferred model. Generally a prudent approach is to choose the model for which the RMS error does not change significantly between iterations (AGI, 2007; Loke, 2010). Some factors used to define a good inversion image consist of a low RMS error (i.e. ≤ 5 %); the anomaly of subsurface structure is geologically interpretable; and reasonable resistivity values are found that are consistent with expected subsurface structure (Loke, 1999).

A data quality control can also be implemented by comparing the forward and reciprocal data. The reciprocal measurements are used for determining noise level since noise contamination can affect the resolution and reliability of ERI images. The quality control process involves two set of measurements in which the first set of measurements is recorded as a forward profile and then a second set of measurements is recorded by switching the current and potential measurement pairs of electrodes for each location. This quality control process doubles survey acquisition times because it essentially measures two surveys. The difference between the two measurements gives an estimate of the measurement error. Theoretically, original and reciprocal measurement pairs should be identical. If the two measurements are not identical, it is assumed there is geologic noise across the electrode pairs. The reciprocal error is the best way to identify the value for the RMS cut off. The data are weighted using the difference between reciprocal measurements as an estimate of their random error. The inversion should be terminated once the difference between successive models reaches the value of the RMS cutoff (Zhou and Dahlin, 2003; AGI, 2007; Gagliano, 2010).

ELECTRICAL RESISTIVITY OF MATERIALS

Electrical Resistivity of Earth Materials

In the earth, electric current flows in water bearing rocks, soils, and minerals by three main mechanisms: electronic and electrolytic conduction and semiconductor. In electronic conductivity, the current flow in materials such as metals is due to free

electrons. In electrolytic conductivity, the current flow is due to the movement of ionic charge carriers mainly in groundwater. Note that electrical flow in dry minerals is mainly by semiconduction (Telford et al., 1990).

Table 2.2 lists characteristic resistivity values for rocks and unconsolidated sediments as given by Cully et al (1975) and Telford et al (1990). Resistivity of earth materials varies over many orders of magnitude. Even individual rock types can exhibit resistivities that vary by several orders of magnitude. Rocks are composed mostly of silicate minerals, which are essentially insulators or semiconductors and have low electrical conductivity (McNeill, 1980). The electric conductivity in most water bearing rocks is principally electrolytic. The electric current paths are through interstitial water networks in pores and fissures (Sharma, 1997). Electrical conductivity of most near-surface materials is due mainly to the groundwater that exists in pore spaces and cracks. The flow of current is largely influenced by the connected porosity of the rock (Adli et al., 2010).

Table 2.2 The resistivity of earth materials (Cully et al., 1975; Telford et al., 1990; Loke, 2010).

Earth materials	Resistivity range (Ωm)
Igneous rocks	
Granite	$4.5x10^3$-$1.3x10^6$
Diorite	$1.9x10^3$-$2.8x10^4$
Andesite	$4.5x10^4$-$1.7x10^7$
Basalt	10-$1.3x10^7$
Gabbro	10^3-10^6
Metamorphic rocks	
Hornfels	$8x10^3$-$6x10^7$
Schists	20-10^4
Mable	10^2-$2.5x10^8$
Quartzite	$2.5x10^2$-$2.5x10^8$
Gneiss	$6.8x10^4$-$3x10^6$

Table 2.2 Continued.

Earth materials	Resistivity range (Ωm)
Slate	$6x10^2$-$4x10^7$
Sedimentary rocks	
Conglomerate	$2x10^3$-10^4
Sandstone	1-$6.4x10^8$
Consolidated shale	20-$2x10^3$
Limestone	50-10^7
Dolomite	$3.5x10^2$-$5x10^3$
Terrain materials	
Unconsolidated wet clay	20
Clays	1-100
Alluvium and sands	10-800
Clay and marl	1-100
Loam	5-80
Top soil	80-120
Clayey soil	100-150
Sandy soil	$8x10^2$-$5x10^3$
Loose sands	10^3-10^5
River sand and gravel	10^2-$9x10^4$
Oil sands	4-800
Glacial till	50-100
Water	
Fresh groundwater	10-100
Sea water	0.2

A bridge foundation is generally built and embedded in firm rock that may be igneous, metamorphic, or sedimentary rocks. The resistivity of subsurface materials should be known or estimated before conducting ERI data acquisition. Igneous rocks typically have higher resistivity values than metamorphic rocks. The resistivity of crystalline rocks is greatly dependent on the degree of fracturing: as a rule, the more

fractured a rock and the higher its water content, the higher the conductivity. Adli et al (2010) tested the resistivity of granite in the field and laboratory. They concluded that field measurements gives generally lower resistivity than laboratory analyses due to the interference form various noise sources in the field. Sedimentary rocks normally have lower resistivity values compared to igneous and metamorphic rocks since they usually have more porosity and a higher water content (Loke, 2010).

Electrical resistivity is described by Archie's Law that gives a relationship between the bulk resistivity and the pore fluid resistivity. Archie's Law is applicable for certain types of rocks and sediments, particularly rock with low clay content. Archie's law assumes that all current is conducted through the pore fluid, and while the grains and air-filled pores are insulators (Taylor and Barker, 2006). A common statement of Archie's Law is

$$\rho_b = a\rho_w S^{-n}\phi^{-m}, \qquad 26$$

where ρ_b is the resistivity of the porous medium, a, m, and n are petro physical constants that are characteristic of the porous medium, ρ_w is the pore-water resistivity, ϕ is the fraction of the rock filled with the fluid, and S is saturation (i.e. ratio of the water content and porosity) (Archie, 1942).

There are many geological processes such as dissolution, faulting, shearing, columnar jointing, weathering, and hydrothermal alteration, which can alter a rock and significantly lower its resistivity (Sharma, 1997). In addition, the geologic age and lithology can determine the resistivity of particular rock types because the porosity of the rock and salinity of the contained water are affected by both. It is also found that electrical resistivity decreases as temperature and pressure increase (Telford et al., 1990).

Unconsolidated sediments generally have much lower resistivity values than consolidated rocks (Loke, 2010). Soil resistivity values are dependent on: (1) degree of saturation; (2) resistivity of pore fluid; (3) porosity; (4) shape and size of solid particles/distribution (Fukue et al., 1999). Soil-water is the most important determining factor of electric current conduction (Saarenketo, 1998). Air filled pores or cracks in

soils represent resistive structures (Samouëlian et al., 2003). The electrical resistivity of soils varies across a large range of values from 1 Ωm for saline soil to about 10^5 Ωm for dry soil. Electrical current in soils vary with the amount of water in the connected pores and on the quantity of dissolved salts (Samouëlian et al., 2005). The electrical resistivity is also related to the mobility of the ions present in the fluid filling the pores, which in turn depends on the pore fluid viscosity (Scollar et al., 1990).

Figure 2.9 illustrates how the pore space is filled by liquid in different zones of a soil profile. The electrical resistivity of rocks and soils mainly depends on porosity and the degree to which pores are filled with water. The degree of liquid saturation is continuous within the pore space below the water table and in the capillary head. Otherwise, liquid content decreases gradually with height above the water table (Meyboom, 1969). The changes of season also affect the groundwater table and the soil moisture in the pore space. Figure 2.10 shows the movement of moisture from topographic high regions down to the draining streams when the water table is higher than stream level in the flooding season. Movement of the moisture downwards away from stream occurs when the water table is lower than stream level during the dry season (Maxey, 1964).

The basic structure of a typical clay particle consists of alternating layers of two sheet-like crystalline lattices consisting of one sheet of an octahedral lattice sandwiched between two tetrahedral sheets to maintain electrical neutrality. The clay particle attracts cations to its surface from the aqueous solution that surrounds the clay (Mitchell, 1993). The presence of clay reduces the bulk resistivity of soil and rock and sometimes causes the resistivity to become frequency dependent (Telford et al., 1990; Fukue et al., 1999; Loke, 1999). Clay minerals have a net charge distribution on the surface layer. The charged surface affects the electrical resistivity of clay-water mixtures (Mitchell, 1993). In clay soil, the bulk electrical resistivity is related to the particle size by the electrical charge density at the solid surface. The electrical charges at the surface of the clay particles lead to greater electrical conductivity than in coarse-textured soils because of the magnitude of the surface to volume ratio (Fukue et al., 1999). A measurement of the

electric resistivity of a number of natural clays shows that resistivity of clays varies in a significantly narrow range from less than 1 to 12 Ωm (Giao et al., 2003).

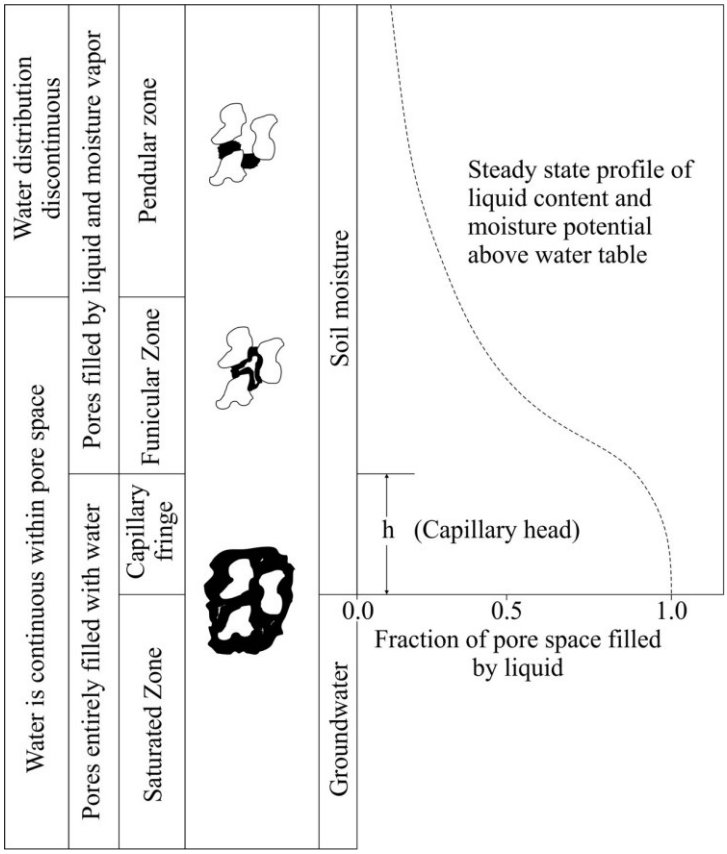

Figure 2.9 Liquid occurrences in soils (Meyboom, 1969).

Clay is exchangeable, in other words, certain ions are replaced by other ions as its aqueous environment changes. Clays remove ions from the aqueous solution and replace them with different ions from their structure. When water is added to clay, the concentration of ions is in solution increases in the vicinity of the clay surface. As clay particles expand surface area per unit weight, ions that are held adjacent to the exposed lattice structure of the surface can be released into solution and ions in the solution can be drawn to the surface. Consequently, a relatively expanding area of small amount of

clay can dramatically increase the bulk conductivity (Mitchell, 1993). All saturated rocks containing clay minerals exhibit high conductivity (Sharma, 1997). Shale and mudstone exhibit resistivity in the range between 10 and 100 Ωm (Stolarczyka and Peng, 2003).

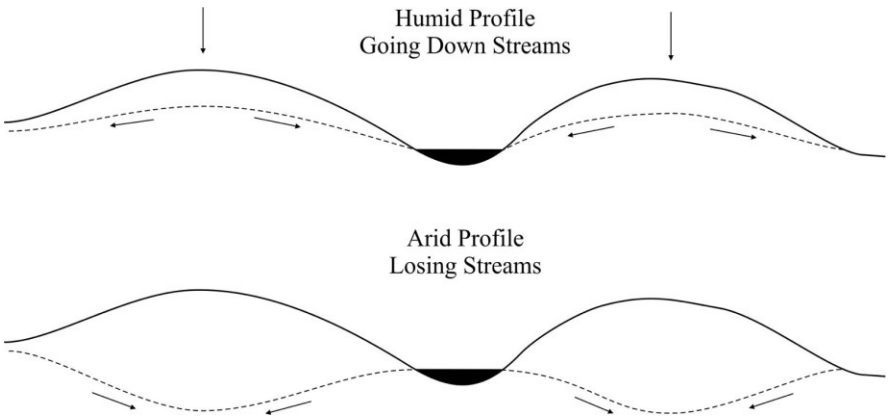

Figure 2.10 Profiles of water tables in arid and humid zones and seasonal movement of moisture (Maxey, 1964).

The electrical resistivity of pore water mainly depends on the concentration of dissolved salt, and temperature. Groundwater has resistivity varying from 10 to 100 Ωm. Seawater with 3 % dissolved salt content has a low resistivity of about 0.2 Ωm (Loke, 2010). The resistivity of water increases with decreasing temperature due to decreasing mobility of the ionic charge carriers. The presence of frost increases the resistivity of the rocks and water. In countries with permafrost, it is difficult to carry out the resistivity survey method (Krautblatter and Hauck, 2007).

Electrical Resistivity of Concrete

The electrical resistivity of concrete is related to the microstructure of the cement matrix, the porosity, and the pore size distribution. The mobility of ions in the pore solution plays an important role in determine bulk conductivity (Humkeler, 1996). As concrete is manufactured, water becomes trapped in pores. When resistivity is measured,

electric current is carried by the ions in the pore water. The electrical resistivity of concrete has been used as an indirect index to evaluate the corrosion of embedded steel (Su et al., 2002). The electrical resistivity of reinforced concrete may vary over a wide range from 10^1 to 10^5 Ωm depending on degree of corrosion; the moisture content and the material composition (Tuutti, 1982).

The electrical resistivity of a concrete structure can be directly measured. The Wenner technique, for example, uses four equally spaced point electrodes pressed onto the concrete surface. The resistance obtained by this method can be converted to apparent resistivity based on equation: $\rho=2\pi aR$, where a is the electrode spacing and $R=V/I$. Due to the heterogeneity of concrete, the true resistivity is reliable only within 25 % error (Polder et al., 2000; Su et al., 2002). Browne (1982) reports that concrete resistivity should be in the range of 500 to 1,000 Ωm to prevent corrosion of the reinforcement steel. Gonzalez et al (1993) added that the corrosion rate is negligible when concrete resistivity is higher than 10,000 Ωm.

Table 2.3 shows reference electrical resistivity values of concrete from several laboratory studies. Resistivity depends on the cement type and its environment. The electrical resistivity of concrete is an important indicator of the extent of corrosion. The amount of corrosion increases as resistivity of the concrete decreases. Concrete materials with low risk of corrosion have high resistivity whereas concrete materials with high risk of corrosion have lower resistivity values, as shown in Table 2.4 (Song and Saraswathy1, 2007). The resistivity of concrete also increases as the concrete dries out (Polder et al., 2000). In reinforced concrete, the electrical resistivity is dependent on: (1) the intrinsic quality of concrete (composition, compressive strength); (2) the condition of surface or bulk deterioration caused by cracking, delamination, and salts; and (3) the distribution of reinforcement bars within the concrete structure (Chouteau and Beavlien, 2010). In case parts of rebars are exposed and contacting to ground, no matter if the foundation is new or old, the ERI images the foundation as a conductive anomaly.

In an ERI survey, the presence of rebar in a concrete foundation can cause interference with the foundation resistivity determination, especially if the rebars are in

direct contact with the ground. The concrete foundation in this case would have high bulk conductivity, and the resistivity contrast of the foundation with its surrounding materials could be small. Practically, if the earth materials surrounding a concrete foundation are high in resistivity, approaching the resistivity of the concrete, an inversion will not be able to distinguish between the concrete foundation and its surrounding materials (Conrad, 2010).

Table 2.3 Global reference values at 20˚C for the electrical resistivity of dense-aggregate concrete of mature structures (age > 10 years); conditions in brackets are corresponding laboratory climates (COST 509, 1997).

Environment	**Resistivity ρ of concrete (Ωm)**
Very wet, submerged, splash zone	50-200
Outside, exposed	100-400
Outside, sheltered, coated, hydrophobised, (20˚C 80 % Relative Humidity)	200-500
Indoor climate, (20˚C 80 % Relative Humidity)	3,000 and higher

Table 2.4 Concrete resistivity and risk of reinforcement corrosion at 20 ˚C for ordinary portland cement concrete (COST 509, 1997).

Resistivity ρ of concrete (Ωm)	**Risk of corrosion**
< 100	High
100 - 500	Moderate
500 - 1,000	Low
> 1,000	Negligible

PREVIOUS ERI STUDIES ON UNKNOWN FOUNDATION

A few studies in the literature have applied the ERI method to investigate unknown foundations. By imaging the distribution of subsurface resistivity, the electrical

resistivity method can provide information on the spatial distribution of the foundation and its surrounding materials. Engineering applications include investigation of bridge and building foundations.

Conrad (2010) carried out a side-looking 2D resistivity profile to investigate the foundation of an old bridge pier. The experiment was performed to determine whether a 2D resistivity profile placed in proximity to a bridge footing would be able to image it from the side. A 28-electrode AGI SuperSting R8 array with 3 m electrode spacing was oriented parallel to the bridge pier and water flow. The line was located approximately 2 m from the pier. An interpretation was performed using the RES2DINV program based on the blocky inversion technique that is suitable for determining sharp boundaries of anomalies caused by concrete adjacent to earth materials. The inversion results indicate that adjacent subsurface structures can be mapped to estimate the size, depth, and orientation of the target structure and surrounding earth materials. Bridge plans showing the original design of the footer were unavailable to verify the results. Other tests have been run at other sites and somewhat similar results were obtained. The general conclusion is that 2D ERI can be used for side scanning of a large buried foundation. Conrad (2010) also reported that the iron rebars in the bridge footing were not in contact with the ground, so the rebar does not appear to cause interference with the resistivity measurements. If the footing exhibited exposed rebar in at least two locations, then the electrical short circuit caused by the rebar might prevent the resistivity configuration from imaging the foundation.

Denil and Canavello (2005) conducted an electrical resistivity survey to evaluate the subsurface material beneath and adjacent to bridge piers. A data acquisition at each of several locations consisted of a dipole-dipole resistivity array. The resistivity line was placed approximately 1.5 m from a pier that had experienced a scour problem. A total of 28 stainless steel electrodes were planted into the ground at 3 m spacing along the survey line, of length 82 m. The resistivity data were inverted using the AGI EarthImager 2D software program. The result shows that low resistivity values of 20 to 200 Ωm were recorded around the base of the pier. This suggests that the pier rests on a layer of soil

and/or highly fractured, broken or weathered rock rather than competent bedrock, which would be highly resistive. Higher resistivity values of 400 to 1200 Ωm were recorded beneath the pier within the depth interval of 6.5 to 12 m. These values suggest the presence of slightly fractured to dense competent bedrock that may provide adequate support for the pier and may not erode or scour if exposed to normal stream flow. Furthermore, the high resistivity values recorded adjacent to the pier walls suggests the presence of competent bedrock that may provide lateral support for the pier.

CHATER III

METHODOLOGY

In this chapter, 2D and 3D forward modeling procedures, ERI data acquisition at existing bridges, and ERI data analyses are illustrated. Data acquisition and objectives will be described for each site. This chapter addresses the ERI experiments in order from small to large foundations and from known to unknown foundations. The data acquisition and analyses comprise both land surface and mixed terrain underwater environments.

EQUIPMENT

Resistivity data were collected for this study using the SuperSting^{TM} R8/IP, Earth Resistivity/IP, Multi-channel Resistivity Imaging System with an internal switchbox system manufactured by Advanced Geosciences Inc. (AGI), Austin, Texas. The SuperSting can simultaneously measure up to 8 voltage channels for a single current injection using a high power transmitter. The equipment included 4 passive electrode cables and 56 stainless steel electrode stakes, each cable with 14 electrode takeouts. Each stainless electrode stake is about 45 cm long and 1 cm in diameter. The maximum allowable distance between two adjacent electrode takeouts is 2 m. Figure 3.1 shows the SuperSting R8/IP system and cable connected to the electrode stakes.

The SuperSting system was powered by an external 12-volt deep cycle marine battery. A field laptop computer was used to upload command files to SuperSting system and download measured data files for subsequent data processing. A tape measure was used to locate positions of electrodes. A hammer was used for planting electrodes into the ground. A Topcon GTS-313 total-station surveying instrument was used to measure elevation data to an accuracy about 1 cm along the resistivity profiles and also to map detailed topography of study areas.

Underwater electrode stakes were designed for ERI surveys in water-covered

environments. The entire length of each stake was waterproofed using a small PVC pipe. Electrode stakes were connected at the top end to an electrical wire. The wire and electrode were inserted into the PVC pipe leaving only about half of the extremity exposed. Hot glue was then injected inside the PVC, and the glue formed into a cone shape at the point end of the PVC. When the electrodes were planted in water area, they could be driven easily into the riverbed. The electrodes are electrically insulated from the water. An electrode test was conducted in an underwater environment at Texas A&M University, Riverside Campus prior to surveys at actual bridges.

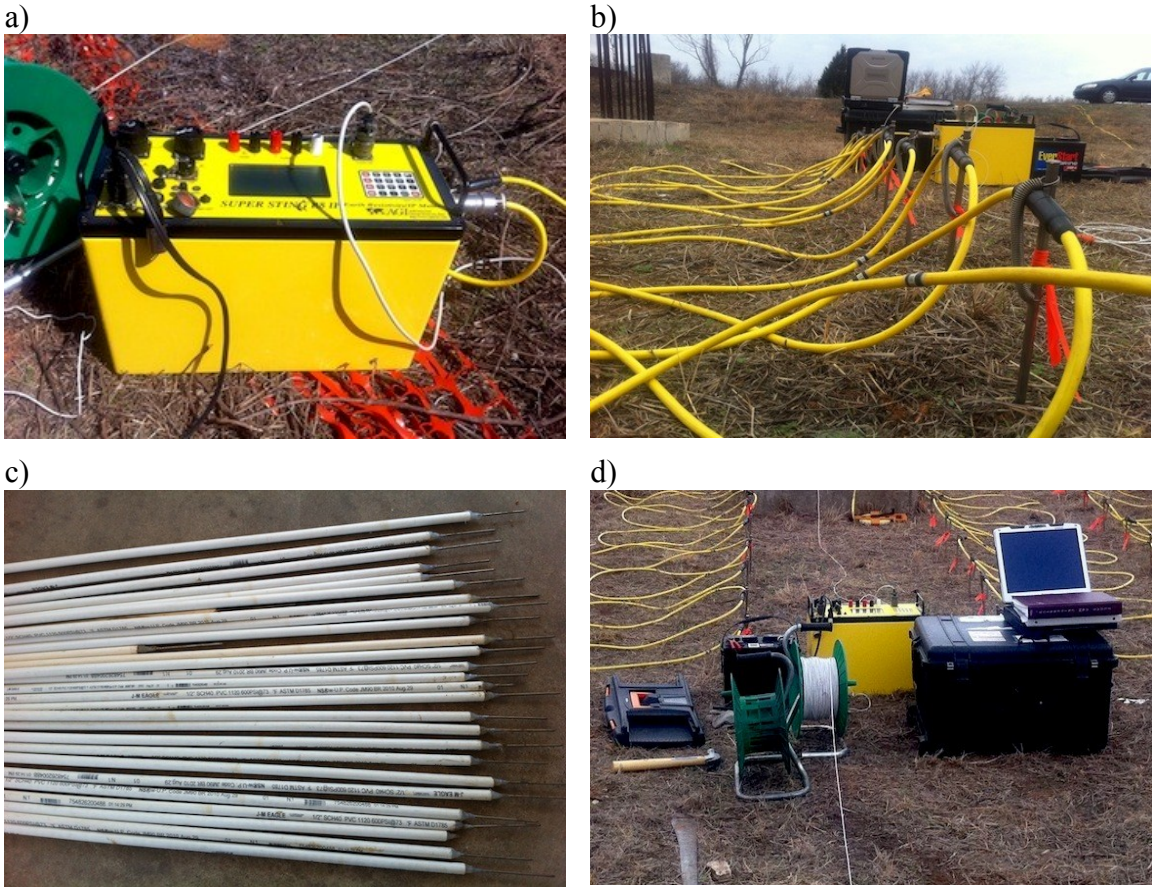

Figure 3.1 (a) Multi-electrode resistivity AGI SuperSting^{TM} R8/IP meter, (b) view of electrodes connected to the cable takeouts, (c) underwater electrodes, and (d) view of equipments set up in the field.

Before a survey is started, an appropriate command file is required. The command file is created by the AGI Administrator software package provided with the SuperSting Resistivity System. The command file is required in order to instruct the SuperSting to execute a pre-defined sequence of electrodes to be used for current injection and measurement of potential difference. The appropriate settings were entered in the command creator module. The software provides tentative information about penetration depth, data coverage, and an estimation of the number data measurements required to perform the survey. Once the creation of the command files is completed, an animation is displayed in order to carefully check the measurement scheme and, if needed, to specify where the reciprocal data are needed. After the command file is verified, it is transferred into the SuperSting RAM memory.

The SuperSting R8/IP is a multi electrode system with a large number of electrode stakes attached to the instrument. An internal switchbox is used to toggle the various electrodes on/off during the acquisition. The 8 receivers measure the potential difference between 9 electrodes simultaneously for each current injection, which uses using two electrodes. Four cables are set out, typically but not necessarily in a straight line, and connected to the resistivity meter system. Electrode stakes are planted into the ground as deep as possible to minimize the electrical contact resistance. Electrode spacing is set to equal intervals as determined by a measuring tape. The cable takeouts are fastened to stainless electrode stakes via spring assemblies. This system can use the roll-along technique that allows 14 additional electrodes at a time to increase the length (although not the penetration depth) of a single survey profile.

Once the survey layout is set up in the field and prior to initiating data acquisition, the SuperSting is tested with a standard receiver test box. Surface coupling tests are conducted to verify proper contact resistance, which should typically range from 0.5 to 5 kΩ. The error code HVOVL usually means poor contact of electrode to ground, while INOVL or TXOVL typically mean loose connections somewhere else in the electrical circuit. If the ground surface at any electrode has anomalously high contact resistance, salt water is added. These tests are carried out before each field survey to

ensure good data quality. The SuperSting system is set as 2-cycle stacking and the standard error of measurements to 5 %. With this setting, each measurement is repeated twice. Repeated measurements with RMS variation greater than 5 % are rejected.

Two-dimensional and three-dimensional electrical resistivity (2D and 3D ERI) surveys are carried out in this study. For the purpose of this investigation, the vertical extent of subsurface structures (i.e. bridge foundations) is of greater interest than the horizontal extent. The dipole-dipole array is well suited for this study. This electrode configuration is selected because it is very sensitive to horizontal resistivity variations, which means that it performs well in the mapping of narrow vertical structures.

FORWARD MODELING

Synthetic models were generated to evaluate the forward response of typical bridge foundations. The subsurface are divided into two main zones; the soil and the concrete foundation. Generally bridge foundations are embedded into the ground and placed on firm bedrock. The earth materials surrounding bridge foundations are classified as alluviums or soils. Using the portable resistivity meter, measured resistivity values of soil at a site are used as input to the forward model. The soil resistivity measurement was conducted using a Miller 400A Analog Resistance Meter. The averaged resistivity at the national geotechnical test site, for example is 116 Ωm. Concrete resistivity is specified in the forward models with trial values that are both lower and higher than the surrounding materials. Concrete foundations with a low risk of corrosion should have a very high resistivity value whereas those with a high risk of corrosion should have a lower value. The amount of corrosion decreases as the resistivity of the concrete foundation increases.

Forward modeling was performed to quantify the influence of the foundation in the inversion results. 3D ERI forward models were completed for 1x1 m dimension with 9 m depth (i.e. a deep foundation), 3x3 and 5x3 m dimension with 5 m depth (i.e. shallow foundation). The synthetic model started with a homogeneous half-space and background resistivity of 116 Ωm. The resistivity of the foundation was assigned in two

trials to be greater and lower than that of the background material. If there is no appropriate resistivity contrast of subsurface structures the ERI method cannot be used efficiently. Trial and error synthetic models were done to find an appropriate range of resistivity contrast between foundation and the measured resistivity of soil.

The 3D synthetic models were generated using RES3DMOD. Synthetic models were designed to simulate land environments. Soils were considered to be the geological background whereas concrete foundations were considered to be the anomalous structure. The dipole-dipole inline configuration was used for both forward modeling and inversion with 1 m electrode spacing along the survey profile and 2 m line spacing. The model configuration is 56 electrodes in the *x* direction and 9 electrodes in the *y* direction with a division of two cells between adjacent electrodes. A single modeled foundation is located in the center of the model, and embedded in a homogenous half-space. The synthetic data are generated based on these assumptions of subsurface resistivity distribution and electrode configuration. Electrodes are assumed to be laid out on flat ground surface so, in this case, topographic information is not incorporated in the model. The resistivity distribution of the foundation and background medium are specified.

The model values are input to the forward modeling program, RES3DMOD. The program allows the user to examine the synthetic pseudo-section and to alter the size and shape of anomalies structures as desired. The forward calculation uses 4 nodes per electrode spacing and is processed with the finite different method. The final apparent resistivity values from the forward calculation are perturbed by 5 % Gaussian distributed random noise in order to represent the realistic response of a foundation and its geological environment. The program calculates apparent resistivities of the 3D synthetic model. Afterwards, 2D profiles along the *x* direction are extracted from the 3D model. For foundations smaller than the electrode spacing, the 2D profile is extracted over the center of the foundation. For foundations greater than electrode spacing, the 2D profile is extracted along the side of the foundation. Each profile is assumed to have 56 electrodes with unit electrode spacing of 1 m. The pseudo-sections consist of

approximated 2400 synthetic apparent resistivity values.

The apparent resistivity data are inverted by RES2DINV. The inverse calculations are conducted by blocky least-squares optimization with a finite element algorithm used to construct the 2D forward model responses. The ratio of the vertical flatness filter is given a greater weight than the horizontal filter, since we require resistivity variations in the vertical direction to be optimally resolved. Successive layer thicknesses increase with depth by 25 %. The model cells are created with widths of half the electrode spacing. The inverted resistivity section is displayed as a resistivity image. This exercise is done to test the validity of using 2D methods in an actual 3D environment.

ELECTRICAL RESISTIVITY EXPERIMENTATIONS AND DATA ACQUISITION

One laboratory experiment and five field surveys were carried out between 2009-2011. The survey design criteria for each site varied based on a range of objectives that are discussed further below. The overall research effort is illustrated schematically in the flow chart shown in Figure 3.2. The bridges are located in Brazos County and neighboring Burleson Country, Texas. Since all bridges are under the responsibility of TxDOT, access to the sites was received from engineers with the Bryan TxDOT District. Data acquisitions were conducted during the non-flood season and the sites were easily accessible. Figure 3.3 shows maps of the five study areas. Summary detail of the acquired data and profiles are presented in Appendix A.

Electrical Resistivity Experimentation

Description of Study Area

The electrical resistivity laboratory experimentation was conducted in the controlled environment of the Haynes Coastal Engineering Laboratory. The Haynes Laboratory is located on the Texas A&M University campus and is designed for research in coastal, ocean, and hydraulic engineering. The laboratory contains a unique towing tank and a 3D wave basin. Electrical resistivity experiment was tested in the towing tank

45.72 m length, 3.66 m width, and 3.35 m depth. There is a sediment pit to allow scour studies that is 9.14 m long, 3.66 m wide, and 1.52 m deep and is located about 2/3 of the way down the tank from the flow inlet end.

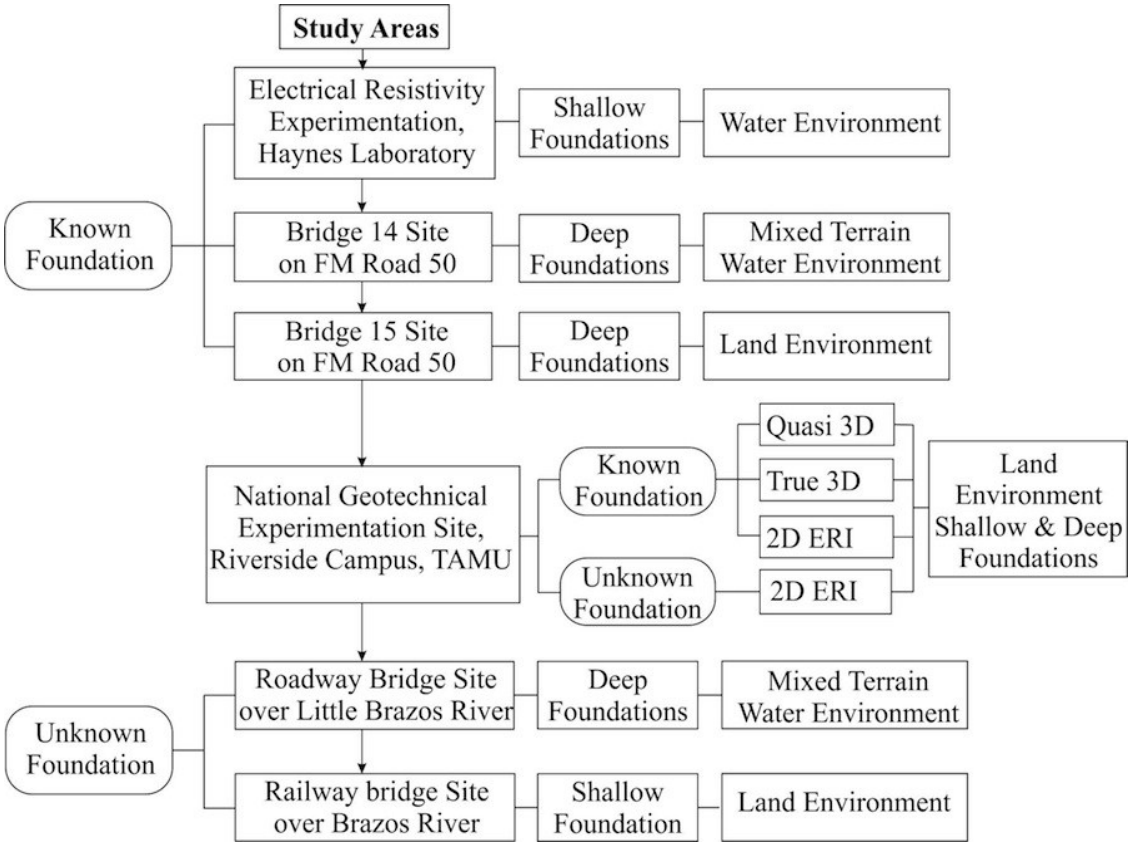

Figure 3.2 Flow chart of ERI experimentation and data acquisition.

Data Acquisition

The goal was to place various lengths and shapes of foundations in the tank and to conduct resistivity surveys with and without water environments. For the first step, two concrete slabs were buried at different depths (i.e. 0.76 and 0.91 m) in the water environment with 0.3 m water depth in order to determine that the different resistivity images would obtain from the slabs buried at different depths. Four underwater

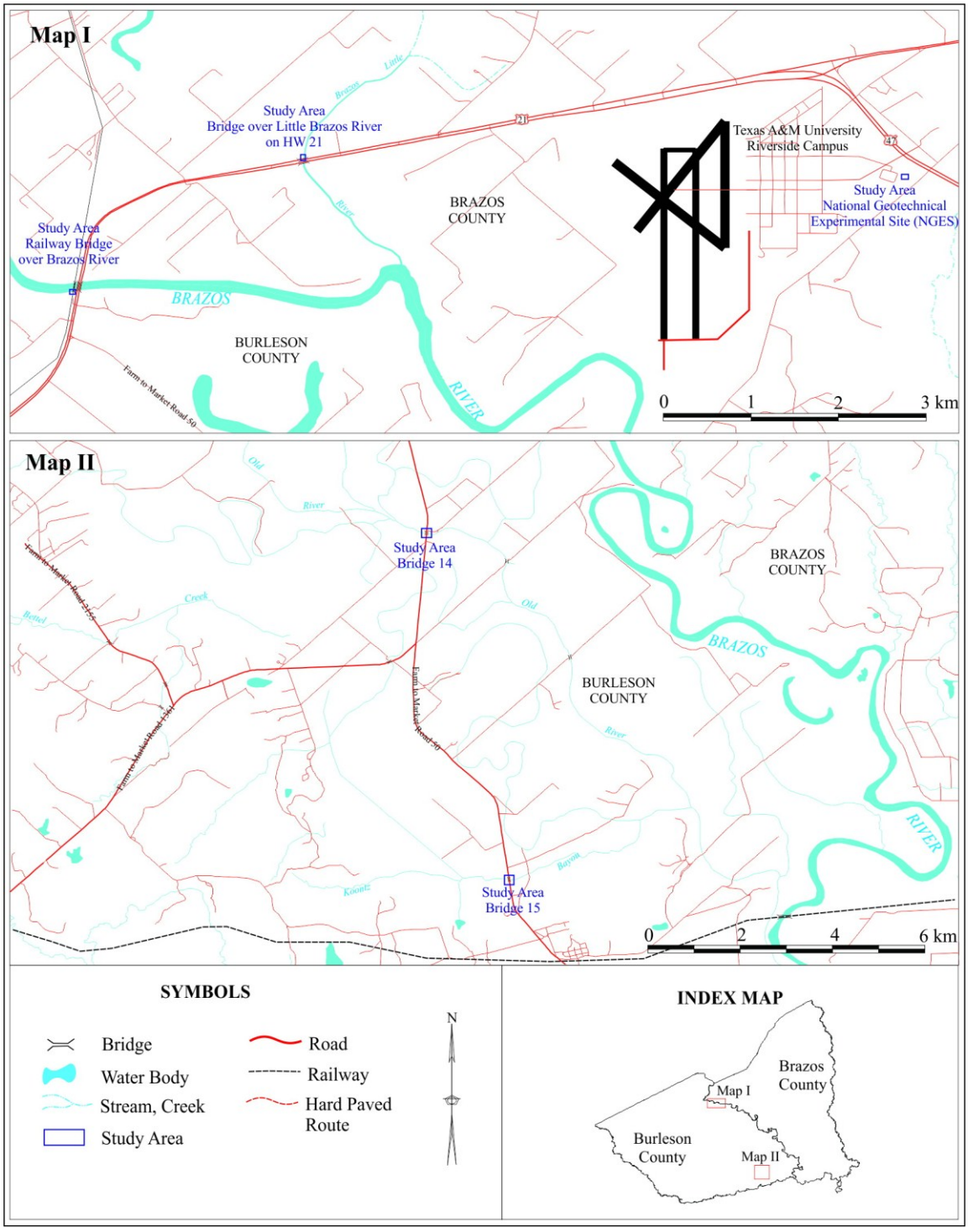

Figure 3.3 Outline maps showing the locations of the five study areas.

electrodes were strung across the tank. The electrical resistivity was first tested in the water with four underwater electrodes in the dipole-dipole configuration, as shown in Figure 3.4. Concrete slabs were placed in the middle of the basin. The measurements were taken with other electrode configurations such as Schlumberger and Wenner at various stations along the horizontal profile. The four underwater electrodes were planted on the ground with 0.25 m electrode spacing. The spacing between electrodes was fixed and the configuration was moved along the profile horizontally between measurements. Measurements were made on the same line for several values of electrode spacing.

a) b)

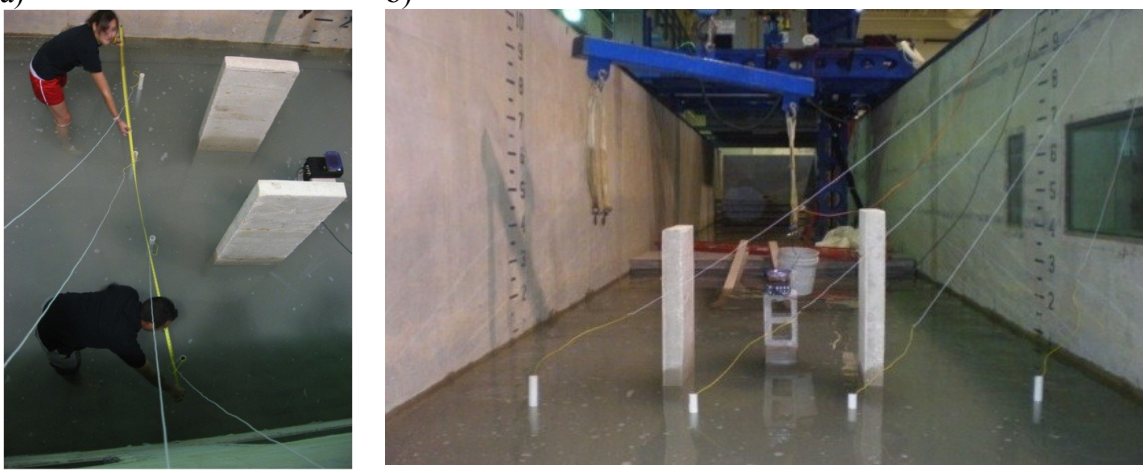

Figure 3.4 Electrical resistivity experiments in water-covered area in towing tank within the Haynes Laboratory (a and b).

From this electrical resistivity experiment, it was found that apparent resistivity values did not change significantly. Although there is a sufficiently high resistivity contrast between the foundation and the sediment, the resistivity values of the environments (i.e. walls and floor) are roughly the same as that of the foundation. The readings were affected by the concrete walls and floor. It was decided that the electrical resistivity method then could not be tested effectively in such an environment.

Accordingly, a field test of underwater electrodes without a concrete slab was conducted at a lake at Riverside Campus, Texas A&M University. It was found in this test that excellent stable readings of apparent resistivity are obtained.

The test was not successful at the Haynes Lab because it was not possible to make the experimental conditions as realistic as an actual bridge site in such a controlled environment. The experiments were therefore ended at Haynes Lab and moved directly to actual bridge sites in field. The field experiments started from bridges with small foundations and worked up in size to larger drilled shafts and spread footings and from known to unknown foundations. With the help of TxDOT, I identified two bridges, Bridge 14 and 15, on FM road 50 where the foundations are small concrete piles. The national geotechnical test site was used as an experimental test site for the 2D and 3D ERI. The other two bridges with larger foundations were then selected. The bridge at HW21 has a drilled shaft and the railway bridge has a footing foundation.

Bridge 14 Site

Description of Study Area

Bridge 14 is located on FM Road 50 in Burleson County about 21 km southwest of College Station (Figure 3.3). This is a site with known concrete pile foundations of small size. The piles are 0.39x0.39 m in square cross-section and the length embedded into the ground varies from 10.1 to 15.8 m according to the bridge design layout obtained from TxDOT. A visual inspection of the foundations revealed that all concrete piles have a hooked metal sling exposed and in contact with the ground. This could lead to a short circuit and cause low apparent resistivity values. The bridge was constructed over the Old River in the North-South direction. The river was about 6 m wide and 1 m deep at the center during the time of the survey. The survey profile has moderate topographic relief. The surface of the site under the bridge is sparsely covered by concrete cobbles and boulders. According to a lithologic log from test holes, the soil geology consists of a layer of red and brown clay about 7.3 m thick followed by a clayey sand layer down to a depth of 10.4 m. A layer of coarse sand and gravel lies between

10.4 and 14.6 m. A silty and clayey sand layer exists from 10.4 to 21 m, the bottom of the hole.

Data Acquisition

The setting of Bridge 14 is a mixed terrain underwater environment with a row of foundations located on the down stream portion of the bridge. The single survey profile BG14 used 56 electrode stakes connected to 4 multi core cables. The roll-along technique was employed in order to extend the length of the survey profile. Figure 3.5 shows the topography of the study area and location of the survey profile. The electrodes were spaced at a distance of 0.5 m apart giving a total profile length of 69.5 m. The first electrode was located on the north end of the bridge, with the line extending to the south end of the bridge. The profile was aligned with the foundation array passing several rows of foundations that are oriented parallel to the road and perpendicular to the river. Figure 3.6 shows photographs of the survey profile and fieldwork. The water body was located approximately at the center of the survey profile. In the water section, underwater electrodes were planted into the riverbed sediments. The underwater electrodes were connected to the multi-core cable using crocodile clips to attach electrical wires to the takeouts. Regular electrode stakes planted on the land surface were connected to the cable takeouts by spring assemblies.

The 2D ERI data acquisition was conducted on November 30, 2009 when the ground was wet due to rainfall the previous night. The time to set up the electrodes and cables took about 1 h. Moving and reinstalling the apparatus for a roll-along measurement took about 20 min. The data measurement time took about 1.5 h for the first deployment plus about 45 min for the roll-along. A total of 6 roll-alongs were carried out. Since we worked partly in a water area, the third roll-along was more time consuming. The elevation was measured at every electrode location using a total station. The resistivity of the water was later measured with a portable meter. Terrain elevation mapping was later undertaken in order to establish a detailed topographic map of the survey area.

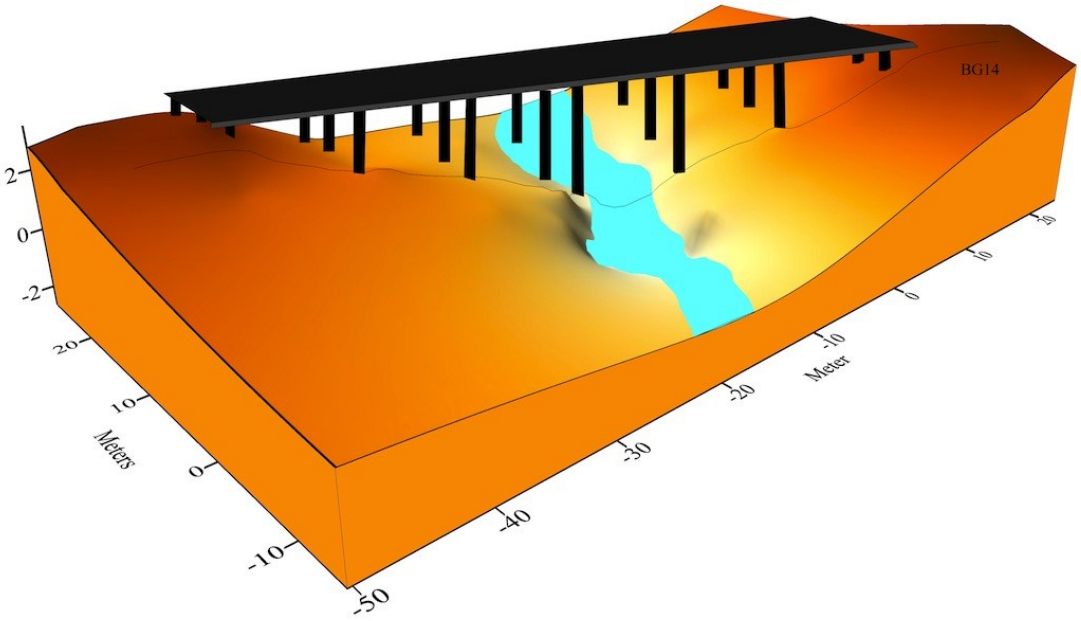

Figure 3.5 A 3D schematic view plan of the Bridge 14 with resistivity survey profile and locations of foundations.

Bridge 15 Site

Description of Study Area

Bridge 15 is located on FM Road 50 in Burleson County. The bridge is under control of the Bryan TxDOT District and located about 34 km southwest of College Station (Figure 3.3). This is another known foundation bridge with the same concrete pile foundations as found at Bridge 14. The bridge was constructed over Koontz Bayou creek in the North-South direction. The creek flows eastward to the Brazos River. The surface of the survey area is rather flat lying and gently slopes toward the creek. The survey profiles were within the flooding area but the water level was low during the fieldwork operation. The site is sparsely covered in concrete cobbles. According to information in the bridge layout, the soil geology consists of a layer of red and grey clay about 16.7 m from the surface. A layer of gravel exists from 16.7 to 19.2 m.

a) b)

Figure 3.6 (a) View of profile BG14 at bridge 14 carried out in water-covered environment. (b) A profile placed coincidently with and row of concrete pile foundations.

Data Acquisition

The experimentation was conducted on a land environment along a row of concrete piles using 56 electrode stakes. Figure 3.7 shows the topography of the study area and location of the survey profiles. The first survey consisted of three parallel profiles with 0.61 m electrode spacing. The total length of each profile was 33.5 m. All three profiles were aligned parallel to the river flow. The first profile B15A was placed alongside the row of concrete piles. The following two profiles B15B and B15C were placed 0.5 and 1 m respectively from the foundations. The second survey consisted of two parallel profiles, BG15A and BG15B, placed at about the same locations as the first survey. They used 1 m electrode spacing with 1 m line spacing and the total profile length was 55 m. Figure 3.8 shows photographs of the fieldwork at Bridge 15.

The ERI data acquisitions were conducted over two days January 27 and 29, 2010. The ground was moist due to precipitation a few days before. The data measurement time was about 1.5 h per profile. Time to setup electrodes generally took 1 h. The terrain elevation was later measured to generate a topographic map of the survey area. The objective of this experiment was to reveal the dominant anomaly of a

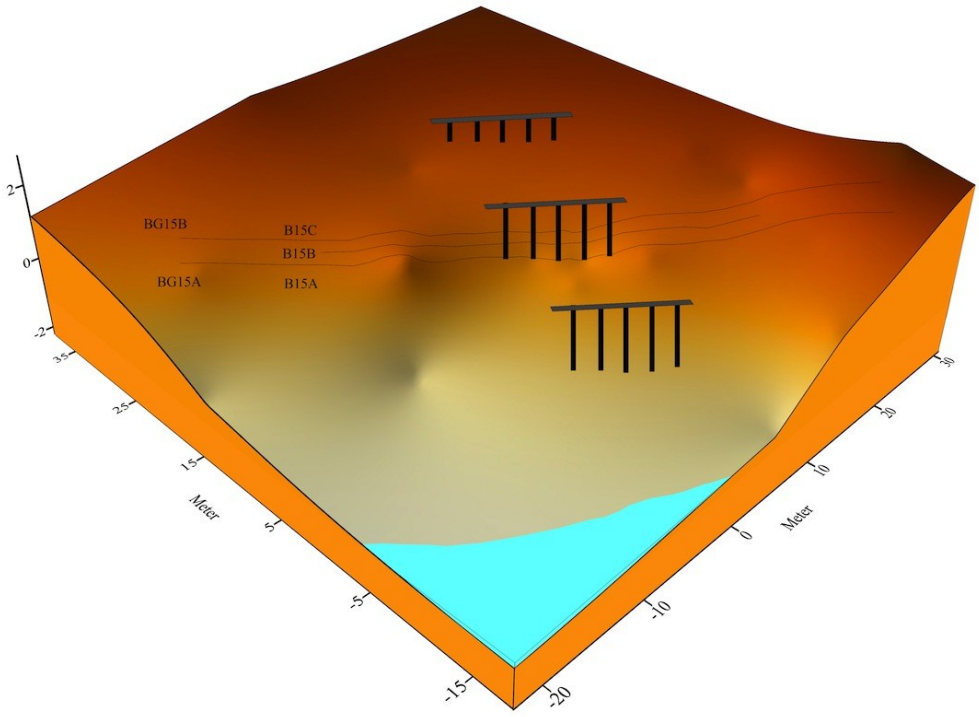

Figure 3.7 A 3D schematic view plan of the Bridge 15 with resistivity survey profiles and locations of foundations.

a)

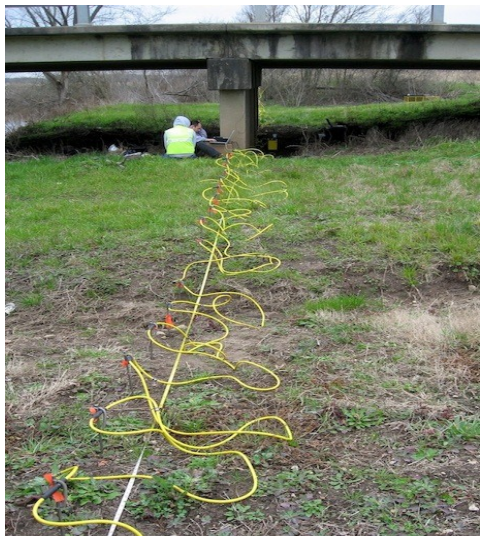

b)

Figure 3.8 View of data acquisition at bridge 15; profiles (a and b) were conducted parallel to the array of foundations and parallel to water flow.

foundation. The primary profile aligned alongside the row of foundations is expected to have more intensive resistivity values indicative of the foundation than secondary profiles that were located farther away from foundations. All profiles were expected to have about the same resistivity values of background. The approach is to subtract the measured resistivity values of the primary profile from those of the secondary profiles. The subtracted data should contain in intensive apparent resistivity values of foundations. There were then inverted using with the same inversion parameters. By this method the inversion may be able to image dominant foundation anomaly.

National Geotechnical Experimentation Site (NGES)

Description of Study Area

The National Geotechnical Experimentation Site **(**NGES) is located on Riverside Campus, Texas A&M University, located on Highway 21, about 16 km west of College Station. An outline map of the area is given in Figure 3.3. This test site has been used for research investigations in engineering over a period of 20 years. There are many large-scale civil and structural engineering projects that have been conducted at this site. The site includes a number of groups of buried, steel-reinforced concrete structures such as spread footings and drilled shafts with square and cylindrical cross-sections. Metal and rebar debris is scattered over the site. These items may cause undesired cultural noise in the electrical resistivity survey.

Groups of unknown and known concrete foundations in the NGES are used in the research as proxies for actual bridge foundations since their depths are well documented and the site is more accessible for testing geophysical methods than a river site. The activity of this study is divided into two main phases: known foundation and unknown foundation tests. The area around the NGES is mixed flat terrain with some undulations due to the excavation and earth shaping for civil engineering experiments. The soil at the site is predominantly sand. The stratigraphy consists of a layer of fine silty sand between the surface and 3.6 m depth, a layer of fine clean sand between 3.6 and 9.1 m depth, and a layer of silty, fine sand, and clay seams between 9.1 and 13.4 m depth. A lower clay

layer exists to a depth of at least 33 m (Ballouz et al., 1991). The known drilled shaft foundations were constructed in December 1991. The shafts included planned defects include neckings, bulbs, soft bottoms, mud cake, and cave-in. There are five drilled shafts with different lengths varying from 10.4 to 15.7 m and they are 0.8 to 1.1 m in diameter.

A group of spread footings and reaction shafts were built in December 1995. Spread footings were built to test stability of spread footings in sand. There are five spread footings and five reaction shafts but only a small footing remained intact that is suitable for resistivity experimentation. Other larger footings were unsuitable due to severe cracking. The suitable footing was a small-unreinforced 0.9 m by 0.9 m by 1.2 m solid concrete footing embedded 0.76 m in the ground. There are three PVC pipes containing rebars embedded into the footing. There exist other drilled shafts and spread footings that are new and intact. From visual inspection, they were built separately from the previous group. Their depths are not available so they are categorized as the unknown foundation group. Two drilled shafts have diameter of 0.91 m and 0.3 m respectively. The spread footing is 3x3 m wide.

3D Data Acquisition

Two main sets of experimentation have been completed in the NGES with different objectives. The first survey was a 3D experimentation conducted over a period of 9 days between 24-28 May 2010. Additional data were collected during 3-5 June 2010. I intended to develop full 3D interpretation based on a series of 2D acquisition profiles to explore the full capabilities of resistivity imaging for evaluating the depths of all concrete foundations. The general approach is to generate 3D resistivity image from a series of parallel acquisition profiles. My goal is to identify which combinations of data in the vicinity of a given foundation offer the most efficient imaging of its deep buried structure. This goal is achieved by constructing different 3D images with selected data subsets and comparing the resulting images.

Data were acquired as a series of continuous dipole-dipole configurations each of

56 electrodes. A total of 23 survey profiles were acquired. This includes 18 parallel primary profiles, labeled NGES1-18 oriented in the *x* direction approximately West-East. The remaining 6 six parallel profiles, labeled NGES19-23, are oriented perpendicular to the primary profiles. Each profile has 1 m electrode spacing and length 55 m. The spacing between the profiles is 2 m. Parallel NGES19-23 profiles were oriented North-South and spaced 5 m apart. Reciprocal measurements were made on all survey profiles. The survey was designed to probe all major clusters of footing and drilled shaft foundations that exist at the site.

The locations of the drilled shafts (circles), the footings (squares) and the resistivity profiles (lines) of the quasi-3D geophysical survey are shown in Figure 3.9. Some of the survey profiles crossed a concrete structure in which case electrodes were placed directly on the concrete and covered by wet clay to ensure good electrical coupling between the electrodes and the concrete. Terrain elevation mapping was undertaken using a total station. The horizontal location of the foundations at the NGES was also determined using the total station. The center of each circular pile foundation was mapped, as were the four corners of each of the square footings.

A true 3D experimentation was conducted over shallow Footing 5. A 3D dataset was collected with electrodes positioned in a rectangular grid. A single dataset, SF1-3D, was conducted on February 25, 2011. A mixed non-standard command file was created manually. The mixed arrays were dipole-dipole + Wenner + Schlumberger + equatorial dipole-dipole. The data collection was designed to measure in all possible directions along the rectangular lines (i.e. in the *x* and *y* directions) and at different angles to the lines. The objective was to test whether mixed arrays offer advantages compared to conventional arrays. The survey used 56 electrode stakes, arranged in a 14x4 rectangular grid with 0.5 m spacing between adjacent electrodes in the *x* direction and 1 m side unit electrode in the *y* direction. Figure 3.10 shows the 3D rectangular grid layout over Footing 5.

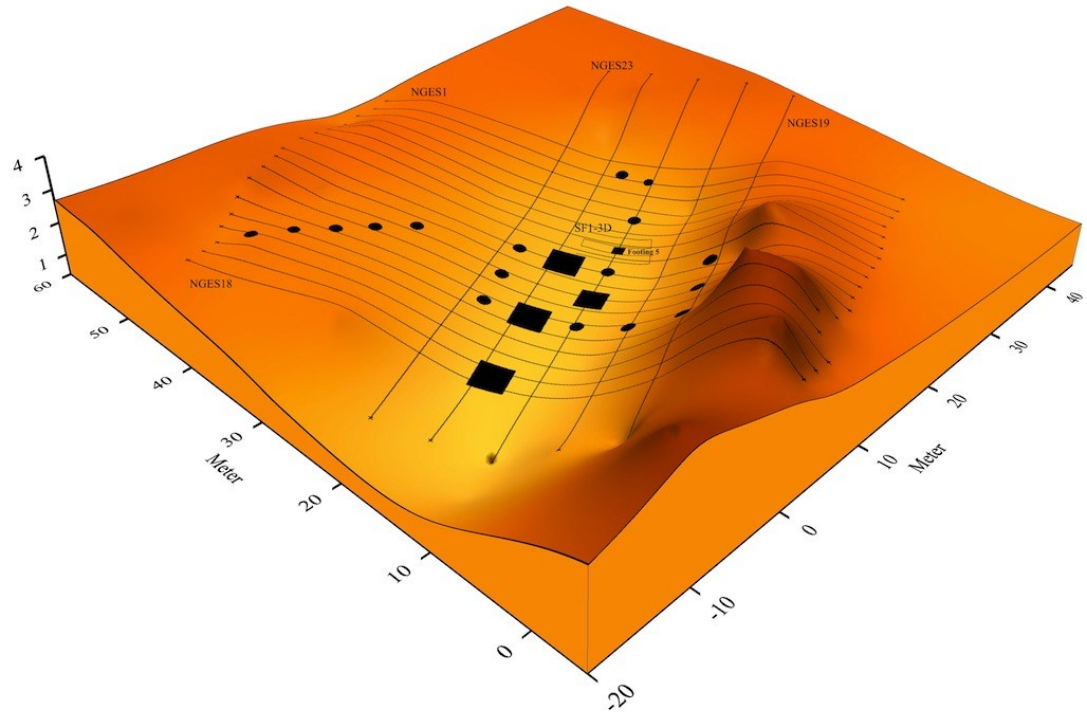

Figure 3.9 A 3D schematic view plan of the NGES site showing resistivity profiles and locations of foundations.

a) b)

Figure 3.10 (a) View of 3D layout in a rectangular grid of electrodes over Footing 5 and (b) a close up view of the Footing 5.

2D Data Acquisition

The second survey was a 2D experimentation conducted in the last week of December 2010 and continued through to the end of February 2011. The 2D ERI profiles were acquired with 28 or 56 electrodes. As measurements were being set up, the SuperSting was placed in the middle of the profile when 56 electrodes were used. If 28 electrodes were used, the SuperSting was connected to one end of the profile. The measurement time for a 28-electrode survey is half that of 56-electrode survey. In these surveys, separate data acquisitions were conducted at individual foundations. The data collections have been done by electrodes being deployed directly over foundations in the case for which a foundation is smaller than or equal to the electrode spacing. An experimentation was also conducted by deploying electrodes to image foundations from the side. This geometry is appropriate in cases for which the foundation is larger than the electrode spacing. Several survey profiles were aligned over spread footings in which some electrodes were placed directly on concrete and covered by wet clay. The inversion results do not provide a good image in these cases. Moreover, this method cannot be applicable to a footing foundation at an actual bridge site. For this reason, the side scanning electrical resistivity profile is preferred. Figure 3.11 shows the survey profiles for the 2D ERI data acquisitions.

At the known foundations, data collections were made for total of six profiles at three individual drilled shafts. The experimentation used 56 electrodes with 1 m electrode spacing. I acquired three, two, and one profiles at drilled shaft TS2, TS4, and RS5 respectively. At drilled shaft TS2, three profiles, TS2A, TS2B, and TS2C, were carried out parallel, shown in Figure 3.12; profile TS2A was conducted across drilled shaft, while profiles TS2B and TS2C were conducted to image the foundation from the side at respectively 0.5 and 1 m from the center of the drilled shaft. At drilled shaft TS4, two profiles, TS4A and TS4B were conducted; profile TS4A was carried out across the drilled shaft, while profile TS4B was conducted parallel to the first profile at 1 m line spacing. At drilled shaft RS5, a single profile RS5A was carried out across the drilled shaft, shown in Figure 3.13. At Footing 5, two profiles, SP1A and SP1B, were carried

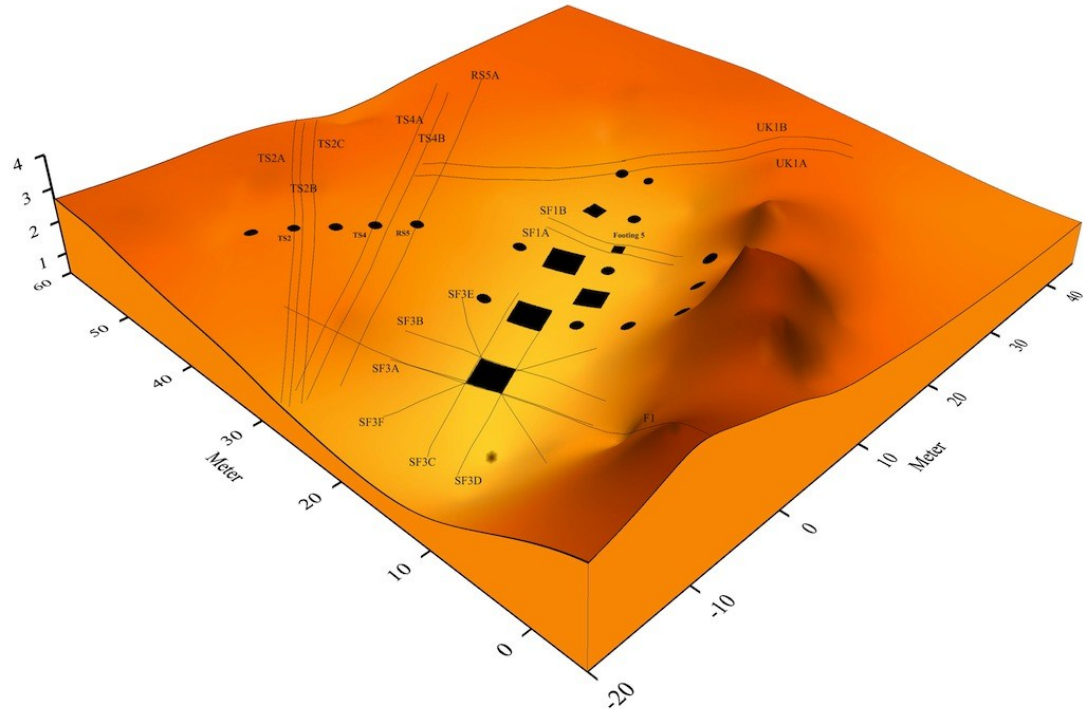

Figure 3.11 A 3D schematic view plan of the NGES site with locations of foundations and 2D resistivity data acquisition profiles at specific foundations.

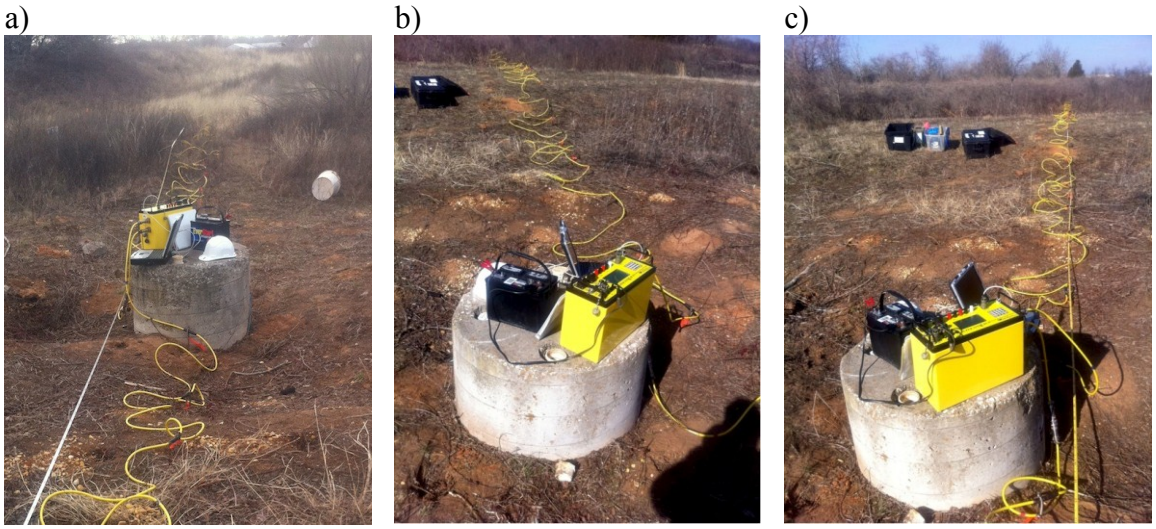

Figure 3.12 View of profiles TS2A (a), TS2B (b), and TS2C (c) carried out parallel over drilled shaft TS2.

out along the two sides of the 1x1 m spread footing, as shown in Figure 3.14. These surveys used 28 electrodes with 0.5 m electrode spacing. The footing is located between electrodes numbered 14 and 16 on each profile.

At the unknown foundation, the experimentation was conducted over a drilled shaft. Profile UK1A was run across the drilled shaft and profile UK1B was conducted on a parallel spread located 0.5 m away from profile UK1A as shown in Figure 3.15. Both profiles used 56 electrodes with 1 m electrode spacing. Another experimentation was conducted over the 3x3 m spread footing as shown in Figure 3.16. There were four profiles, SF3A, SF3B, SF3C, and SF3D, carried out along the four sides of the footing and two profiles, SF3E and SF3F, that were conducted obliquely with respect to the at corners of the footing. The experimentation used 28 electrodes and 1 m electrode spacing. The last 2D ERI experimentation at the NGES was conducted on the spread footing to confirm results of previous experimentation. Profile F1 was carried out along the side of the footing with 56 electrodes and 1 m electrode spacing. The center of the profiles was placed at the center of the foundation.

a) b) c)

Figure 3.13 View of profiles TS4A (a) and TS4B (b) carried out parallel to drilled shaft TS4 and profiles RS5A (c) carried out over drilled shaft RS5.

a) b)

Figure 3.14 Views over profiles SF1A (a) and SF1B (b) carried out along the two sides of Footing 5.

a) b)

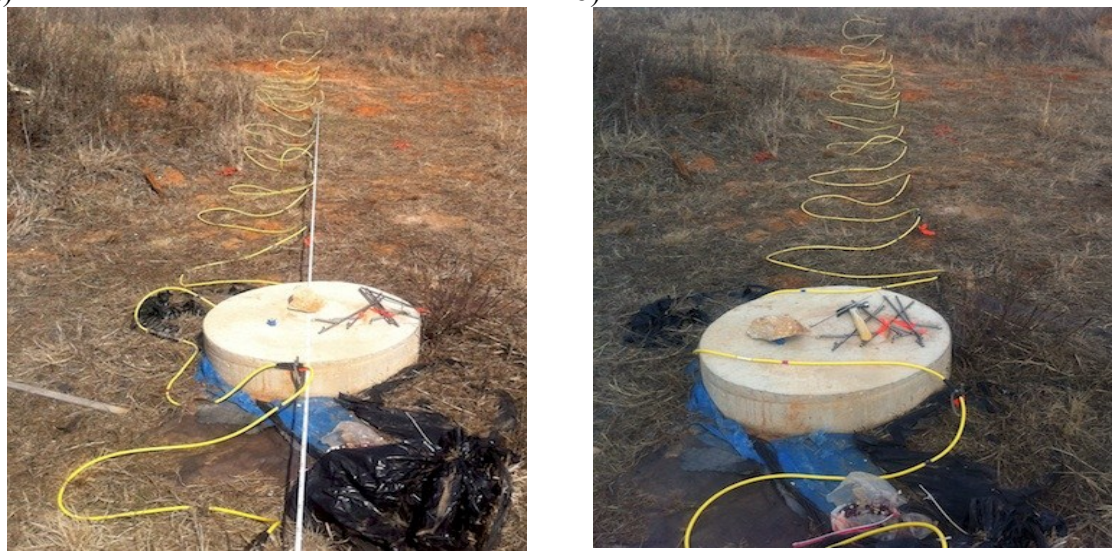

Figure 3.15 Views of profiles UK1A (a) and UK1B (b) carried out over an unknown foundation drilled shaft.

a) b)

Figure 3.16 Views over profiles SF3A (a) and SF3B (b) carried out along the side of 3x3 m spread footing.

Roadway Bridge Site

Description of Study Area

This bridge has unknown foundations and the resistivity profiles were acquired in a mixed terrain water environment. The bridge is located on Highway 21 in Brazos County, within the Bryan TxDOT District, approximately 21 km northwest of College Station. The bridge spans the Little Brazos River in the East-West direction (Figure 3.3). Two sets of foundations support the eastbound and westbound lanes individually. The resistivity profiles were acquired beneath the westbound lane. Actually, I intended to assign these two bridges into known foundation category. Unfortunately, the TxDOT layout of westbound bridge is not available. The layout of the eastbound bridge is available and is used as a good indicator for the westbound bridge information.

The topography around the bridge has high relief, as the terrain slopes toward the river. The west bank has a steeper slope than the east bank. The study area is covered with heavy bush vegetation along both sides of river so alignment of the electrodes was difficult. The river is approximately 25 m wide and flows from north to south. The

maximum depth of water in the river during the survey was 1.4 m during the time of the survey. The bridge site is easily accessible during the non-flood season. The site is underlain by brown and grey shale exposed in outcrops on the riverbed and along the bank. According to TxDOT layout of the eastbound bridge, a layer of brown shale extends from the riverbed to 3.1 m depth. Shale and siltstone exists between 3.1 to 12.2 m depth.

The foundations are drilled shafts of 0.91 m in diameter and 22.55 m total length according to the eastbound bridge layout. The section of the foundation embedded in the ground is only 10.36 m in the water-covered area. There are embedded a total of six foundations in the water-covered area, three foundations on each bent (or beam). The 2D ERI surveys were carried out at the foundations of the westbound bridge. The foundation condition was visually inspected. It was found that parts of foundation are eroded and corroding rebars are exposed and in contact with water. Broken concrete boulders and rebars from a previous demolished bridge are sparsely scattered across the bridge site in the water and on the bank. This rubble is the main obstacle to electrode installation and causes accessibility limitations in the field. The discarded rebars are considered to be a significant noise source.

Data Acquisition

Two survey profiles were acquired at this site. The surveys were completed using 56 electrode stakes and 1 m electrode spacing. The 3D topography of the study area and survey profiles is shown in Figure 3.17. The total length of profiles is 55 m, which is adequate to image the foundation depth. The survey profiles were designed to collect resistivity data at just one of the drilled shaft foundations, located near the middle of the profile.

The BHW21A profile was conducted on April 7, 2011 over a foundation in the North riverbank. The profile was deployed directly across the foundation and is oriented N-S and parallel to the water flow. The profile started on flat, wet ground surface and continued parallel the river, ending up on the riverbank. The BHW21B profile was

carried out on April 26, 2011 over a foundation near the South bank. The profile was deployed directly across the foundation and trended NE-SW, oblique to the river flow. The path was cleared of vegetation for ease in using the measure tape and deploying electrodes. The water body was located approximately at the center of the survey profiles. Figure 3.18 shows data acquisition in the mixed water terrain environment at Little Brazos River site.

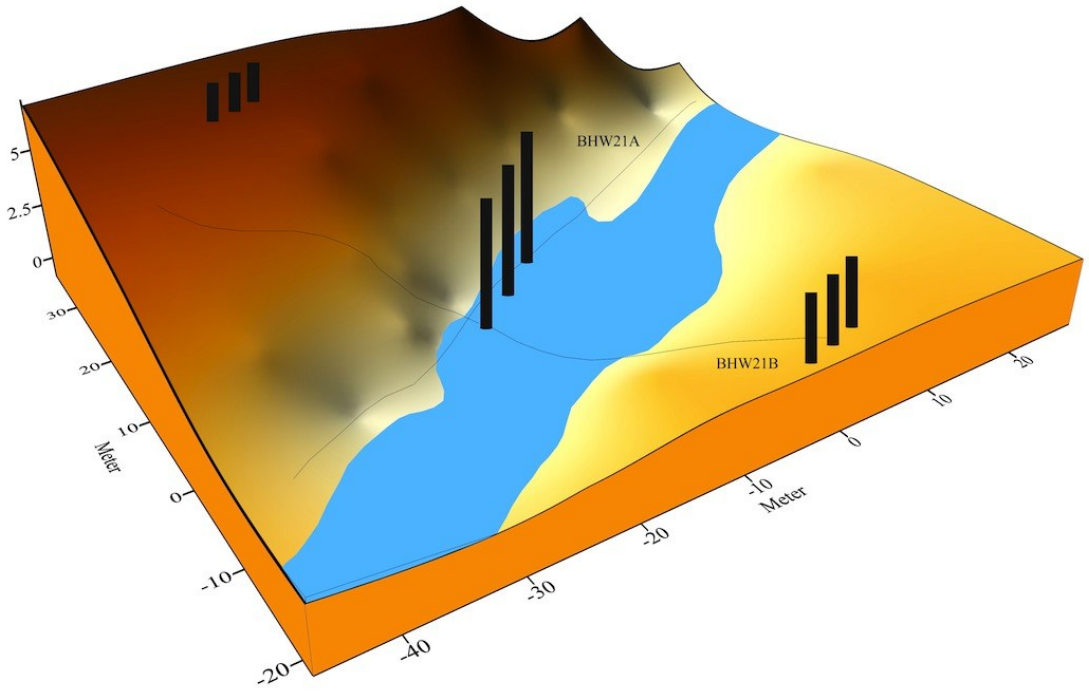

Figure 3.17 A 3D schematic view plan of the bridge on Highway 21 site with resistivity survey profiles and locations of foundations.

At the places where the survey line crosses the river, underwater electrodes were planted on the riverbed sediments (i.e. weathered shale). The deployment leaves part of the waterproof PVC in the water and part above the water surface. Regular stainless steel electrode stakes were planted on the land surface. The SuperSting system and battery were connected in the middle of the profile near the foundation and placed in waterproof

a) b)

Figure 3.18 View of data acquisition in water-covered environment at bridge over Little Brazos River; (a) profile BHW21A electrodes were aligned parallel the river and (b) profile BHW21B electrodes were aligned oblique to the river.

plastic boxes. The vertical and horizontal electrode coordinates were measured using the total station. The resistivity of the water was measured with a portable meter. Detailed terrain elevation was later measured to construct a topographic map of the survey area. The depth of the water column at the locations of the underwater electrodes were measured for inclusion in the inversion process.

The data acquisitions were undertaken in summer, the weather on both days was sunny and the ground was dry. Water was poured over the base of some electrode stakes in order to improve the electrical contact between the dry soil and the electrodes. Since we worked for a large part in a water-covered area, it took much effort and time for electrode installation. The electrode and cable set up time generally took about 3.5 h and the time for data measurement took about 1.5 h per profile. Reciprocal measurements were recorded on both profiles.

Railway Bridge Site

Description of Study Area

This is the second actual bridge site containing unknown foundations and experimentation was conducted on a land environment. The railway bridge is located

adjacent to Highway 21 in the Bryan TxDOT District. This bridge spans the Brazos River in NE-SW direction between Brazos County and Burleson County, Texas. The bridge is located approximately 24 km, northwest of College Station (Figure 3.3). The foundation cross-section is of hexagonal shape with 8, 3, and 3 m side lengths. The topography around the site is undulated excepted along the river. The riverbank is rugged and slopes toward the river. Vegetation is moderately heavy on the riverbank. The ground surface is covered by light bush and grass. The river flows from west to east in the study area. The site is underlain by weathered grey and brown shale rock exposed as outcrops along the riverbank. Reddish brown sandstone is exposed on the steep slope in the formed of scattered boulders near the foundation. Incidentally a large number of shell fossils were found in the bedrock.

Data Acquisition

Two profiles were acquired at this site on July 6, 2011. Figure 3.19 illustrates the topography of the study area and approximate location of the survey profiles. The weather was sunny and the ground surface was very dry. The 2D ERI was conducted with 28 electrode stakes and 2 m electrode spacing. The total length of the survey profile is 54 m. It was difficult to deploy the electrodes in a straight line due to the hard bedrock, so the electrode stakes were offset in some locations. The survey profiles were about 0.5 m away from the foundation and the profile is about centered at the foundation.

The E-W profile RWB1 is located parallel to river on the slope of the riverbank and deployed on rugged terrain of weathered shale. The profile RWB2 is located perpendicular to the river and continues the slope. The path was cleared of heavy vegetation. The two profiles intersected near their center points. Due to the dry ground surface, water was poured at base of electrodes. Reciprocal measurements were carried out on both profiles. The elevation was measured of at every electrode location of both profiles and terrain elevation mapping was undertaken to make a detailed topographic map of the survey area. Figure 3.20 shows photographs of data acquisition at the railway

bridge site.

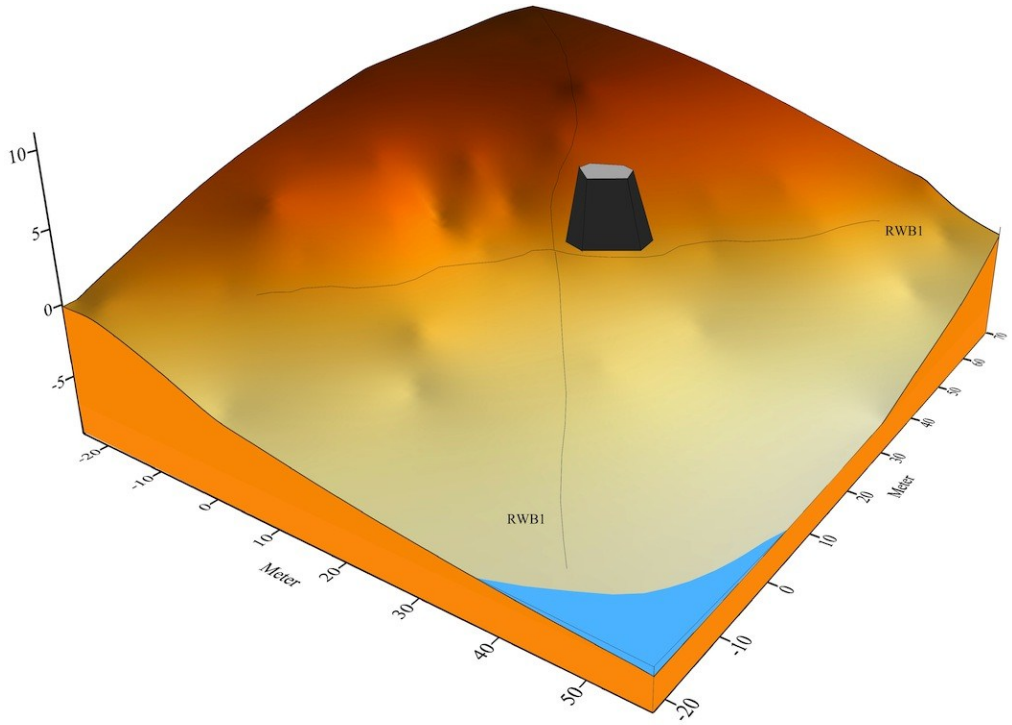

Figure 3.19 A 3D schematic view plan of the railway bridge site over Brazos River with resistivity survey profiles and locations of foundations.

DATA ANALYSES

Apparent resistivity data are displayed as a type of contour map termed a pseudo-section. The layout of the plot varies depending on the electrode configuration used (AGI, 2009; Loke, 2000). A pseudo-section is not a true cross-section of subsurface resistivity. The pseudo-sections must be converted into a true resistivity section by the process of data inversion. The true resistivities are then used to interpret subsurface features. Several steps have to be done in the 2D analysis stage such as data preparation, data quality checks, and inverse simulation. The ERI data from all surveys were inverted using the RES2DINV and RES3DINV programs. Data measurements in this research

were conducted using the SuperSting system. However, the SuperSting system is not integrated with the RES2DINV and RES3DINV inversion programs, so that the measured data are required to be converted into an appropriate format before the analyses proceeds. The measured data stored in the SuperSting were saved in binary form. They consist of induced current, potential difference, and apparent resistivity data. A data conversion module was used to filter and convert the SuperSting data for use with RES2DINV.

a) b)

Figure 3.20 View of data acquisition at railway bridge over Brazos River; (a) profile RWB1 electrode were aligned parallel the river and (b) view of foundation and the intersected point of two profiles near the foundation (inset).

Once data were input to RES2DINV, the first task is to conduct quality control on the measured apparent resistivity data, displayed as a pseudo-section plot and a profile plot. In profile plots, data quality control is performed by checking for bad data points. Bad data points stand out as outliers with unusually low or high resistivity values compared to the neighboring data points. They were manually identified and eliminated before the inversion process. Note that bad data has several causes such as low battery,

poor contact of an electrode to the ground due to dry soil, bad connection of the cable to an electrode, shorting across electrodes due to very wet ground conditions etc. Almost all the 2D data were good quality, only a few bad data points were removed except datasets for 3D inversion that were carried out across concrete slabs. Figure 3.21 shows an example of a profile plot with a few bad points. The noise estimate was also measured by reciprocal measurements. The reciprocal errors were found to be always < 10 % for the survey. Measurements with reciprocal errors > 5 % were removed.

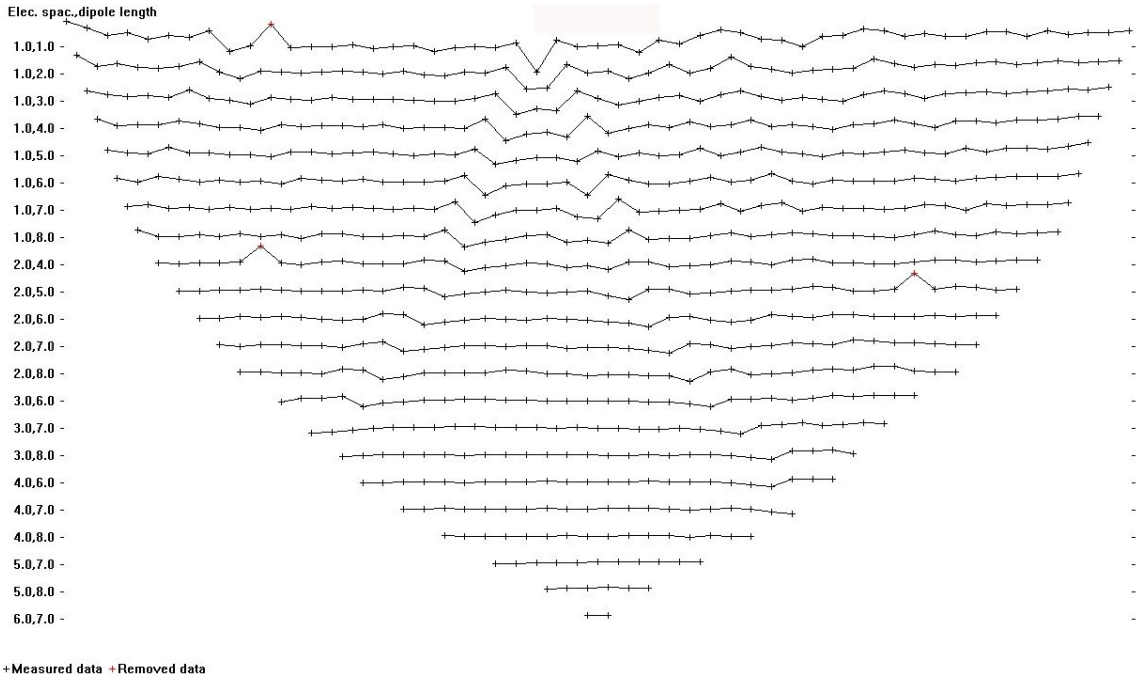

Figure 3.21 Example of a data set with a few bad data points, profile BHW21B.

RES2DINV provides a set of default parameters that are designed to give reasonable results for the inversion process. However, the inversion process was adjusted to optimize the result by changing some of the default parameters. An important setting of ERI data inversion is the width of a model cell in the finite element algorithm. The default value is equal to the unit electrode spacing. By narrowing the model cell

width to 4 nodes between unit electrode spacing, the calculated apparent resistivity values may become more accurate. However, as the quality and accurate increase, so does the number of nodes and thus the run time. By default, equal weighting of the damping factor is used for the vertical flatness filter and the horizontal flatness filter. However, bridge foundation anomalies have predominantly vertical elongation, so that the vertical flatness filter is given a greater weight than the horizontal filter. Note that the ratio of the damping factor for the vertical flatness filter to the horizontal flatness filter produces models that are elongated either vertically or horizontally. Using trial and error, the initial and minimum damping factors were set to 0.15 and 0.01 respectively.

A regular flat mesh was generated in cases where surveys were conducted over flat ground surface. Along survey profiles over areas with significant topographic relief, the horizontal distance and elevation from total station survey were incorporated into the forward mesh. Note that it is not necessary to acquire the elevation of every electrode but the elevation of the first and last electrodes is required. This was done at Bridge 14, the roadway bridge on Highway 21, and the railway bridge. At Bridge 14 and the roadway bridge on Highway 21, surveys were conducted with some of the electrodes above the water surface and some of the electrodes under the water surface. The water layer was manually input into the model. Resistivity values and boundaries of the water layer were included in the model.

The blocky least square inversion optimization method was used to produce the resistivity images. This inversion method is suitable since bridge foundations have sharp boundaries with the surrounding geological medium. The blocky inversion method emphasizes the resistivity contrast between the bridge foundation and its surroundings. When the blocky inversion method is used, it gives greater weight to the sides and bottom cells of the inversion model compared to the interior cells. This effect can be reduced by reducing the effect of side blocks. For consistency, all 2D datasets were inverted using the same inversion parameters. The initial parameters used for all inversions are shown in Appendix B.

The next step was to carry out the inversion. The RMS error was reduced from

iteration to iteration. The RMS error terminated when the error reduction was less than 0.5 % between two consecutive iterations. The number of iterations was limited to seven in order to avoid over-fitting. Further iterations result in only a small decrease in RMS, and this may be the result of the software over-refining the model to fit small data variations caused by noise rather than imaging required features of the subsurface. However, if the RMS error did not converge to below 5 %, the data are regarded as noisy. In all cases, the inversion result is displayed as a model section. At this step, topography is incorporated as required into the model section. Since variable terrain has a potentially large effect on voltage measurements, the capability to incorporate topography into the software leads to more accurate and reliable imaging of the subsurface resistivity. Ultimately this leads to better foundation depth estimates. The vertical exaggeration factor and horizontal plotting scale are adjustable. By default, RES2DINV uses logarithmic contour intervals for the pseudo-sections and model sections. Since the range of resistivity values is different from profile to profile and site to site, universal contour intervals are necessary to provide uniform contouring, prevent misinterpretation, and maintain data integrity for all measurements at the same site.

Figure 3.22 illustrates an example of the RES2DINV inversion result for profile TS2A. The top and middle cross sections are the contour plots from the measured and calculated apparent resistivity data pseudo-section, respectively. The bottom cross-section is the imaged resistivity model. The RMS error is an indicator of the difference between the calculated and measured apparent resistivity values. The resistivity model obtained at the first several iterations has a larger RMS error. The last iteration usually has the lowest RMS error. If there is a good fit, the measured apparent resistivities will match the calculated apparent resistivity pseudo-section to a low RMS. The color bar indicates the range of electrical resistivity values in unit of ohm-meters (Ωm). The color scale is logarithmic and consistent with contour intervals. Cool colors (i.e. blue) represent areas of low resistivity values. Warm colors (i.e. red) represent areas of high resistivity values.

The next step is to display a histogram of the RMS error statistics. The histogram

shows the distribution of the percentage difference between the logarithms of the measured and calculated apparent resistivity values. Relatively large percent of error > 100 % was identified as bad data. The bad data were removed and the inversion performed again. The same inversion process normally results in a smaller RMS error. In this research, an apparent resistivity error exceeding 40 % is considered as a bad data point and removed from the data set. The removal of bad data points was found to reduce effectively the RMS error. Many of data sets did not require removal of bad data provided the RMS error became less than 5 % after five iterations.

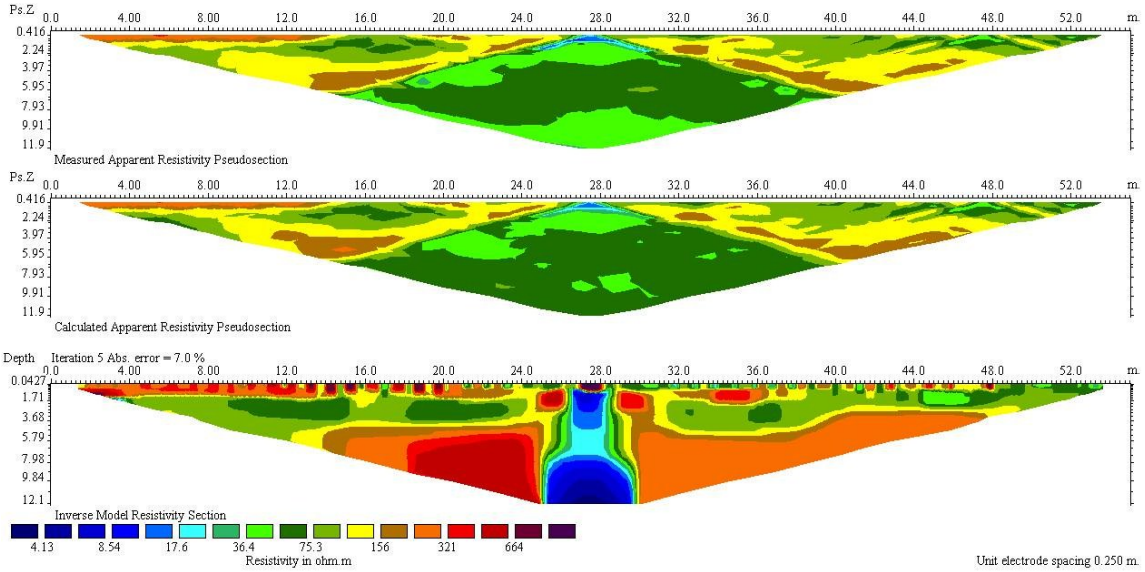

Figure 3.22 Electrical resistivity section of profile TS2A: (a) measured apparent resistivity pseudo-section, (b) calculated apparent resistivity pseudo-section, (c) and inverted resistivity model after the five iteration (RMS error: 7.0).

Initially, 3D inversions were interpreted with the advanced 3D resistivity imaging software BERT (Boundless Electrical Resistivity Tomography) developed at the Institute for Applied Geosciences in Hanover, Germany. The BERT is based on the inversion method described in Günther et al (2006) and is available under the Linux operating system. However, it was soon found that the BERT software needs a fast

computer with powerful CPU processing and capability large amounts of RAM memory. This program does not have a user-friendly interface. I decided that this program is not suitable for foundation investigation for practical engineering use since the inversion procedures are rather complicated. Moreover the computer run time is long. Super computers are necessary to handle larger datasets. For this reason the commercial RES3DINV program was substituted. Figure 3.23 shows a 3D inversion result as determined by BERT.

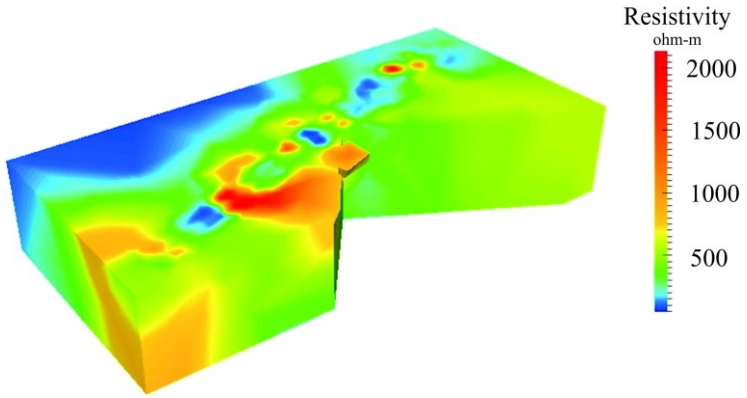

Figure 3.23 3D inversion model of profiles NGES 15-18 using BERT inversion software and visualizing by ParaView.

The eighteen 2D data profiles from the NGES were collected into a 3D resistivity dataset. Data quality control was done in the 2D analysis stage before combining the 3D dataset. The 2D data with topographic elevation were initially inverted individually using RES2DINV. Most of survey profiles subjected to the inversion process converged with a data misfit error of less than 6 % after six iterations except the survey profiles aligned across the concrete slab. Those survey profiles were unusually noisy, so bad data points were removed from the data set at the post-inversion stage. The inversion was then repeated until the RMS error fell below 10 %. The number of iterations was limited to seven in order to prevent over-fitting. The inversion process converged with the data misfit errors shown in Table 3.1. The 2D inversion images for all twenty-three profiles

are illustrated in Appendix C.

Table 3.1 Data misfit error (%) for eighteen data sets after five iterations of the inversion process.

Profile Number	**1**	**2**	**3**	**4**	**5**	**6**	**7**	**8**	**9**
Misfit Error (%)	3.4	2.8	3.6	3.9	4.5	3.7	3.7	4.2	11.6*
Profile Number	**10**	**11**	**12**	**13**	**14**	**15**	**16**	**17**	**18**
Misfit Error (%)	6.1*	8.6*	7.3*	12.4*	5.9*	4.86	5.1	5.7*	10.4*

* There are some of electrodes put on concrete slab.

The edited 2D data files with bad data points removed were collected and the coordinates (i.e. x and y locations) of each survey profile were noted. Next, the 2D datasets were combined using a module in RES2DINV. When 2D profiles were combined into a single 3D data set in the appropriate format, the 3D dataset is properly called "quasi-3D". Once the 3D data file was obtained, the next step is to carry out 3D inversion by RES3DINV. The same inversion parameters were used as for the 2D inversion models but a higher initial damping factor λ was required in order to minimize the model roughness. Once the inversion was completed, the 3D result is visualized as 2D horizontal slices and vertical slices with topography. At this step, the error distribution bar chart is displayed and the removal of bad data points from dataset is again carried out, as noted in the 2D inversion. The RES3DINV was then run again. Computer run time of the 3D inversion is about 2.5 h.

CHAPTER IV

RESULTS AND DATA INTERPRETATION

In this chapter, the 2D and 3D inversion results are presented and discussed. For known foundations, the interpretation of each profile is verified for accuracy using the layout provided by TxDOT. For unknown foundations, data acquisition with profiles arranged in different orientations is shown to increase reliability.

Generally, a limitation of the resistivity method is that interpretation rapidly becomes more challenging with increasingly complex subsurface features. The advantages of the electrical resistivity method however are the well-understood theory and the well-established field procedures. The ERI method for foundation determination has the advantage that the known foundation position is known a priori, and most sites have no complex resistivity structures. Since the position of the foundation is observed on the survey profile, interpretation is usually done by qualitative comparison of the observed surface position with the anomalies found on the inversion image. The interpreted depth of the foundation is also inferred by an examination of the inversion result. Good inversion results depend on a number of factors such as data quality, data coverage, and robustness of the inversion algorithm.

The ERI method to image slender bridge foundations is challenging. Bridge foundations have different characteristics compared to vertical geological structures such as dykes. Moreover it is well known that interpretation of all potential field geophysical data (including resistivity data) is non-unique or ambiguous. More than one model can produce the same response but there is no way to verify which ones if any are correct. The interpretation of the result is based somewhat on the expected subsurface geology. Verification of an inversion result then must include comparison with auxiliary data such as drill core, geophysical logs, or results of other types of geophysical surveys.

The bulk resistivity of a reinforced concrete foundation may be higher or lower than its surrounding geological materials, depending to some extent on its physical condition. For example, a zone of low resistivity in an ERI image could be caused by the

presence of a conductive rebar cage embedded in deteriorating concrete. On the other hand, a zone of high resistivity could be caused by an intact foundation with no cracks or exposed rebar. Careful interpretation of resistivity imaging results is necessary to estimate the physical condition of the buried part of a foundation.

RESULTS AND INTERPRETATION OF FORWARD MODELING

3D synthetic models were generated using various depths and sizes for the foundations. Resistivity values of foundation were selected to be lower and higher than surrounding materials. The 3D synthetic models are shown in Appendix D.

Figure 4.1 shows inversion images of a 1x1x9 m, deep foundation. The resistivity of the foundation of in upper image was random and set to be 50 Ωm intercalated with 0.01 Ωm zones. Since the resistivity of the foundation was set into a homogeneous 50 Ωm background, the inversion was not able to image the entire body of the foundation. The inversion image shows only a clear zone of low resistivity anomaly to a few meters beneath the surface. Various smaller resistivity values were trially intercalated. In the upper image, the inversion image shows a low-resistivity anomaly of the foundation in the middle of the profile with a consistent low-resistivity zone, 50 Ωm, in the synthetic model. The shape is greater than in the synthetic model. The inversion image is characterized by the occurrence of artifacts particularly at the side. The bottom boundary of the foundation cannot be detected. The low resistivity zone is gradually enlarged as depth increases. The resistivity of the lower image was first modeled randomly from a homogeneous model as low as 200 to 10,000 Ωm and an intercalated model with lower or higher resistivity values. The inversion results are not still able to image the shape of foundation. In the lower image, an example result of inversion illustrates a zone of high resistivity close to the surface. The resistivity of background is consistent with the synthetic model.

Figure 4.2 shows the inversion images for a 3x3x5 m shallow foundation. the resistivity of the foundation in the upper and lower images was set to be 50 and 200 Ωm, respectively. The simulated noise and resistivities produce significant variation of

artifacts especially near the surface. This is caused by reducing the widths of the unit spacing to half in the inversion process. It produces significant resistivity anomalies, which tend to be slightly smeared out along the boundary. The foundation is identified at different spatial resolutions. In upper image, the zone of low resistivity is located correctly. However, the resolution is relatively degraded around the edges. Resistivity anomalies of the foundation and background are close to the model resistivity values. The depth of the low resistivity zone is approximately 5 m. In the lower image, the image shows a degraded shape of the foundation located in the middle. The magnitude of resistivity is lower than that of the synthetic model. The bottom boundary is about 5 m deep.

Figure 4.3 shows resistivity inversion images of a 5x3x5 m shallow footing. Resistivity values of the foundation were set as in previous 3x3x5 model. The inverted resistivity images are quite clear. The low and high resistivity zones of anomaly are similar as in the previous image. Obviously, there are artificial oscillations of high resistivity above the foundation anomaly. The depth of anomalous zone is about 5 m. Resistivity values of the foundation and background are consistent with the synthetic model. Anomaly zone of low resistivity shows lower boundary at about 4 m. this is shallower than in the synthetic model. In the lower image, the inversion model resembles the synthetic model. The bottom and sides of the high-resistivity zone are well defined. The shape of the high-resistivity feature is rather well imaged as a shallow footing. The depth of the high resistivity zone is 5 m. A side effect is visible as a low-resistivity zone (lower than 90 Ωm) beneath the foundation anomaly. These effects are more pronounced at greater depths in the sections. The smaller and longer foundation produces more artifacts than a bigger and shorter foundation.

The synthetic model and inversion results above indicate that the 2D ERI method is a reasonable approach for practical application to bridge foundation determination. Applying an appropriate electrode configuration with an appropriate foundation geometry is able to detect the presence of the bridge foundation although it is unable to resolve its precise shape and depth. Increasing the size of the foundation seems to

a)

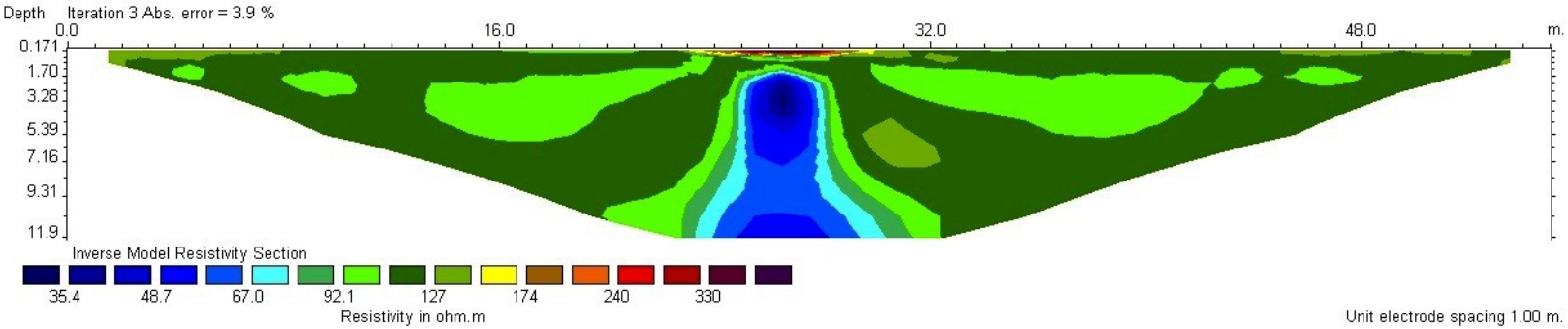

b)

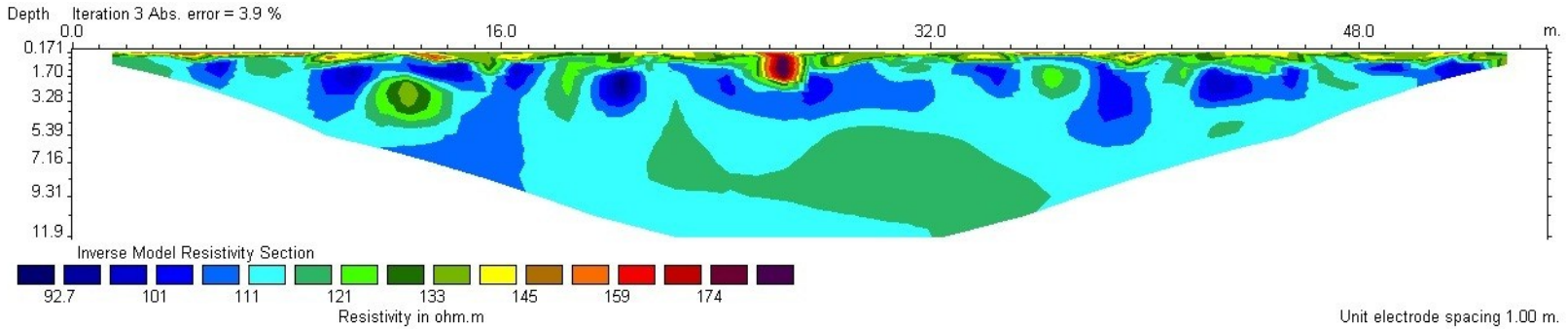

Figure 4.1 The inversion image of the profile extracted from the 3D synthetic model of 1x1x9 m, deep foundation, (a) the resistivity of foundation is lesser than the geological background, (b) the resistivity of foundation is greater than the geological background.

a)

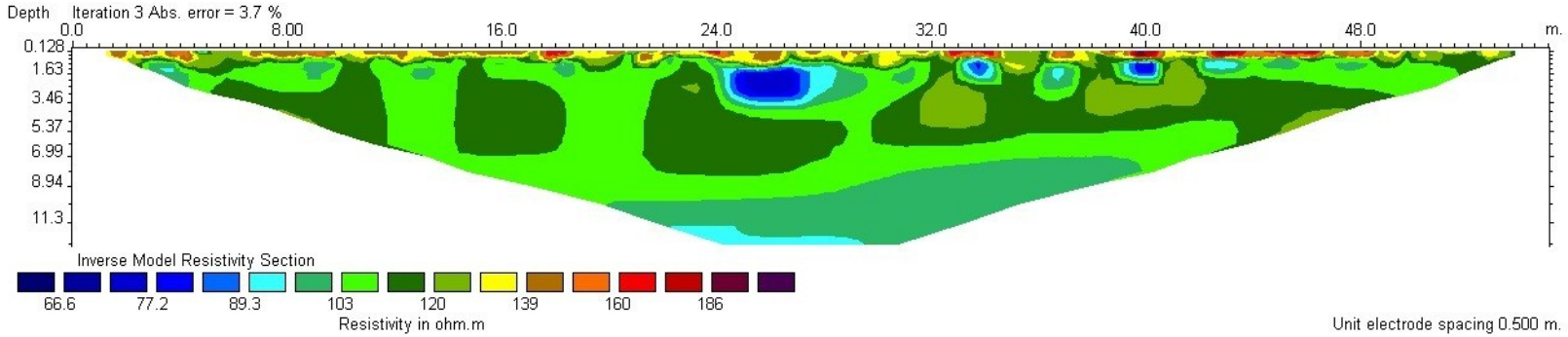

b)

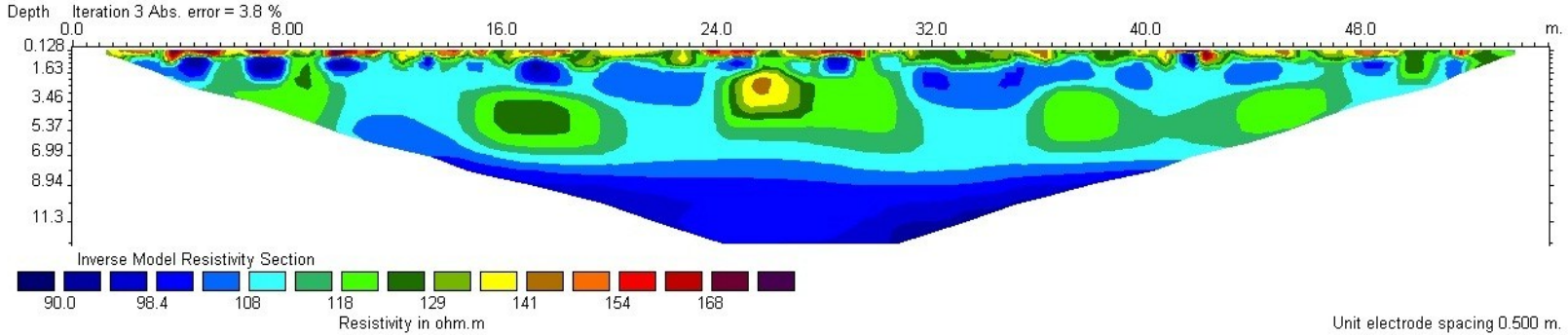

Figure 4.2 The inversion image of the profile extracted from the 3D synthetic model of 3x3x5 m, shallow foundation, (a) the resistivity of foundation is lesser than the geological background, (b) the resistivity of foundation is greater than the geological background.

a)

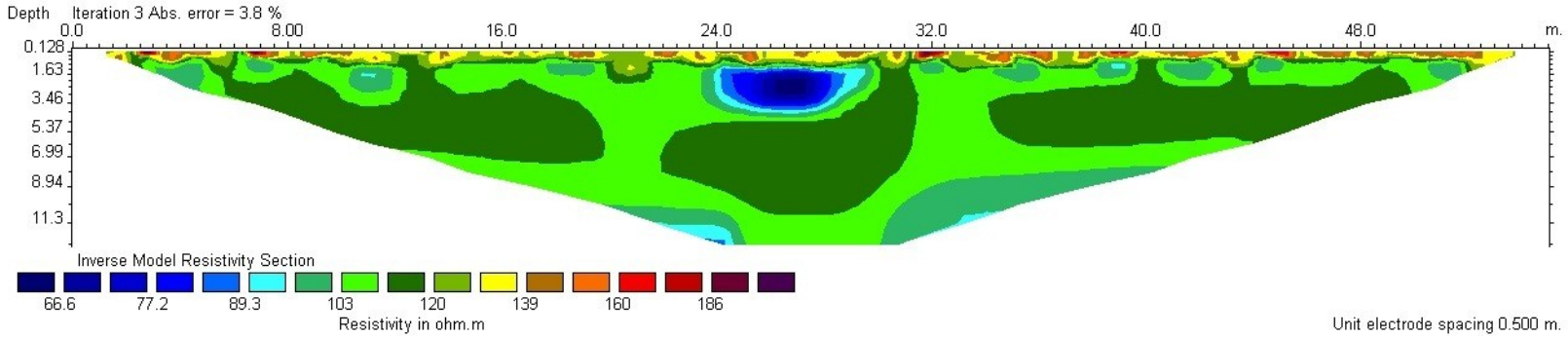

b)

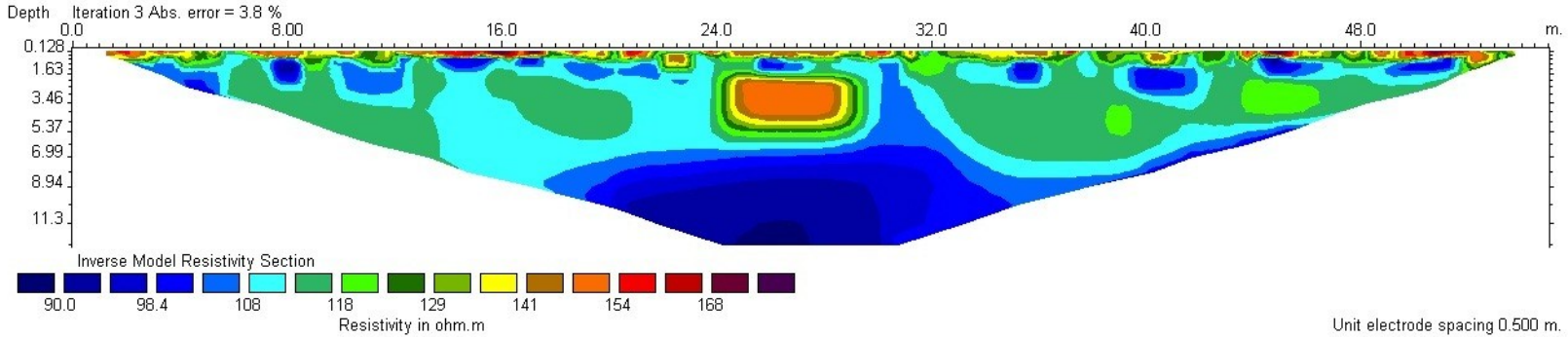

Figure 4.3 The inversion image of the profile extracted from the 3D synthetic model of 5x3x5 m, shallow foundation, (a) the resistivity of foundation is lesser than the geological background, (b) the resistivity of foundation is greater than the geological background.

provide better images of the shape and depth. The appropriate electrode spacing and configuration can optimize the resolution of subsurface resistivity distribution. However, it is not possible to accurately image small and deep foundations that have higher resistivity values than surrounding materials. In real data acquisition, noise can vary significantly depending on several factors as mentioned previously in Chapter III. Several important factors should be considered to gain spatial resolution and reduce noise effects. Although the actual depth of the foundation cannot be detected precisely, this is not a big impediment to estimate scour because severe critical scour is usually near the surface. The important point is the determination of a foundation to be deeper or shallower than the depth of critical scour (i.e. 5 m).

RESULTS AND INTERPRETATION OF BRIDGE 14 SITE

The experimentation was carried out in the mixed terrain underwater environment at Bridge 14 over the Old River in Burleson County, Texas. In this experiment, electrode stakes were inserted into the ground surface as well as placed underwater into the riverbed at locations where the survey profile crossed the river. The electrode stakes were placed coincidently with a row of the concrete pile foundations. The roll-along technique was used to span the entire length of the survey profile. It was expected that a very small inter-electrode spacing is required to reliable image, the individual piles. However, with the loss of resolution with depth, the piles could quickly become undetectable. An appropriate electrode spacing was initially used to yield sufficient resolution, as high data density must be used to detect small anomalies in resistivity images.

Figure 4.4 shows the inversion result from profile BG14 at Bridge 14. The inversion process converged with a RMS misfit of 6.0 after six iterations. The underwater segment of the profile is marked by the blue zone above the ground surface. Small tick marks on the ground surface are half the electrode spacing. Since the electrode spacing is 0.5 m, the maximum depth of inversion is about 6 m. The survey profile intersected eight concrete pile foundations. Several possible foundation bodies

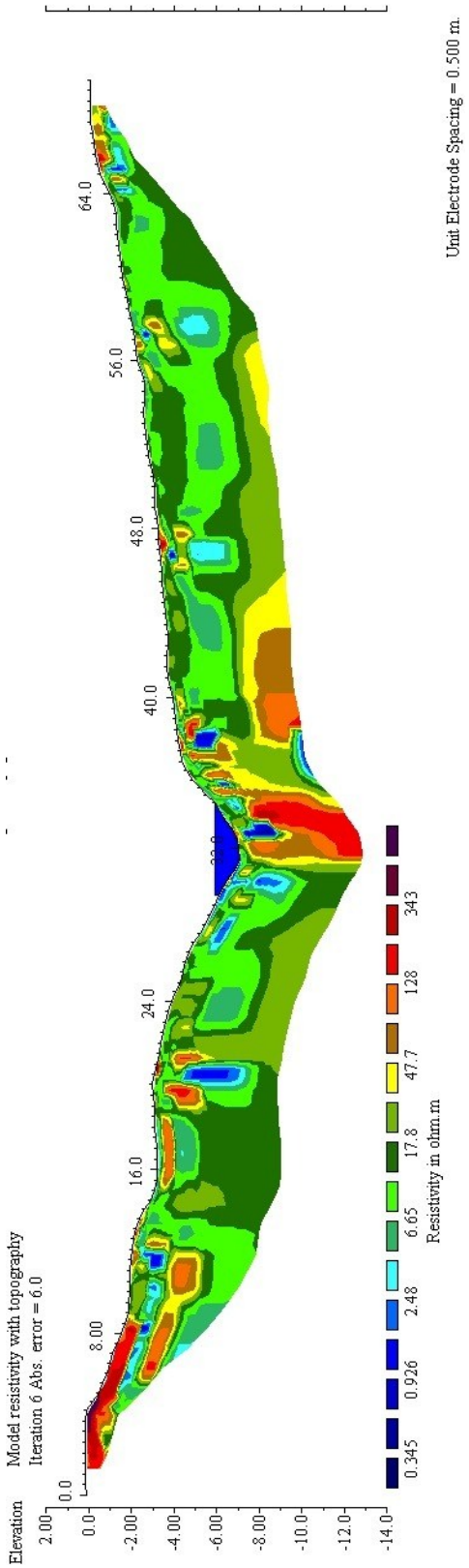

Figure 4.4 The inversion image for profile BG14 at Bridge 14 after six iterations. Vertical exaggeration factor is 1:1.

are outlined in the resistivity images based on their relatively low resistivity (< 3 Ωm). The actual location of the concrete piles was marked and compared with the inversion result. The first pile foundation is located at 11.5 m. The inversion result shows a small, low resistivity body at depth 1-1.5 m below the surface. The second pile is located at 20.5 m. The depth of a low resistivity body at this location extends between 1 to 5 m depth. There does not appear to be a low resistivity anomaly corresponding to the third foundation located at 28 m. At the fourth to seventh foundations, low resistivity anomalies are present as small bodies located a few meters below the surface. Since the resistivity of the geological medium ranges between 5-45 Ωm and the ERI method cannot penetrate to greater depth, the geology is interpreted to be consolidated sediments. A relatively high resistivity body (> 100 Ωm) below the river section is interpreted to be slightly weathered bedrock. A thin high resistivity layer near the surface at the beginning of profile is supposed to be the consolidated material of an asphalt road.

The inversion result can be appraised for accuracy by comparison with the TxDOT design layout of bridge 14 shown in Appendix E. The piles are 0.39x0.39 m in cross-section and the length embedded into the ground varies from 10.1 to 15.8 m. From the resistivity image, there is not a good indication of a long and slender anomaly that represents accurately the shape of the concrete pile foundations. However, a visual inspection at the concrete piles supports the appearance of a low resistivity anomaly. All concrete piles at bridge 14 have few signs of cracking or corrosion. However, a hooked metal sling is found and it is exposed and contacting the ground. These metal cables are used for holding or lifting the piles up and down during bridge construction. The cables generate low resistivity anomalies. Although concrete piles have sufficient resistivity contrast, the slender cylindrical shape is poorly imaged by the electrical resistivity method.

At this site, a small electrode spacing was used but the concrete piles are still not clearly detectable. Decreasing the electrode spacing increases the resolution. If the electrode spacings were to be smaller than 0.5 m, a clearer foundation anomaly might be

obtained but it remains challenging to determine the depth of the long and slender foundation because the depth of penetration would be reduced. With the roll-along technique, increasing the number of electrodes does not increase depth of penetration, so that rolling the array is not considered further due to its time consuming and labor-intensive nature. Generally, most of the foundations should have similar depths at a given bridge site. The recommended procedure is to focus on an individual foundation as proxy of all foundations in a site.

RESULTS AND INTERPRETATION OF BRIDGE 15 SITE

Further experimentation was carried out on a land surface environment at Bridge 15 over Koontz Bayou creek. Surveys were initially carried out along three parallel profiles. The first profile (B15A) was aligned coincidently to a row of concrete pile foundations. The second (B15B) and third (B15C) profiles were aligned parallel to the first profile with 0.5 m line spacing. A second set of surveys was conducted with two parallel profiles BG15A and BG15B at the same location but using greater electrode spacing and line spacings. The experimentation tested the effect of electrode spacings on the quality and resolution of the resistivity images. The primary profile is coincident with a row of five regularly spaced concrete pile foundations. The secondary profiles are located some distance from the row of the foundations but are parallel to the primary profile.

Figure 4.5 shows the inversion results from the first survey. Topographic information was not included here due to the relatively flat ground surface. The electrode spacing is 0.61 m, the total length of the profiles is approximately 33.5 m, and the depth of penetration is about 7 m. After five iterations, the inversion process converged with a RMS misfit of 2.8, 1.96, and 1.37 for profiles B15A, B15B, and B15C, respectively. The inversion result from profile BG15A shows the locations of foundations marked by regularly spaced high resistivity bodies near the ground surface. The resistivity values are > 35 Ωm and located at 12.9, 15.0, 17.1, 19.2, and 21.3 m respectively extending to 1 m depth. Resistivity bodies as low as 3 Ωm are found

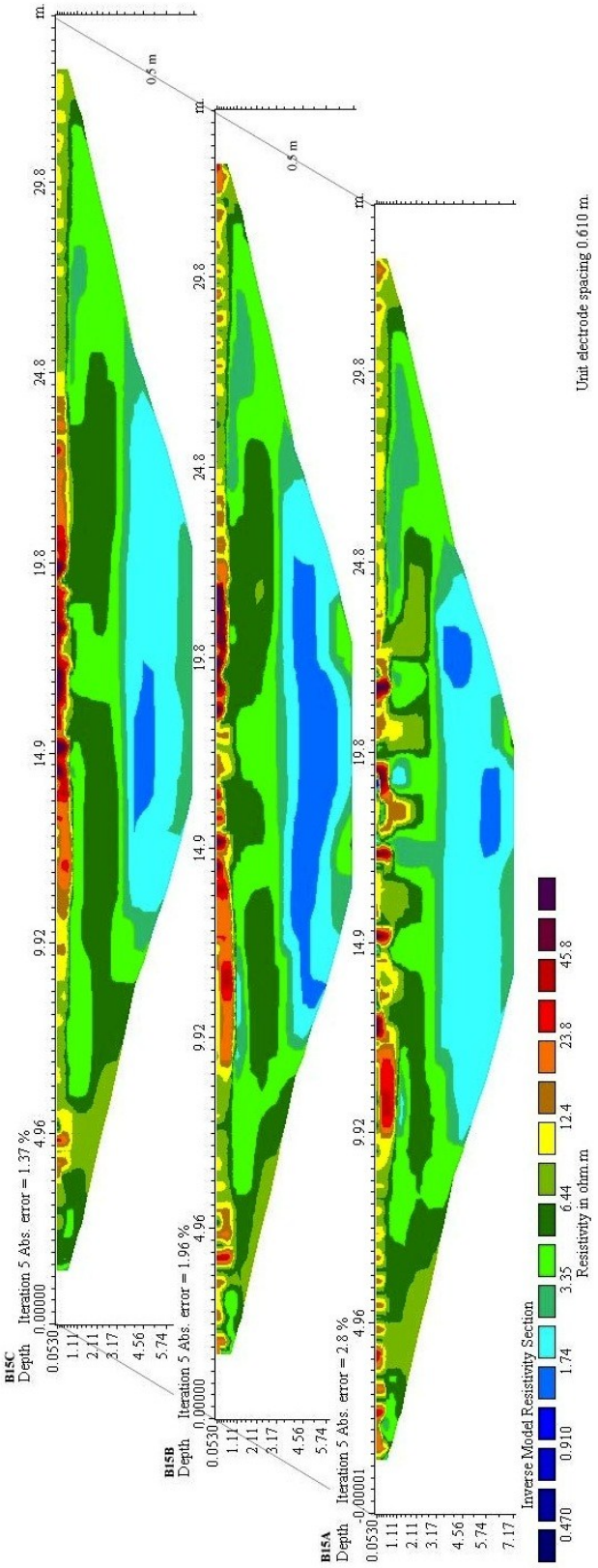

Figure 4.5 The inversion image for the first test at Bridge 15 on FM 50 after five iterations. Vertical exaggeration factor is 2:1.

beneath the anomalies of the third and fourth foundations. The inversion results from profiles B15B and B15C show somewhat similar results but there is not such a clear indication of concrete pile anomalies appearing near the surface as in profile BG15A. A thin layer of high resistivity > 35 Ωm is found near the surface between 8-23 m. This corresponds to the location of concrete boulders exposed under the bridge. All profiles show a low resistivity layer at 3 m deep that is interpreted as the saturated zone beneath the groundwater table. The data were then reanalyzed by subtracting the apparent resistivity of profiles B15B and B15C from that of profile BG15A. The new data were inverted again using the same parameters. This method tests whether the subtracted data would more clearly show the resistivity anomalies of concrete piles. However, the inversion result does not show clear signature of the foundations.

Figure 4.6 shows inversion results of the second survey at Bridge 15. The electrode spacing is 1 m yielding a total length of the profiles of 55 m. The depth of penetration is about 11 m. After five iterations, the inversion process converged with a RMS misfit of 1.32 and 1.10 for profiles BG15A and BG15B, respectively. Somewhat similar results to the first survey are obtained but the locations of concrete pile foundations are not imaged as clearly. A discontinuous thin layer of resistivity > 20 Ωm is found near the surface between 22 m to 34 m. The parallel profile BG15B shows a very similar inversion result. The low resistivity zone of about 2 Ωm is interpreted as the zone of groundwater saturation. A reanalysis was completed, as in the previous survey by subtracting the apparent resistivity of profile BG15B from that of profile BG15A. The new data were inverted again using the same parameters. However, there is no clear signature of an anomaly found that can be identified as a concrete pile foundation.

From the TxDOT layout shown in Appendix E, small concrete piles of 0.39x0.39 m in cross-section with a length embedded into the ground of 13.1 m are present at this site. The inversion results image small higher resistivity bodies near the ground surface but do not capture the long concrete pile shape and depth. In general, the maximum depth of penetration is approximately one-fifth of the total length of survey profile; in this case 56 electrodes were used. Using a larger electrode spacing with the same

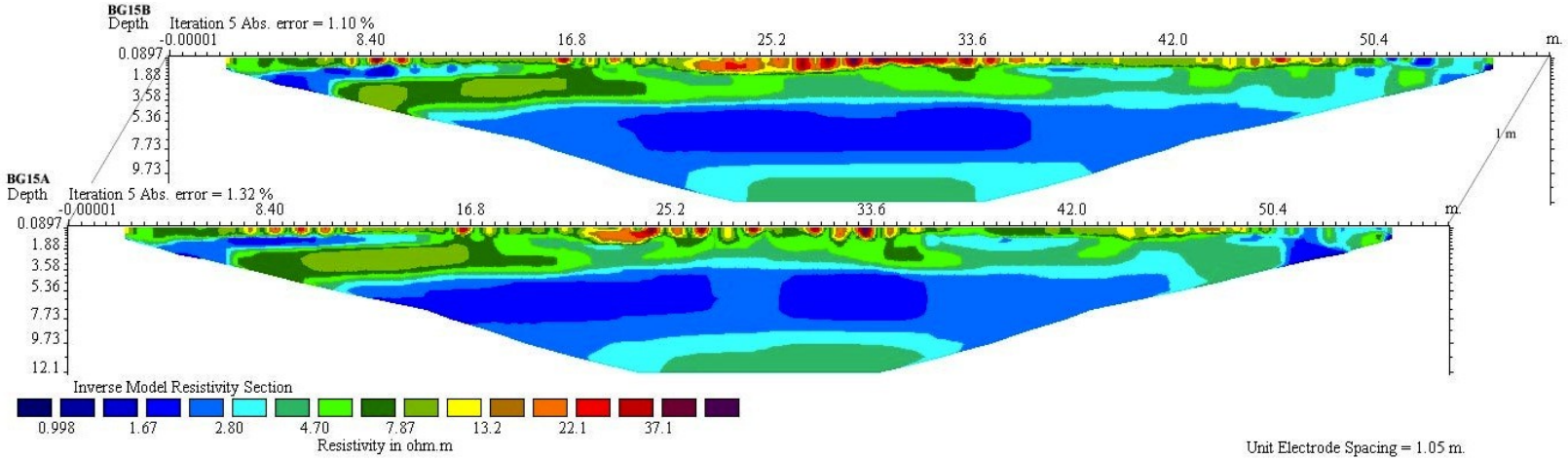

Figure 4.6 The inversion image for the second test at Bridge 15 on FM 50 after five iterations; Note a vertical exaggeration factor of 0.5 is used in the display.

number of electrodes increases the depth of penetration but reduces the spatial resolution. However, increasing the number of electrodes does not always increase the depth of survey under certain circumstances for a fixed electrode spacing *a* and dipole factor *n*. The parallel survey and subtraction method was used but the concrete piles are still not clearly detectable. The concrete piles have sufficient resistivity contrast but they are too slender to be imaged by the resistivity method. I conclude that the ERI method is not capable of reliably characterizing long and slender concrete pile foundation.

The 2D ERI experimentation was conducted at actual bridge sites. The method could not effectively provide images of long slender foundations. The method of deploying parallel cables across a row of foundations was not completely successful. I decided to postpone further experimentation at actual bridge sites and move to the National Geotechnical Experimentation Site (NGES), to investigate a variety of 2D and 3D electrode configurations over known and unknown foundations.

RESULTS AND INTERPRETATION OF NGES

3D Inversion Result

The experimentation was conducted over a number of shallow and deep concrete foundations at the NGES. A number of 2D profiles was acquired with each line of electrodes arranged as part of a series of regularly-spaced profiles. A quasi-3D image of the survey area was merged from sets of 2D data collected from eighteen parallel lines. However, five perpendicular profiles were not included in a 3D imaging because they extends beyond the edge of the rectangular area formed by the parallel eighteen profiles. The 2D inversion images for all twenty-three profiles are shown in Appendix C. Due to the regular spacing of each profile; it is not possible to obtain a uniform coverage of all major clusters of spread footings and drilled shafts. Some profiles have electrodes placed directly on spread footings whereas others have electrodes placed adjacent to foundations. The 3D resistivity image is shown as a series of horizontal and vertical slices at different depths spanning the study area.

Figures 4.7-4.8 present horizontal depth slices of the 3D resistivity image at

NGES. A RMS error of 7.9 was achieved after five iterations. Looking at depth slices, I have tried to match zones of anomalous resistivity with known positions of the foundations that appear on the site map in Appendix E. Scattering of small-scale high resistivity bodies is found on the near-surface layers 1-3. There is however no clear indication of a foundation located in these depth slices. Cultural interference from metal fences, and discarded metal such as rebars, may cause many undesired anomalies. Distinct, localized high resistivity zones are found at a depth of 1-3 m below ground level in the middle to south portion, see layers 3-6. These zones are consistent with a group of drilled shafts and a spread footing. However, the inferred depths are greater than expected and the precise shape of the foundations cannot be determined.

Figures 4.9-4.10 present vertical slices extracted from the 3D inversion result at roughly the locations of the 2D acquisition profiles. Distinct low resistivity zones are found in x/z planes 8, 9, 10, 11, and 13. These zones are in locations that are consistent with positions of reaction shafts. Zones of high resistivity interpreted as spread footings have greater depth than expected and are of larger size. The extracted 2D images from the 3D inversion may be compared directly with the 2D inversion results from individual profiles. The images from 2D inversion and the sliced 2D images at the same location are rather different. The 2D inversion images are much more consistent with the layout shown in Appendix E. The 2D images sliced from the 3D inversion result are distorted. The distortions and artifacts present in the sliced 2D images may cause misinterpretation.

Fully 3D experimentation was carried out over Footing 5. The dataset SF1-3D was not processed however due to very poor data quality. A poor quality datum may be caused by faulty connections of electrodes or low battery. The number of remaining data was not sufficient to process the inversion after the bad data were removed. This dataset consequently was discarded and not considered further in the analysis. A repeat of data acquisition was not carried out because I decided to end the 3D ERI method and proceed further with 2D ERI experimentation.

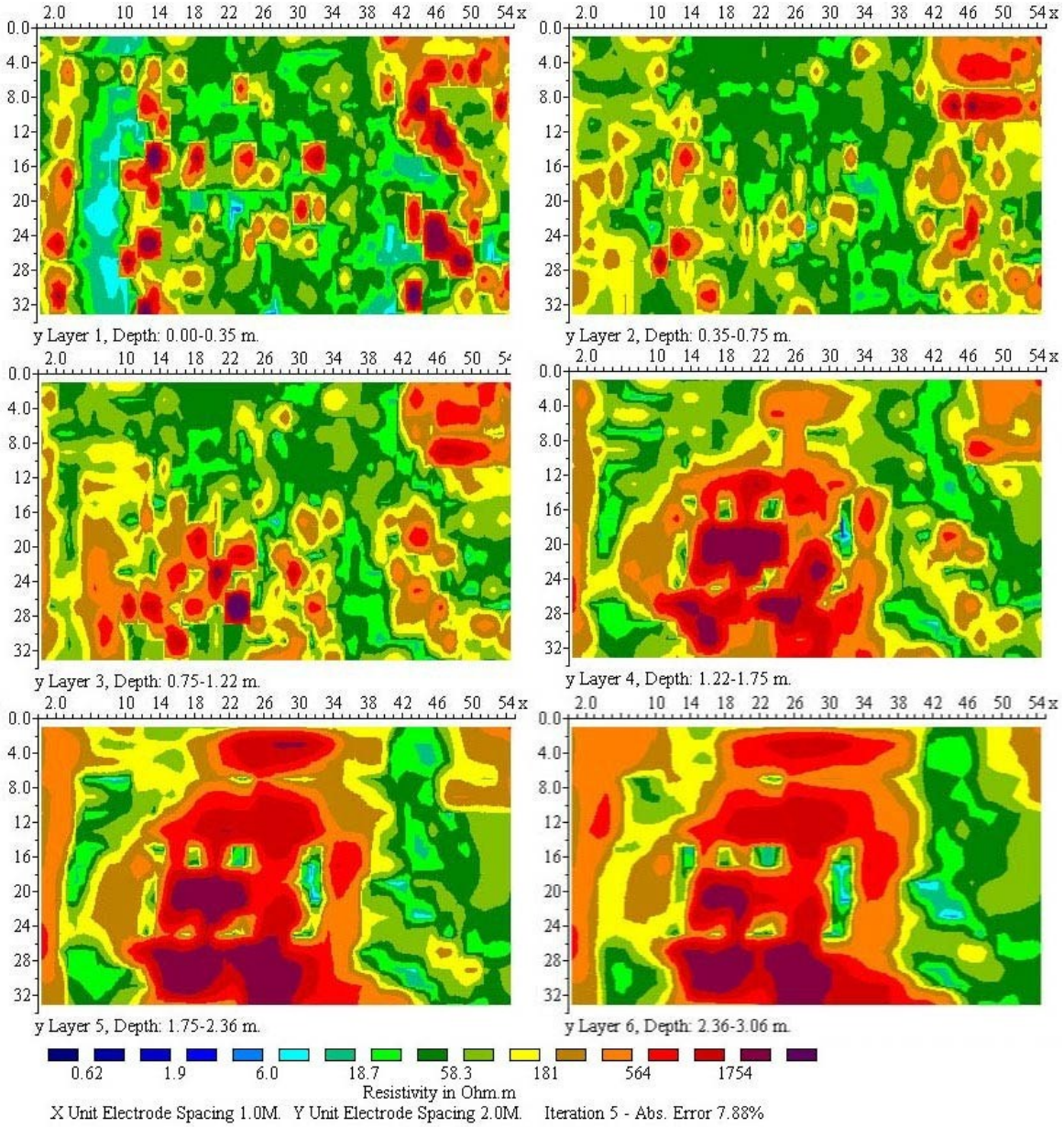

Figure 4.7 Depth slices of the 3D model between 0-3.06 m depth ranges obtained from the inversion of the NGES3D data set.

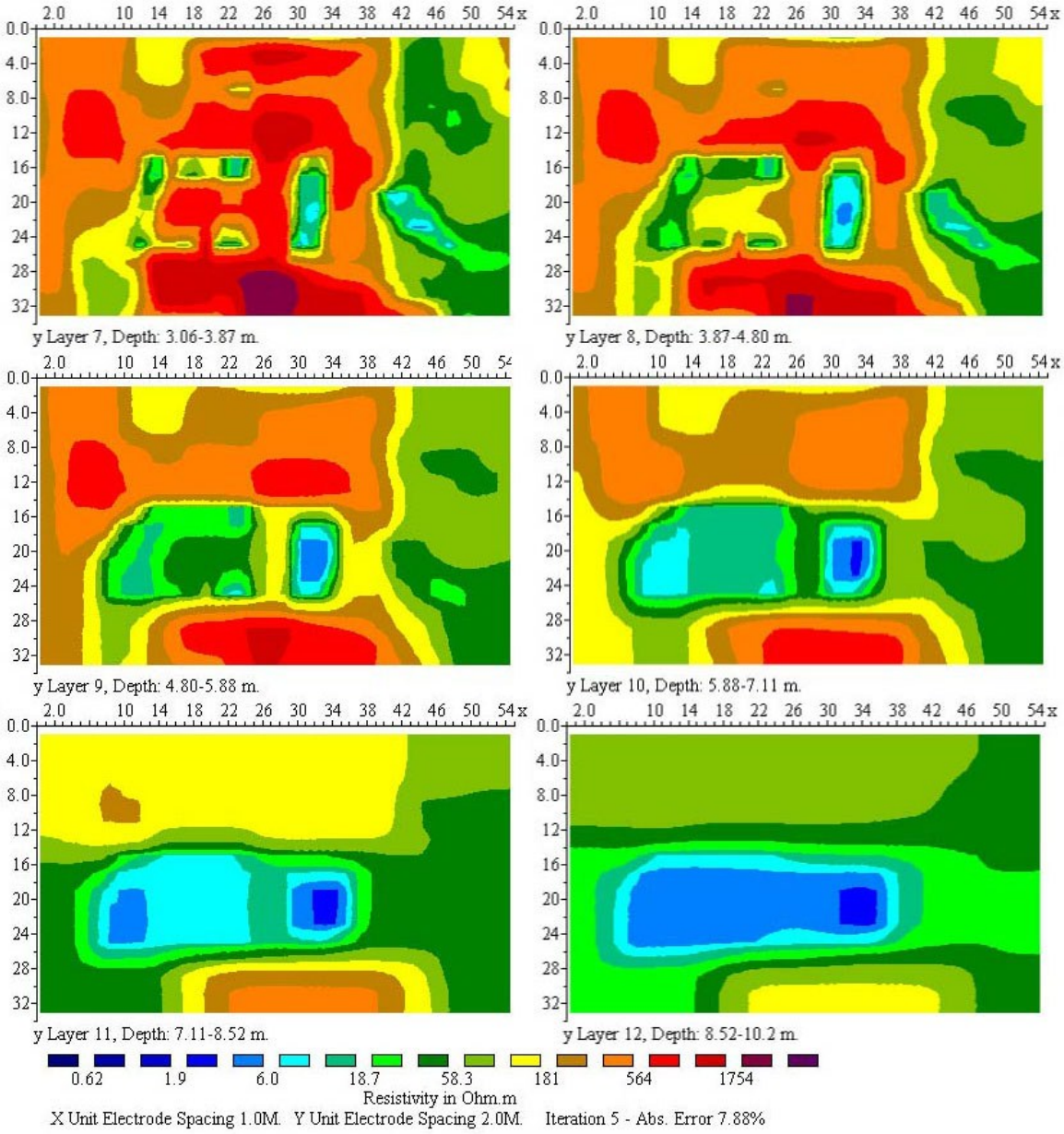

Figure 4.8 Depth slices of the 3D model between 3.06-10.2 m depth ranges obtained from the inversion of the NGES3D data set.

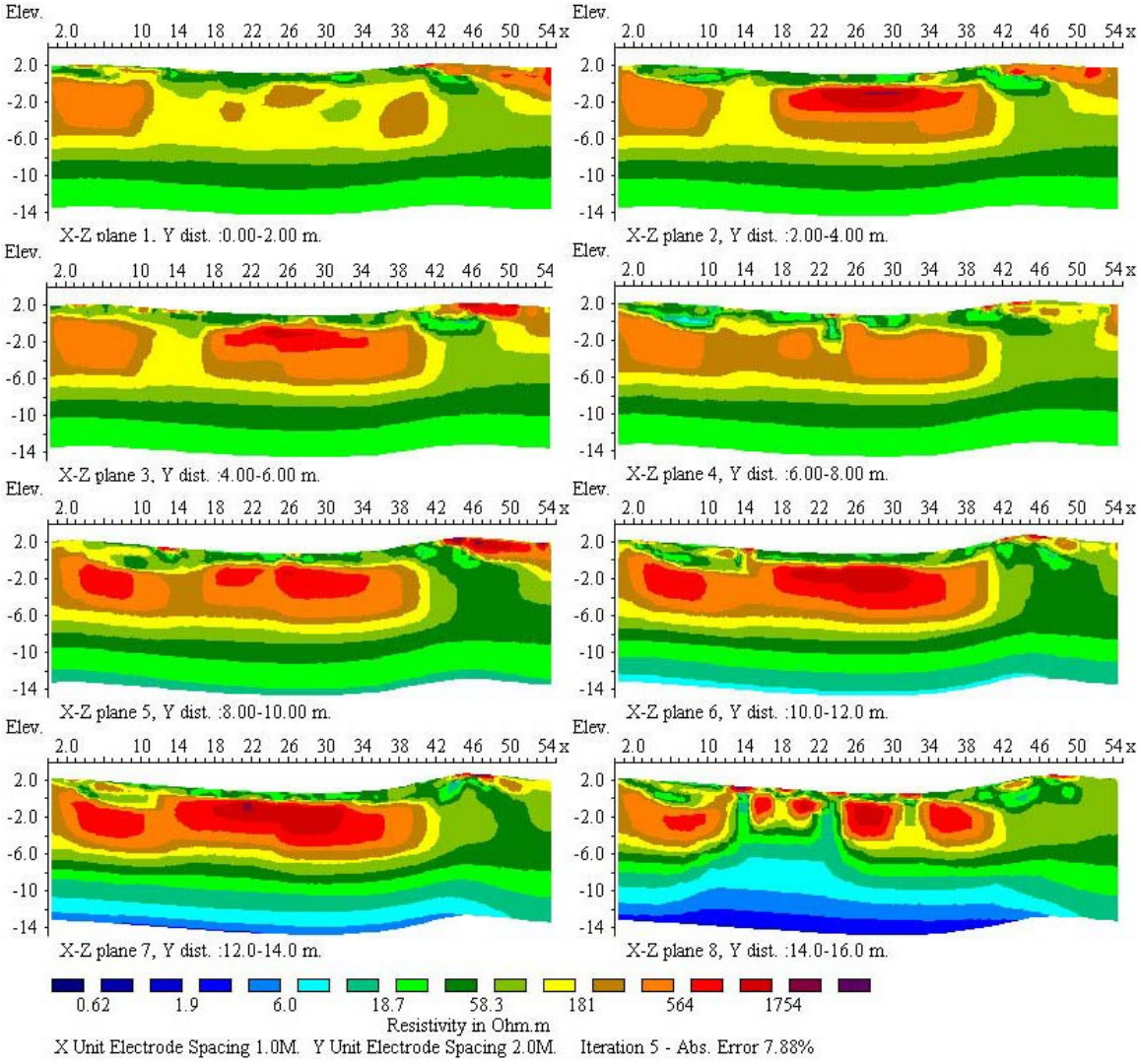

Figure 4.9 Vertical slices of the 3D model between 0-16 m ranges obtained from the inversion of the NGES3D data set coinciding with the 2D profiles measured.

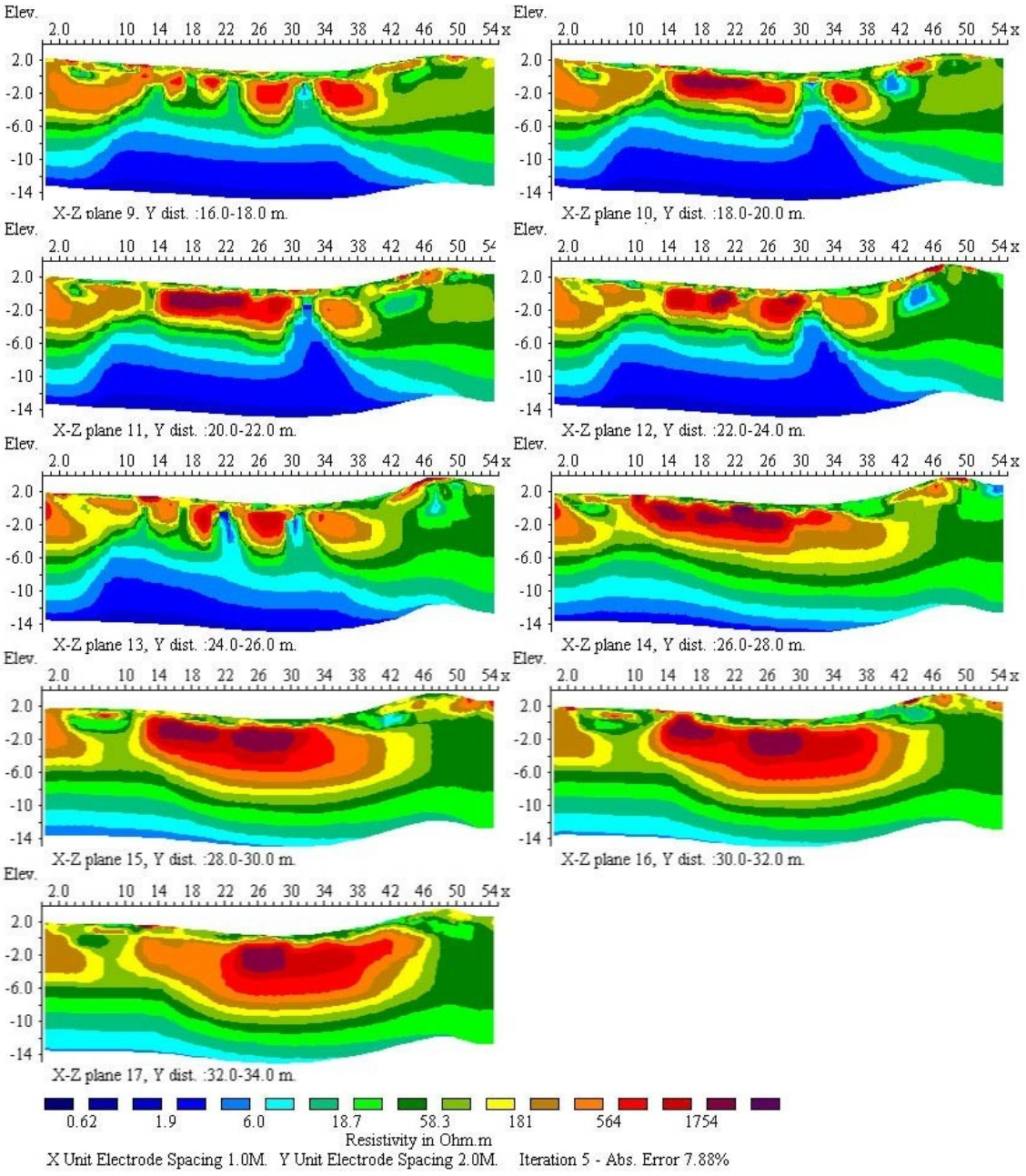

Figure 4.10 Vertical slices of the 3D model between 16-34 m ranges obtained from the inversion of the NGES3D data set coinciding with the 2D profiles measured.

The 3D ERI method in principle should provide the most accurate images of 3D subsurface structures. In the case of foundation determination, it was found that the quasi-3D inversion procedure does not provide precise or clear images of known foundations. A possible exploration is that the survey profiles did not sufficiently cover all major clusters of spread footings and drilled shafts. Moreover the various foundations are not all elongated and vertical structures so that the 3D images provide a wide range of anomaly shapes that are difficult to interpret. One important practical limitation of the 3D survey at bridge site is the need to have sufficient space for the electrode layout. The number of electrodes must be greater than other conventional electrode configurations to ensure adequate vertical and horizontal data coverage. The ERI method for bridge foundation determination is usually conducted in an undulated terrain and accessibility may be limited to survey in one direction. In summary the 3D ERI technique is not likely to be a useful practical technique for bridge engineering geophysics investigations.

2D Inversion Result

Separate 2D experiments were carried out at the NGES site over three drilled shafts and a shallow spread footing. Topographic information was not incorporated in the inversion process due to the presence of relatively flat ground. A resistivity pseudo-section is displayed as an example in Figure 3.21. All profiles conducted over drilled shafts provided similar pseudo-sections. The pseudo-sections provide some information about the shape and position of foundations using dipole-dipole configuration. The pseudo-section plot illustrates a zone of low apparent resistivity values. The foundation in the subsurface appears as the lineaments that incline separately from the center. This indicates good data quality.

Figure 4.11 shows the inversion results for profiles TS2A, TS2B, and TS2C conducted over drilled shaft TS2. The inversion results have an RMS error of 4.8, 5.6, and 3.7 respectively. The length of the profiles is 55 m and depth of penetration is about 12 m. The inversion results show a somewhat low resistivity zone (< 20 Ωm) corresponding to the drilled shaft at the middle of each of the profiles. The width of the

low resistivity zone gradually increases from 1.5 m near the surface to 4 m at the bottom. A high resistivity body appears close to the surface, while the surrounding geological materials dominantly show high resistivity values. From the NGES site layout, the length of the drilled shaft is 10.8 m so that the zone of low resistivity is wider and longer than the actual structure. Figure 4.12 shows the inversion results for profiles TS4A and TS4B conducted over drilled shaft TS4. The inversion results have an RMS error of 7.0, and 3.5 respectively. Figure 4.13 shows the inversion results for profile RS5A conducted over drilled shaft RS5. The inversion result has an RMS error of 6.2. The inversion results show similar images to those for drilled shaft TS2 but the high resistivity zone near the surface is not present.

The accuracy of the results may be verified using the site layout in Appendix E. A vertical zone of low resistivity extends from the surface to the bottom of each image. However, the depth of drilled shaft cannot be estimated from resistivity images due to a lack of sufficient coverage. Moreover, 3D effects might cause distortions at depth in the lower sections of the image and also the presence of conductive rebar might affect background resistivity. A different electrode configuration to better constrain the depth of this anomaly was not carried out because these results are sufficient to determine that the drilled shafts are long enough (> 5 m) to be safe from scour. The images are consistent with the hypothesis that as the drilled shaft was being constructed, the rebar cage was exposed along and at the bottom of the hole and has made contact with the ground. The exposed steel rebar in contacted with the soil electrolyte can generate an electrode potential in the subsurface. For this reason, the IP method may be able to determine the foundation depth and shape as a complement to the ERI method.

Figure 4.14 show the inversions results for profiles SF1A and SF1B conducted over a 1x1 m spread footing. After five iterations, the inversion process converged with a RMS misfit of 1.6 and 1.5, respectively. The length of the profiles is 13.5 m. The inversion results indicate a penetration depth of about 3 m. The profile SF1A shows a body of low resistivity of 20 to 40 Ωm located between 6.5-7.5 m. This zone represents the footing buried to a depth of about 1 m from the ground surface. A somewhat similar

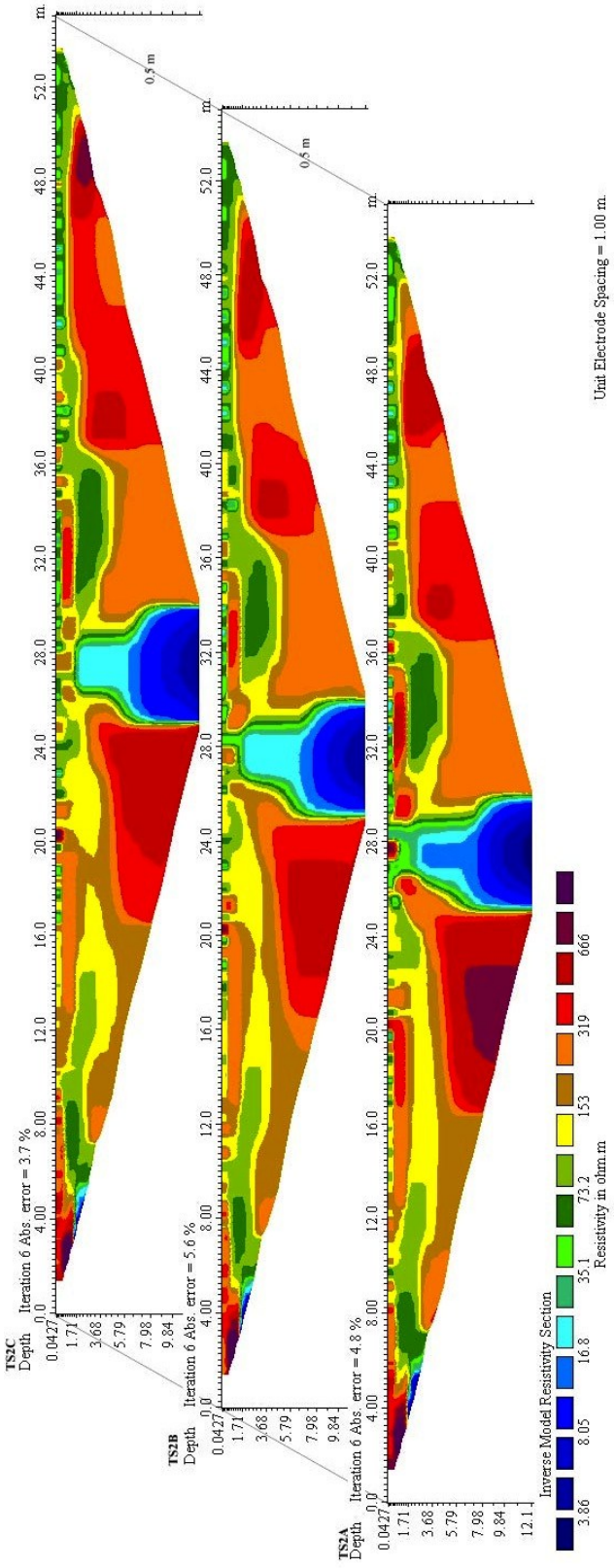

Figure 4.11 The inversion result for profiles TS2A, TS2B, and TS2C at drilled shaft TS2 after six iteration.

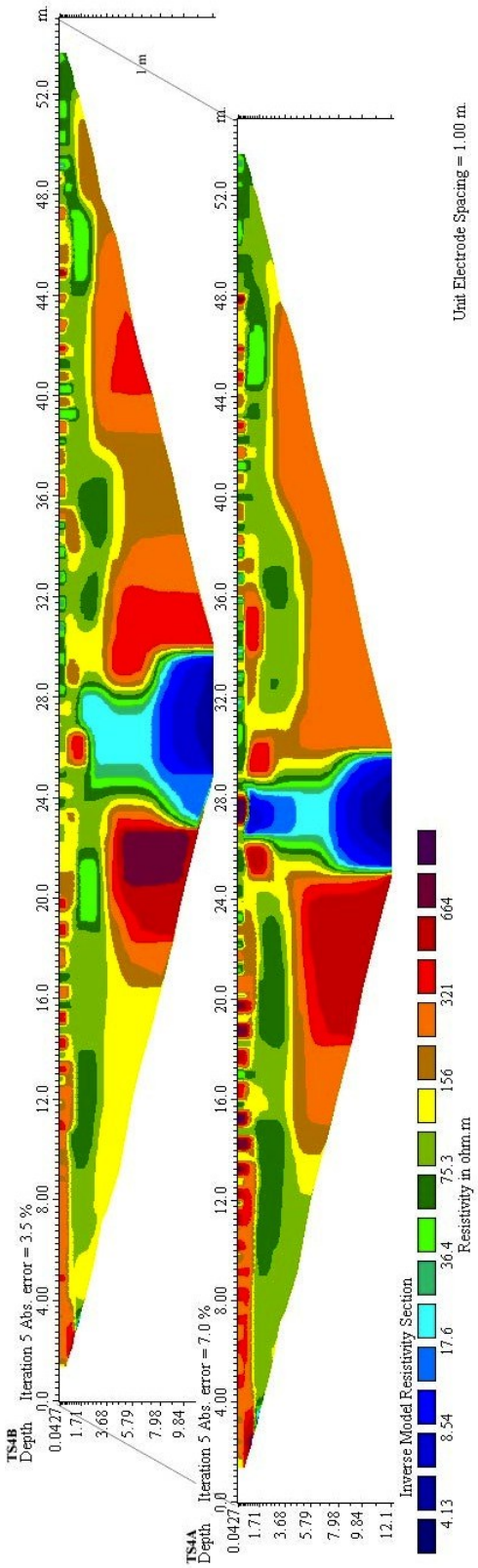

Figure 4.12 The inversion result for profiles TS4A and TS4B at drilled shaft TS4 after five iteration.

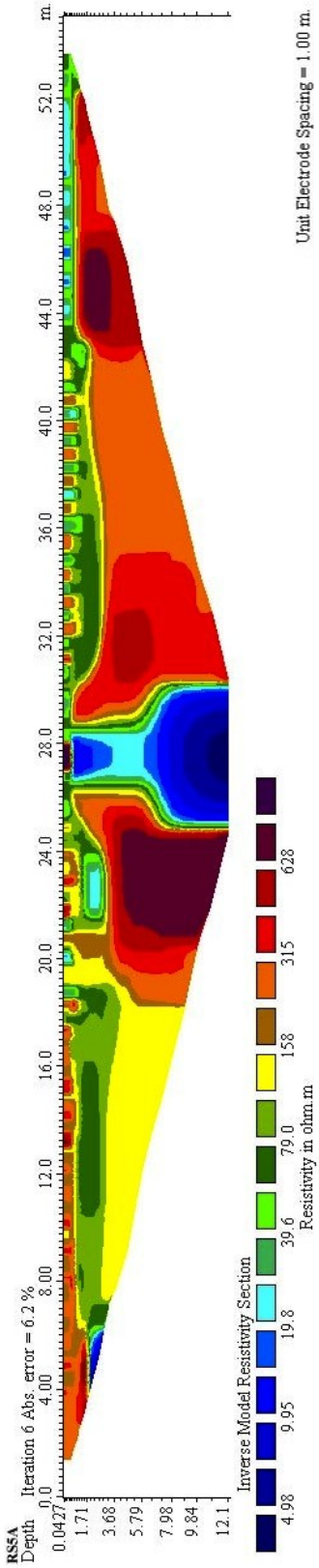

Figure 4.13 The inversion result for profile RS5 at drilled shaft RS5 after six iteration.

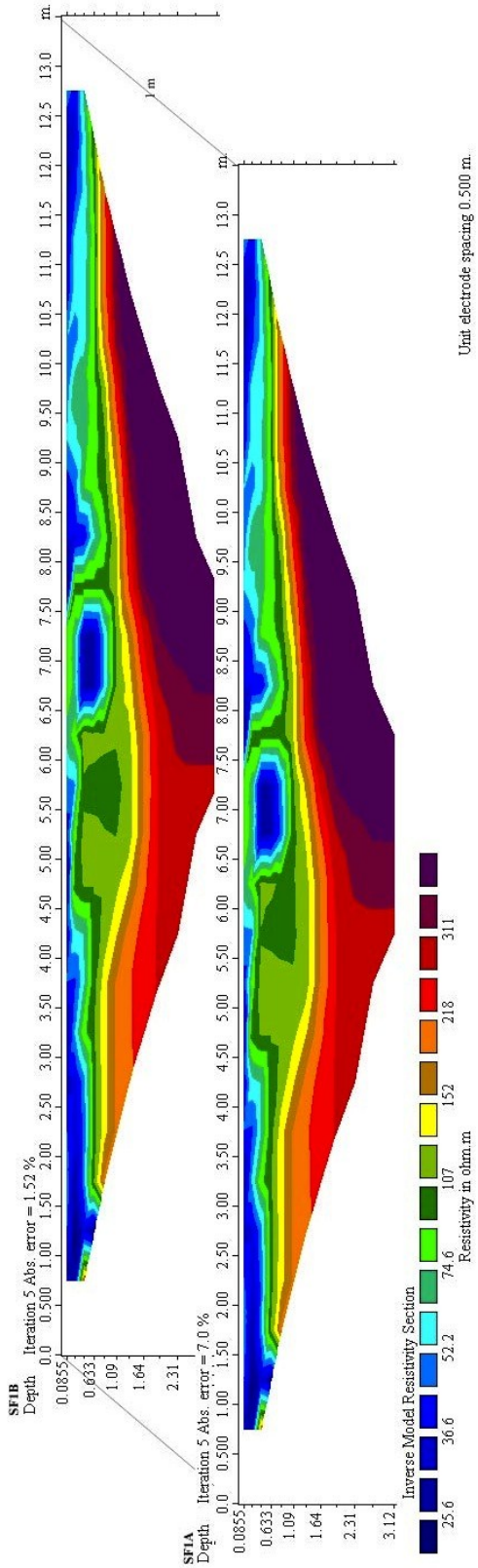

Figure 4.14 The inversion result for profile SF1A and SF1B at a shallow spread footing after five iteration.

result is found for profile SF1B. The accuracy is verified according to original design in Appendix E and visual inspection. The zone of low resistivity of about 1 m width and 1 m depth is approximately to actual size of the spread footing. Again, the presence of rebars exposed to ground strongly affects the results of a resistivity survey and likely causes the low resistivity values associated with the anomaly of the spread footing.

Further experimentation was conducted over a drilled shaft and a 3x3 m shallow spread footing that are categorized as unknown foundations. Figure 4.15 shows inversions results for profiles UK1A and UK1B conducted over the drilled shaft. The length of the profiles is 55 m and the depth of penetration is about 12 m. The inversion images of profile UK1A show a high resistivity zone (> 250 Ωm) compared to the location of the foundation at the center of the profiles. The zone is 1 m wide and 3 m deep. The inversion result for the profile UK1B has a smaller zone of high resistivity than that of profile UK1A. The central anomaly is interpreted as an unreinforced concrete drilled shaft or solid concrete of 0.9 m diameter embedded about 3 m in the ground. According to the forward modeling of the resistive drilled shaft, the anomaly cannot image slender and vertical foundation so, for this reason, is can be considered that this foundation might be longer than the interpreted length but the ERI technique is not capable to detect such a foundation.

Four profiles, SF3A, SF3B, SF3C, and SF3D, were carried out along the four sides of the footing and two profiles, SF3E and SF3F, were conducted across opposite corners of the footing. Only the first two inversion results are illustrated here because other two profiles provide an identical result. Moreover the profiles carried out access the opposite corners are of very poor quality data, so they were discarded. Figure 4.16 shows inversions results of profiles SF3A and SF3B conducted over the 3x3 m spread footing. The depth of penetration is 5 m. Both profiles give a similar result, showing high resistivity zones (> 1500 Ωm) at the location of the footing with a low resistivity zone above. The high resistivity zones of depth about 3 m from ground surface and width about 5 to 6 m indicate that the anomaly shape is larger than actual the footing size, 3 m. The profile SF3B provided a similar result but its high resistivity zone is

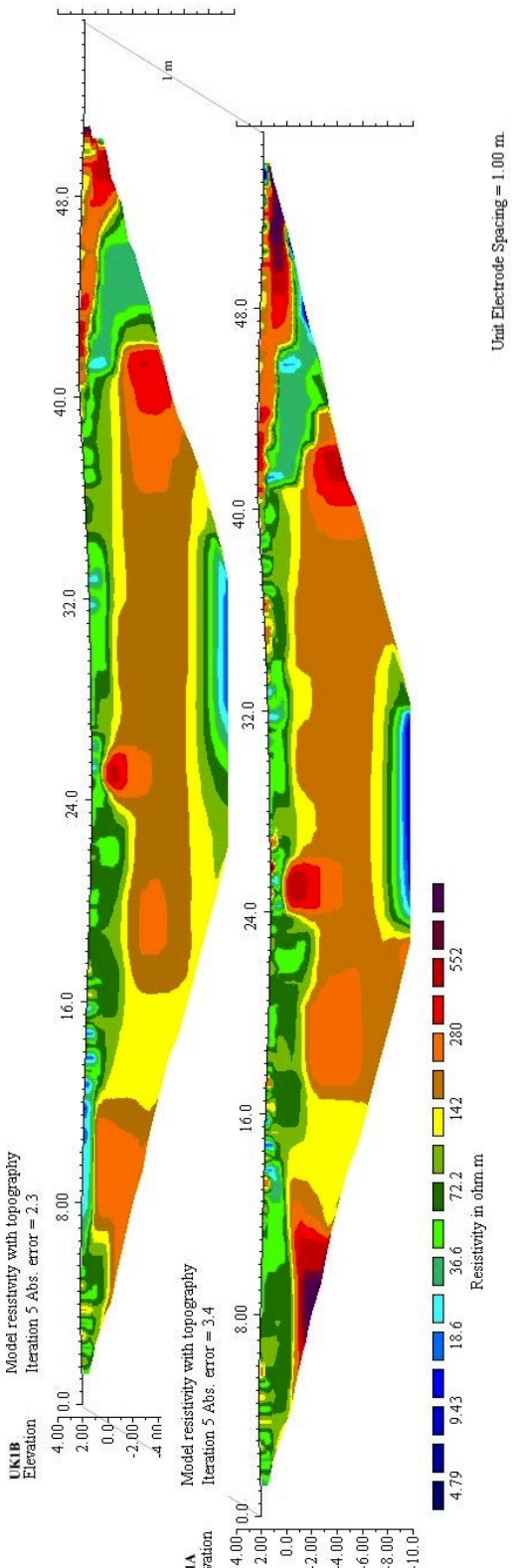

Figure 4.15 The inversion result for profiles UK1A and UK1B at drilled shaft.

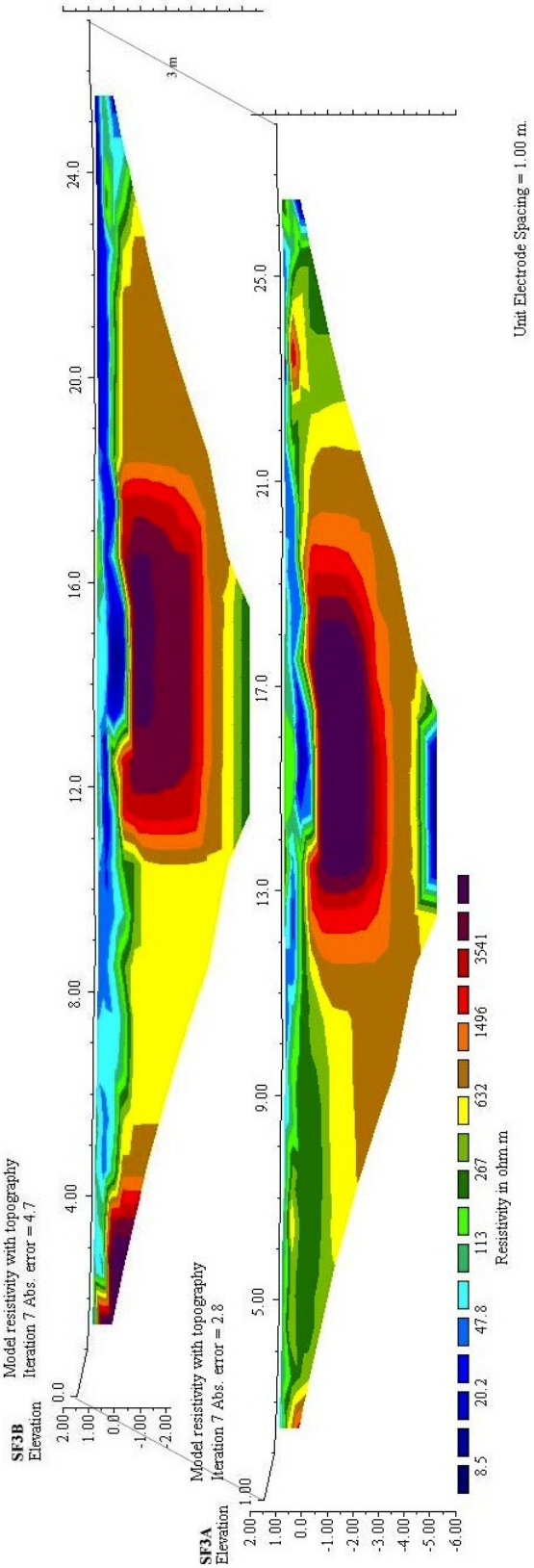

Figure 4.16 The inversion result for profile SF3A and SF3B at a shallow spread footing after seven iteration.

slightly larger. The low resistivity zone is caused by wet ground during the survey; it is assumed that the highly resistive concrete slab might not be strong enough to affect conductive ground. A low resistivity zone appears close to the surface. Since the electrode spacing and dipole factor are small, the low apparent resistivies are measured close to the surface.

Profile F1 was carried out to confirm from the previous experimentation that the depth of penetration image is only 5 m deep. The bottom of the spread footing might not have enough data coverage and be poorly resolved due to shallow the penetration. Figure 4.17 shows the inversions result for profile F1 conducted over the 3x3 m spread footing. A RMS error of 4.2 was achieved at the sixth iteration. The length of the profile is 55 m and depth is about 12 m. Topographic information was incorporated into the inversion process. At the position of the spread footing, the image shows a high resistivity zone with values > 2000 Ωm between 25-29 m and 1-4 m depth. A low resistivity zone appears on the top of the image as in the previous experimentation. The design layout of this spread footing is not available. However, this profile confirms the result of the previous experimentation of this spread footing.

Several 2D ERI experimentations have been completed at the NGES and bridge sites Bridge 14 and 15. It can be summarized that using electrode spacings < 1 m for detecting a foundation smaller than 1 m diameter is not recommended. Due to the exponential loss of resolution of the resistivity method with depth, imaging such a slender foundation to a depth of greater than 10 m is not feasible. The smallest advisable electrode spacing is 1 m. Since the dipole-dipole configuration has comparatively low signal strength, the method of overlapping data levels is recommended. The lessons learned from the successful experimentation at the NGES were applied further at actual bridge sites.

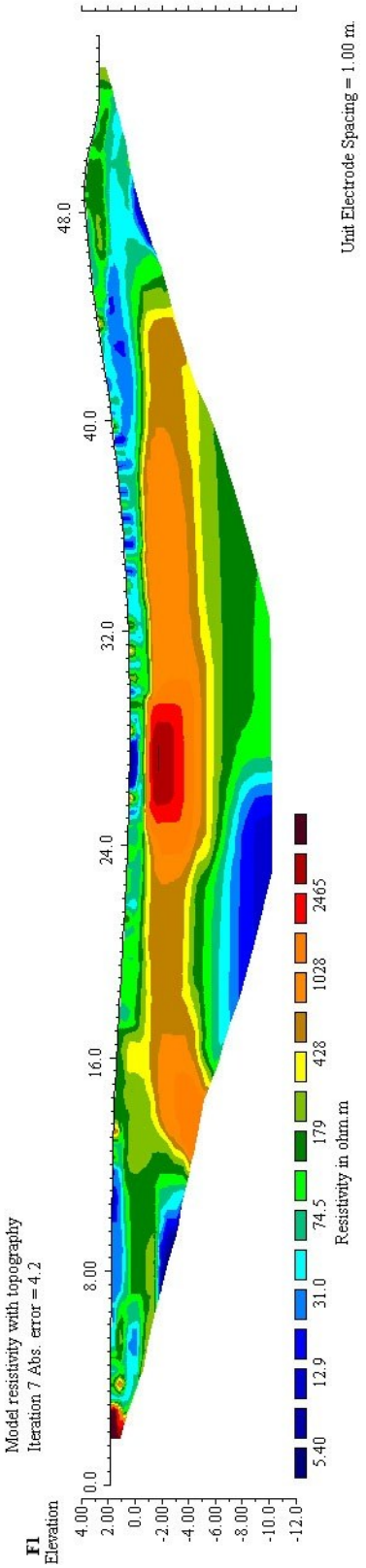

Figure 4.17 The inversion result for profile F1 at a shallow spread footing after seven iteration.

RESULTS AND INTERPRETATION OF ROADWAY BRIDGE SITE

Experimentation was carried out in mixed terrain underwater environment at a highway bridge over the Little Brazos River. The two selected bridge foundations were embedded in the riverbed. Electrode stakes were installed on the ground surface as well as underwater on the riverbed. The acquisition was carried out with the foundation located near the center of the survey profile. Two profiles were carried out on two separate drilled shaft foundations of the bridge. The first profile is oriented approximately parallel to the river flow while the second profile is oblique to the river. The inversion results are shown in Figure 4.18. The length of the profiles is 55 m and depth of penetration is about 11 m. The water in the river where electrodes are underwater is marked by the blue zone above the ground surface. Small ticks marked on the ground surface denote half the electrode spacing. The water body is shown in blue. The overall resistivity values range from about 0.3 to 70 Ωm. The foundation anomaly is outlined as a relatively low resistivity zone.

In the inversion result for profile BHW21A after five iterations, the inversion process converged with a RMS misfit of 3.8. The image shows a small range of resistivity values indicating a small degree of heterogeneity in subsurface geology. The geological medium shows resistivity values between 5-23 Ωm. These are consistent with prior information from this area that indicates clay and shale to 3.1 m depth from an available borehole. Sandstone and siltstone lies between 3.1 to 12.2 m depth. There also exists near-surface materials with resistivity values > 23 Ωm located between 44-49 m. Field investigation indicated that this highly resistive region is related to debris from a previously demolished bridge. A distinct low resistivity body between 0.5-5 Ωm is also clearly seen. The location of this zone is consistent with the foundation position at the middle of the profile. This body has width which is much greater than the actual 1 m of the foundation diameter. The bottle like shape is about 2 m wide from 0-4 m deep and widens to 4.5 m at 4 m depth. The interpreted depth of the foundation is about 10 m.

In the inversion result for profile BHW21B, the resistivity data were processed through four iterations yielding an RMS error of 4.4. Although this profile was

a)

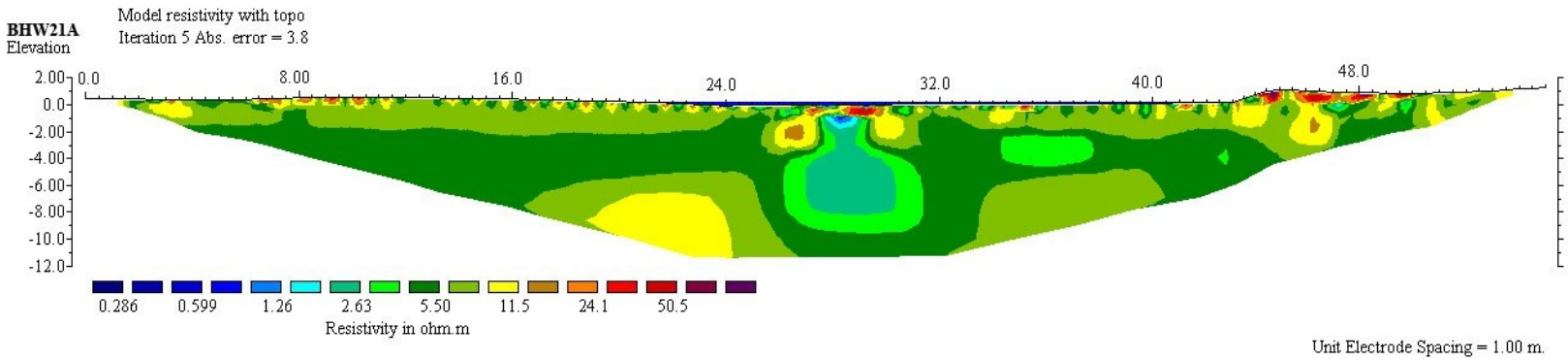

b)

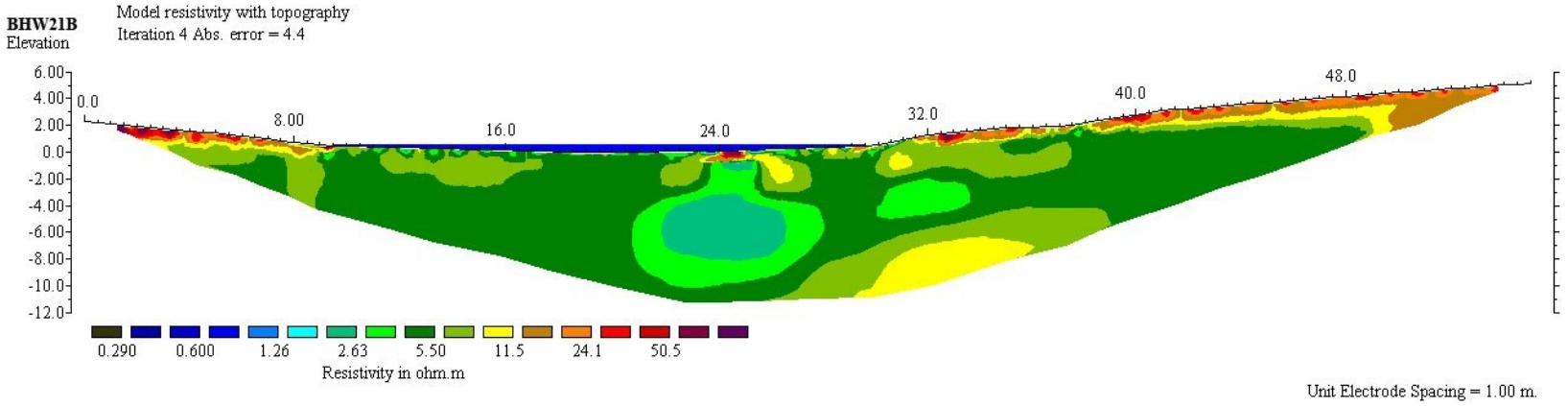

Figure 4.18 The inversion result for profiles BHW21A (a) and BHW21B (b) at roadway bridge over Little Brazos River after five iteration, vertical exaggeration 2:1.

conducted at a different drilled shaft, similar and consistent results to the first profile were obtained. Resistivity values of riverbed materials are between 5-23 Ωm, which is consistent with observation and the geologic log from this area. A thin layer of higher resistivity values exists the near surface on both sides of the model section where the land surface electrodes were deployed. This layer has resistivity values > 23 Ωm and is typically about 1 m in thickness. It is interpreted to be a hard soil layer plus demolished bridge material. A low resistivity body between 0.5-5 Ωm associated with the foundation exists relative to the higher resistivity values of the surrounding geological materials. Higher resistivity anomalies appear near the surface, perhaps caused by the heterogeneity of the concrete body. The interpreted depth of the foundation is about 10 m.

Visual inspection around the drilled shaft foundations confirms the inversion results. It was found that parts of the foundation are corroded and the rusting rebars are exposed and in contact with water. Broken concrete boulders and rebars from the previous bridge were scattered under the bridge in water and on the bank. The inversion result shows a lower resistivity for the foundations than the surrounding geological materials. It is assumed that cracks or corrosion have degraded the reinforced concrete foundation and caused the iron rebars to come into contact with the ground, causing the transport of ions through the concrete and the surrounding materials. These ions affect the resistivity measurements by increasing the surface conductivity. If the foundations are intact with no cracks or corrosion, then the inversion images would show a higher resistivity anomaly compared to the surrounding geological materials.

In order to access the reliability of the inversion results, the images are compared with known information from the TxDOT layout of the eastbound lane. The eastbound bridge was constructed beside the westbound bridge so the two bridges should be very similar. The drilled shaft foundation at the eastbound lane is known to be 0.91 m in diameter and 22.55 m in total length. The foundations were located in water-covered area, such that a 10.36 m long section was embedded into the ground. The resistivity image is consistent with the layout. Although the resolution of the 2D ERI in a mixed

terrain underwater area is lower than 2D ERI performed over a land surface area, the inversion results clearly and consistently show the existence of low resistivity anomalies at the known foundation positions on the survey profiles. Moreover, the low resistivity zone of the foundations is clearly imaged in both inversion results. Although the images do not indicate the precise shape of the foundation, the horizontal and vertical extent of the anomaly is sufficient to estimate the size and depth of the foundation. From the inversion result, it can be summarized that the 2D ERI method that has been widely used for land surface surveys can be adapted effectively in water-covered environments at actual sites.

RESULTS AND INTERPRETATION OF RAILWAY BRIDGE SITE

ERI data were acquired at the railway bridge over Brazos River to determine whether a 2D resistivity profile placed in proximity to a very large bridge footing would be able to image it from the side. Two profiles RWB1 and RWB2 were placed perpendicularly and passed 0.5 m from the footing. Both profiles give similar and consistent results. Figure 4.19 shows the inversion result of 2D REI at the railway bridge. Small ticks marked on the ground surface correspond to half the electrode spacing. Profiles RWB1 and RWB2 were oriented perpendicular to each other. The length of the profiles is 54 m and the depth of penetration is about 10 m. The inversion results clearly indicate a strong contrast in resistivity of the foundation and the surrounding geological materials. The inversion results generally show lower resistivity values of geological materials and higher resistivity values of the concrete foundation.

From the inversion result for profile RWB1, the inversion process converged with a RMS misfit of 2.8 after five iterations. A high resistivity anomaly > 80 Ωm is located between 20-31 m. This location is consistent with that of the concrete foundation. Its shape is somewhat rectangular with a width of 11 m and a depth of 5 m. This zone is interpreted to be the resistivity anomaly of the large spread footing. A thin zone of high resistivity anomaly close to the footing is caused by overapping boulders

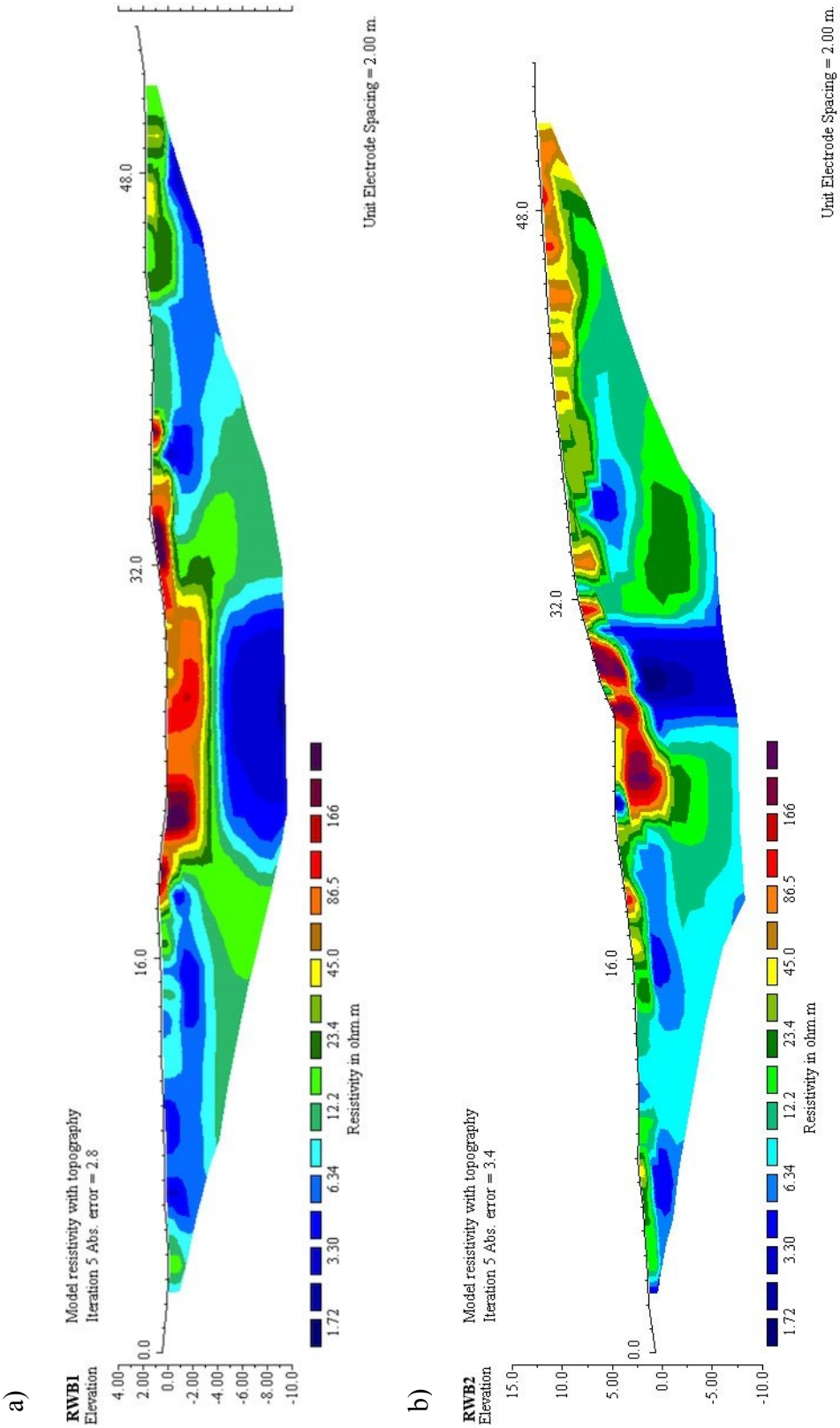

Figure 4.19 The inversion result for profiles RWB1 (a) and RWB2 (b) at the railway bridge over Brazos River after five iteration., vertical exaggeration 2:1.

and discontinuous bedrock. The lower resistivity values correspond to weathered rock materials. A subsurface layer of comparatively low resistivity values < 10 Ωm located beneath the bottom of the spread footing anomaly is considered to be typical of weathered materials of the underlying rocks in the area. This zone of low resistivity also appears toward both end sections of the profile where clay particles and elevated moisture act to increase electrical conductivity. The shallowest bedrock is found close to the foundation, with resistivity values ranging between 10-40 Ωm. This layer represents weathered to moderately weathered shale, as observed on the surface.

The inversion process at RWB2 converged with a RMS misfit of 3.4 after five iterations. This inversion result provides important additional information. The center of this profile was placed a few meters away from the foundation due to lack of access caused by the river. A high resistivity anomaly > 80 Ωm corresponds to the footing foundation and is located between 22-25 m with a somewhat rectangular shape of 3x5 m width and depth. Discontinuous bedrock is assumed to underlie the foundation, as in the previous profile. The sloping section between 25-32 m reveals discontinuous high resistivity bodies > 80 Ωm. This location marks the occurrence of exposed sandstone outcrops. Conversely, a low resistivity zone (< 5 Ωm) beneath the high resistivity bodies is interpreted as a highly weathered zone, perhaps also high in water content. Lower resistivity values are found near the surface close to the foundation; these can be interpreted as weathered rocks. A near surface thin layer from 37 m the end of profile with a comparatively high resistivity value is interpreted as hard ground surface.

From the two resistivity images, the size of the footing foundation anomaly is consistent with the actual size of foundation (11x3 m wide and 5 m deep). The foundation has high resistivity in accordance with the observation that the iron rebar did not appear to be in contact with the ground. Visual inspection shows that the foundation footing is in intact condition. There is no rebar metal exposed although small metal items such as nails and wires were noticed. Those metal items did not cause applicable lower resistivity anomalies than the surrounding geological materials. The inversion results show that the 2D ERI method is a very effective tool for delineating large, shallow

bridge foundations. The 2D ERI can be used for side scanning of a buried concrete foundation, that is much larger than the electrode spacing. Unfortunately the bridge layout showing the original design of the footing is not available so the interpretation was not verified. Without confirmation documentation, two profile surveys conducted perpendicularly can increase the reliability relative to a single profile in any direction.

CHAPTER V

CONCLUSIONS AND DISCUSSION

CONCLUSIONS

The 2D ERI method that has been widely used for land surface surveys can be adapted effectively in water-covered environments. The method is selected as the most appropriate geophysical method for contribution to unknown bridge foundation determination. The method used in this investigation is a cost-effective and rapid method to obtain wide area subsurface information. The notable advantages of ERI are related to low cost, site accessibility, portability, non-invasiveness, fast investigating speed, operator safety, and good resolution. The equipments and field method can often be effectively deployed beneath bridge on land or in water environments over densely vegetated areas that might not be easily accessible to invasive methods. Resistivity data were collected using the SuperSting^{TM} R8/IP, Earth Resistivity/IP, Multi-channel Resistivity Imaging System with 56 stainless steel electrode stakes. The underwater electrodes were built for surveys in mixed terrain underwater environments. The dipole-dipole configuration was used because it provides good sensitivity to horizontal changes and powerful imaging abilities for mapping narrow vertical structures.

The experimentation was divided into one laboratory experimentation at Haynes Laboratory and five experimentations in the field consisting of Bridge 14 and Bridge 15 on FM road 50, the NGES at Texas A&M University, a roadway bridge over the Little Brazos River on highway 21, and a railway bridge over the Brazos River. The experimentation began working on the actual bridge from the smallest foundation, Bridge 14 and Bridge 15, and working up in size to the drilled shafts at a roadway bridge and spread footing at a railway bridge and from known to unknown foundations. The data acquisition has been carried out using two methods of electrode deployments; electrodes are deployed directly across foundations for those foundations that are smaller or equal to the electrode spacing and mainly conducted at drilled shaft and concrete pile foundations. Another approach is to deploy electrodes in proximity to foundations to

image foundations from the side. This is preferred for foundations that are larger than the electrode spacing such as a spread footing. Waterproof underwater electrodes are made and planted on the riverbed in mixed terrain water environments. Data acquisitions were conducted to image foundation in different orientations.

Generally, the ERI method for foundation determination is somewhat straightforward to interpret due to the presence of a fixed foundation position. Since the known position of foundation can be located on the survey profile, interpretation is usually done by qualitative comparison of the observed surface location with that inferred on the specific inversion image. The depth of foundation can be interpreted from the inversion result. The ERI method to image slender foundations is challenging because bridge foundations are cylindrical and vertical. General geological subsurface features such as faults, fractures, or igneous dykes are vertical but spatially elongated features. Optimizing interpretation of the results is necessary to understand the physical condition of the foundation and the resistivity of the subsurface materials. Possible obtained resistivity anomaly of reinforced concrete foundation is related its physical condition. It can be a zone of low resistivity if there exists a conductive rebar cage. Conversely, it can be a zone of high resistivity if there exists an intact condition of foundation.

According to the 2D resistivity forward modeling, the ERI method is a reasonable approach for practical application to bridge foundation determination. The method is more effective when conducted on shallow, large foundations. The laboratory experimentation conducted in the water environment at the Haynes Laboratory found that apparent resistivity values did not change significantly. Resistivity values of the environment (i.e. walls and floor) and foundation are not different significantly. So the experiment was ended and moved to actual bridges in the field to investigate a various sizes of foundations. Experimentation was conducted on small concrete pile foundations in a mixed terrain underwater environment at Bridge 14. A small electrode spacing was used but the concrete piles are still clearly undetectable. If electrode spacing is smaller, clearer foundation anomaly might be obtained but it is not possible to detect the full

depth of a long slender foundation. The experimentation moved to the land environment at Bridge 15. The test was conducted in a row of concrete pile foundations. The surveys were carried out along parallel profiles. The data were reanalyzed by subtracting the measured apparent resistivity values of secondary profiles from those of the primary profile. Subsequently, the processed inversion was repeated. The concrete piles are still not clearly detectable. The conclusion is that the ERI method is not capable of reliably characterizing long and slender concrete pile foundations.

Further experimentation was moved to the NGES to investigate a variety of known 2D and 3D configurations. The 3D data were combined from 2D data sets collected from the eighteen parallel profiles. The 3D inversion model does not yield meaningful results because the designed survey could not cover all major clusters of spread footings and drilled shafts. The 2D experimentation was then substituted and conducted over individual drilled shafts. The depth of drilled shaft cannot be precisely determined with the available data due to a lack of sufficient coverage further than the bottom of the drilled shafts. The inversion images are consistent with results of forward modeling. It can be concluded that these drilled shafts are safe for scour (i.e. they are > 5 m deep). The experiment precisely gave the size and depth of a shallow solid concrete footing, that is 1 m width and 1 m depth. The experimentation was extended to cover two unknown foundations; drilled shaft and spread footing. The anomaly of the unreinforced drilled shaft shows high resistivity near the surface but the interpretation does not precisely indicate its actual depth. The depth of the spread footing is shallower than 5 m. The successful experimentation at the NGES was applied further at actual bridge sites.

The experimentation was moved to an actual roadway bridge. The foundation is a drilled shaft with 1 m in diameter. Two profiles were acquired across foundations in mixed terrain underwater environment. The inversion results can image clearly and consistently the existence of low resistivity anomalies. However, the inversion results cannot reveal a clear shape of the foundation. The shape of the anomaly near the surface and at greater depth are sufficient to interpret and delineate the depth and size of the

foundation. This method can work effectively in a mixed terrain underwater environment. The last experimentation was conducted over an 11x3 m length foundation on a land environment at a railway bridge. Two profiles were perpendicularly deployed near the foundation. The inversion results reveal a good resistivity contrast and image clearly the high resistivity anomalies of the spread footing. The findings are consistent with the forward modeling results of a large foundation. The ERI method is an effective technique for delineating large bridge foundations in terms of depth and size with relatively shallow depth. This method can also be used for side scanning of a large buried concrete foundation in which the foundation is larger than the electrode spacing.

The ERI method has been tested at variable sites using different electrode spacings for different sizes of foundation to understand the effects of electrode spacing on data quality and resolution of resistivity results. From the experiments, it can be summarized that electrodes must be placed at appropriate spacings. Figure 5.1 shows a graph of the appropriate electrode spacing for bridge foundation investigations. Using smaller electrode spacing than 1 m for detecting slender foundations that are smaller than 1 m in diameter is not recommended. Due to the reduction of resolution of the resistivity method with depth, imaging a small and slender foundation with a size of smaller than 1 m at a depth of greater than 5 m is challenging. The smaller the electrode spacing, the finer the resolution. Therefore, the smallest advisable electrode spacing is 1 m.

Generally the maximum depth of dipole-dipole configuration is approximately 20 % of the total length of survey profile. Using greater electrode spacing with the same number of electrodes increases the depth of investigation but reduces the resolution. However, increasing the number of electrodes does not increase depth of survey under certain circumstances because the median depth of investigation of this configuration depends on the electrode spacing a and the dipole factor n. Since the dipole-dipole configuration has comparatively low signal strength, the method of overlapping data levels is recommended. Appropriate electrode spacing recommended imaging foundations between 1-2 m in diameter is 1-1.5 m. For foundation sizes of 2-3 m in

diameter, appropriate electrode spacing is 1.5 m. For large foundations of > 3 m, appropriate electrode spacing is 1.5 m to a maximum of half the foundation size. The greater the electrode spacing, the lower the resolution. Generally the largest foundations are shallow spread footings. A minimum of two integrated profile surveys conducted at different orientations is advisable.

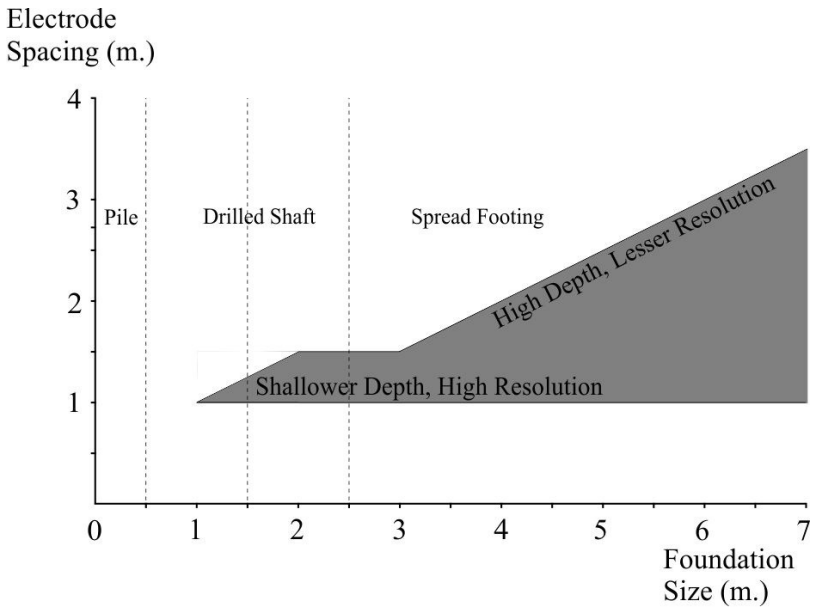

Figure 5.1 The appropriate electrode spacing designed for bridge foundation investigations.

DISCUSSION

There are several geophysical NDT methods that can delineate bridge foundations. However, these methods are limited to one dimension and cannot provide wide-area subsurface coverage. The electrical resistivity method is a geophysics method widely used in engineering and environment applications. The method is somewhat simple in theory and implementation. The method is poorly documented and has not yet been widely applied to unknown foundation determination. From this research, it has

been tested and proven to be applicable and effective to image foundations and surrounding geological materials.

The electrical resistivity of earth materials is mainly related to bulk physical properties such as porosity, water content, clay content, lithology, and fracture density. The electrical resistivity survey method uses the resistivity contrast of subsurface materials to image subsurface structures. If there is not sufficient resistivity contrast of subsurface structures, the method cannot be used efficiently. For example if the earth materials surrounding the foundation, such as intact rocks, are high in resistivity and approach the resistivity of the reinforced concrete foundation; on the other hand if the earth materials surrounding the foundation, such as clay or shale, are low in resistivity approaching the resistivity of the bulk reinforced concrete foundation due to the exposed rebars, the resistivity method is not effectively able to clearly image the zone of foundation anomaly.

For ERI surveys in water-covered areas, direct contact of electrode stakes to the riverbed is advisable. This method can increase the current injected into the earth, and the sensitivity to the subsurface anomaly is much greater than with the floating electrode method. However, it is time consuming and requires effort to install electrodes on the riverbed. Underwater electrodes are simple to design. Although the electrical sensitivity and current strength are lower than that of the land surface environment, it is sufficient to image and identify foundation depth in term of safe or critical for scour. Depth of water that is greater than twice of electrode spacing is not qualified for this method. The sites should be easily accessible during non-flood season. If it is possible, the survey should be conducted on land surface.

A particular bridge site must be evaluated in terms of expected substructure and geological conditions before making survey. The foundation material may be steel, wood, concrete, or masonry. Approximate resistivity of bridge materials and geological materials must be known. In this research, the ERI method has been carried out on only concrete foundations. There is no verification that this method can be applied effectively to other types of foundation materials. Generally scour is critical to only a few meters

deep (i.e. 5 m deep maximum). It is therefore sufficient to image only the upper portion of the foundation to assess bridge safety from scour hazard. Imaging slender foundations at great depths is unlikely because electrical sensitivity and current strength become weaker at increasing depth. However, it may not be necessary for adequate scour hazard assessment.

The electrical resistivity method has drawbacks. The method lacks reliability in some case, and other complementary geophysical methods are advisable in an integrated exploration. For example the induced polarization (IP) method should be also involved in case of a very conductive foundation. The IP may be able to distinguish between the depth, shape of the foundation and subsurface geological materials much clearer than the ERI method, so it is recommended these two methods are deployed simultaneously.

REFERENCES

Adli, Z.H., Musa, M.H., and Arifin, M.N., 2010, Electrical resistivity of subsurface; field and laboratory assessment, world academy of science: Engineering and Technology, **69**, 805-808.

AGI, 2006, Instruction manual for the SuperSting™ with swift™ automatic resistivity and IP system: Advanced Geosciences Inc.

___, 2007, 2D resistivity and IP inversion software instruction manual: Advanced Geosciences Inc.

___, 2010, Advanced resistivity imaging: Advanced Geosciences Inc.

Amidu, S.A., and Olayinka, A.I., 2006, Environmental assessment of sewage disposal systems using 2D electrical resistivity imaging and geochemical analysis; A case study from Ibadan, Southwestern Nigeria: Environmental & Engineering Geoscience, **12**, 261-272.

Anderson, N., Hoover, R., and Sirles, P., 2008, Geophysical methods commonly employed for geotechnical site characterization: Transportation Research Broad of the National Academies.

Archie, G.I., 1942, The electrical resistivity log as an aid in determining some reservoir characteristics: Transaction American Institute of Mining and Metallurgical Engineering, **146**, 54-62.

Aristodemou, E., and Thomas, A., 2000, DC resistivity and induced polarization investigations at a waste disposal site and its environments: Journal Applied Geophysics, **44**, 275-302.

Ballouz, M., Nasr, G., and Briaud, J.L., 1991, Dynamic and static testing of nine drilled shafts at Texas A&M University geotechnical research sites: Geotechnical Engineering Department of Civil Engineering, Texas A&M University.

Barkdoll, D., Ettema, R., and Melville, B., 2007, Countermeasures to protect bridge abutments from scour: National Cooperative Highway Research Program.

Barker, P., 1993, Techniques of archaeological excavation: Taylor & Francis e-Library.

Barker, R.D., 1996, The application of electrical tomography in groundwater contamination studies: EAGE 58th Conference and Technical Exhibition, Extended Abstracts, P082.

Beard, J., 2009, FHWA unknown foundations summit, investigating unknown foundations in North Carolina: North Carolina Department of Transportation, North Carolina.

Bernard, J., 2003, The depth of investigation of electrical methods: IRIS-instruments.

_____, J., Leite, O., and Vermeersch, F., 2005, Multi-electrode resistivity imaging for environmental and mining applications: IRIS Instruments.

Bichler, A., P. Bobrowsky, M. Best, M. Douma, J. Hunter, T. Calvert, and R. Burns, 2004, 3D mapping of a landslide using a multi–geophysical approach; the Quesnel Forks Landslide: Landslides, **1**, 29-40.

Breen, R., Brown, T.M., Collins, T.J., Dillworth, B., Garlich, M., Kaderbek, S., O'Toole, M.A., Stromberg, D., and Triandafilou, N., 2010, Indiana bridge inspection manual: Collins Engineers Inc.

Browne, D., 1982, Design prediction of the life for reinforced concrete in marine and other chloride environments. In: Su, J.K., Yang, C.C., Wu, W.B., and Huang, R., 2002, Effect of moisture content on concrete resistivity measurement: Journal of the Chinese Institute of Engineers, **25**, 117-122.

Buselli, G., and Lu, K., 2001, Groundwater contamination monitoring with multichannel electrical and electromagnetic methods: Journal of Applied Geophysics, **48**, 11-23.

Castilho, G., and Maia, D., 2008, A successful mixed land underwater 3D resistivity survey in an extremely challenging environment in Amazônia: 21th EEGS Symposium on the Application of Geophysics to Engineering and Environmental Problems, 1150-1158.

Chen, W.F., and Duan, L., 2000, Bridge engineering handbook: CRC Press.

Chouteau, M., and Beaulieu, S., 2010, An investigation on application of the electrical resistivity tomography method to concrete structures: 4th International Conference on Seismic Retrofitting.

Chung, H.J., Kim, J.H., Park, K.P., Kwon, H.S., Choi, H.S., Kim, K.S., and Kim, J.S., 2001, Application of geophysical results to designing bridge over a large fault: 4th Asian Young Geotechnical Engineers Conference.

Conrad, C., 2010, Electrical resistivity side scanning for bridge foundation investigation: GTS Technologies Inc.

COST 509, 1997, Corrosion and protection of metals in contact with concrete. In: Polder R., 2000, Test methods for on site measurement of resistivity of concrete, Materials and Structures, **33**, 603-611.

Cully, R.W., Jagodits, F.L., and Middleton, R.S., 1975, E-phase system for detection of buried granular deposits: Symposium on Modern Innovations in Subsurface Exploration, 54th Annual Meeting of Transportation Research Board.

Dahlin, T., 2001, The development of DC resistivity imaging techniques: Computers & Geosciences, **27**, 1019-1029.

_____, T., and Bernstone, C., 1997, A roll-along technique for 3D resistivity data acquisition with multi-electrode arrays: Symposium on the Application of Geophysics to Engineering and Environmental Problems, **2**, 927-935.

_____, T., and Zhou, B., 2004, A numerical comparison of 2D resistivity imaging with 10 electrode arrays: Geophysical Prospecting, **52**, 379-398.

Day-Lewis, F.D., White, E.A., Johnson, C.D., and Lane, J.W., 2006, Continuous resistivity profiling to delineate submarine groundwater discharge; examples and limitations: The Leading Edge, **25**, 724-728.

Delphia, J., 2010, PowerPoint presentation on an action to address bridges with unknown foundation for scour: Texas Department of Transportation, Texas.

Denil, M., and Canavello, D., 2005, Geophysical investigation report; electrical resistivity investigation: Pyramid Environmental & Engineering.

Ellis, R.G., and Oldenburg, D.W., 1994, Applied geophysical inversion: Geophysical Journal International, **116**, 5-11.

FHWA, 2004, Determination of unknown bridge foundations: Federal Highway Administration, U.S. Department of Transportation.

_____, 2006, Scour technology: Federal Highway Administration, U.S. Department of Transportation.

Fukue, M., Minatoa, T., Horibe, H., and Taya, N., 1999, The microstructure of clay given by resistivity measurements: Engineering Geology, **54**, 43-53.

Gagliano, M., 2010, Assessment of electrical resistivity method to map groundwater seepage zones in heterogeneous sediments at Mirror Lake, NH: Master Thesis, Temple University.

Gakkai, B.T., 2004, Application of geophysical methods to engineering and environmental problems: Society of Exploration Geophysicist of Japan.

Garcia, M., 2007, ASSC manuals and report on engineering practice; sedimentation engineering, processes, measurements, modeling, and practice: American Society of Civil Engineer.

Gharibi, M., and Bentley, R., 2005, Resolution of 3D electrical resistivity images from inversions of 2D orthogonal lines: Journal of Environmental & Engineering Geophysics, **10**, 339-349.

Giao, P.H., Chung, S.G., Kim, D.Y., and Tanaka, H., 2003, Electric imaging and laboratory resistivity testing for geotechnical investigation of Pusan clay deposits: Journal Applied Geophysics, **52**, 157-175.

Gibbend, R.M.V,. 1995, Load tests on five large spread footing on sand and evaluation of prediction methods: Master Thesis, Texas A&M University.

Gonzalez, J.A., Lopez, W., and Rodriguez, P., 1993, Effect of moisture availability on corrosion kinetics of steel embedded in concrete. In: Su, J.K., Yang, C.C., Wu, W.B., and Huang, R., 2002, Effect of moisture content on concrete resistivity measurement: Journal of the Chinese Institute of Engineers, **25**, 117-122.

Griffiths, D.H., and Barker, R.D., 1993, 2D resistivity imaging and modeling in areas of complex geology: Journal Applied Geophysics, **29**, 211-226.

Günther, T., Rucker, C., and Spitzer, K., 2006, 3D modeling and inversion of DC resistivity data incorporating topography - part II; Inversion: Geophysics Journal International, **166**, 506-517.

Harrigan, E., and Reynaud, A., 2008, Research results digest 334; joint workshop on abutment scour: National Cooperative Highway Research Program.

Hiltunen, D. and Roth, M., 2003, Investigation of bridge foundation sites in karst terrain via multi-electrode electrical resistivity: 3rd International Conference on Applied Geophysics - Geophysics 2003.

Hsu, H., Yanites, B., Chen, C., and Chen, Y, 2010, Bedrock detection using 2D electrical resistivity imaging along the Peikang River, central Taiwan: Geomorphology, **114**, 406-414.

Humkeler, F., 1996, The resistivity of pore water solution-a decisive parameter of rebar corrosion and repair methods: Construction and Building Materials, **10**, 381-389.

INDOT, 2010, Bridge inspection manual: Indiana Department of Transportation, Indiana.

Kearey, P., and Brooks, M., 2002, An introduction to geophysical exploration: Blackwell Science Publications.

Khwairakpam1, P., and Mazumdar, A., 2009, Local scour around hydraulic structures: International Journal of Recent Trends in Engineering, **1**, 69-61.

Kim, J.H., Yi, M.J., Song, Y., Cho, S.-J. Chung, S.-H., and Kim, K.S., 2002, DC resistivity survey to image faults beneath a riverbed: 15th EEGS Symposium on the Application of Geophysics to Engineering and Environmental Problems.

Kimmerling, R.E., 2002, Shallow foundations: Federal Highway Administration, U.S. Department of Transportation.

Krautblatter, M., Hauck, C., 2007, Electrical resistivity tomography monitoring of permafrost in solid rock walls: Journal of Geophysics Research, **112**, F02S20.

Kress, W.H., and Teeple, A.P., 2005, 2D resistivity investigation of the North Cavalcade street site, Houston, Texas: U.S. Geological Survey.

Kwon, H.S., Kim, J.H., Ahn, H.Y., Yoon, J.S., Kim, K.S., Jung, C.K., Lee, S.B., and Uchida, T., 2005, Delineation of a fault zone beneath a riverbed by an electrical resistivity survey using a floating streamer cable: Geophysical Exploration, **58**, 50-58.

Lagasse, P., Clopper, P., Zevenbergen, L., and Girard, L., 2007, Countermeasures to protect bridge piers from scour: National Cooperative Highway Research Program.

Leftor, J., 1993, Instrumentation for measuring scour at bridge piers and abutments: Transportation Research Board of the National Academies.

Loke, M.H., 1994, The inversion of 2D resistivity data: PhD thesis, University of Birmingham. In: Loke, M.H., 2010, 2D and 3D electric imaging surveys:

Geoelectric Company.

____, M.H, 1999, Rapid 2D resistivity forward modeling using the finite difference and finite element methods: Geotomo Software Sdn Bsd.

____, M.H., 2000, Electrical imaging surveys for environmental and engineering studies; a practical guide to 2D and 3D surveys: Geotomo Software Sdn Bsd.

____, M.H., 2001, RES3DMOD ver. 2.1: Geotomo Software Sdn Bsd.

____, M.H., 2002, RES2DMOD ver. 3.01: Geotomo Software Sdn Bsd.

____, M.H., 2004a, RES2DINV ver. 3.54: Geotomo Software Sdn Bsd.

____, M.H., 2004b, RES3DINV ver. 2.14: Geotomo Software Sdn Bsd.

____, M.H., 2010, 2D and 3D electric imaging surveys: Geotomo Software Sdn Bsd.

____, M.H., Acworth I., and Dahlin T., 2003, A comparison of smooth and blocky inversion methods in 2D electrical imaging surveys: Exploration Geophysics, **34**, 182-187.

____, M.H., and Barker, R.D., 1996, Practical techniques for 3D resistivity surveys and data inversion: Geophysical Prospecting, **44**, 499-523.

____, M.H. and Lane, J.W., 2004, Inversion of data from electrical resistivity imaging surveys in water covered areas: Exploration Geophysics, **35**, 266-271.

Louis, C., 1995, Nondestructive testing: ASM International.

Maxey, G.B., 1964, Handbook of applied hydrology: McGraw Hill.

McNeill, J.D., 1980, Electrical resistivity of rocks and soils: Geonics Limited.

MDOT, 2008, MDOT geotechnical manual: Minnesota Department of Transportation, Minnesota.

Melville, B., and Coleman, S., 2000, Bridge scour: Water Resources Publications.

Meyboom, P., 1969, Hydrogeology groundwater in Canada: Geological Survey of Canada.

Mitchell, J.K., 1993, Fundamentals of soil behavior: John Wiley & Sons.

ODOT, 2011, Introduction to bridge foundations: The Oregon Department of Transportation, Oregon.

Olson, L D., 2002, Determination of unknown bridge foundation depths with NDE methods: 1st International Conference on Scour of Foundations.

_____, L.D., 2003, Determination of unknown bridge foundation depths with NDE methods: TRB 2003 Annual Meeting, Louisiana Transportation Research Center.

_____, D.L., and Aouad, M.F., 1998, Research results on determination of unknown bridge foundation depths: Olson Engineering Inc.

_____, D., Jalinoos, F., and Aouad, M., 1998, Determination of unknown subsurface bridge foundations: National Cooperative Highway Research Program.

_____, L.D., Liu, M., and Aouad, M.F., 1996, Borehole NDT techniques for unknown subsurface bridge foundation testing: Proceeding of SPIE 2946.

Ostrom, T.A., Post, S.H., and Barbour, M.A., 2000, Deep foundation: California Department of Transportation, California.

Polder, R., 2001, Test methods for on site measurement of resistivity of concrete: Construction and Building Material, **15**, 125-131.

_____, R., Andrade, C., Elsener, B., Vennesland, O., Gulikers, J., Weidertand, R., and Raupach, M., 2000, Test methods for on site measurement of resistivity of concrete: Materials and Structures , **33**, 603-611.

Richardson, V., and Davies, R., 1995, Evaluating scour at bridges: Federal Highway Administration, U.S. Department of Transportation.

Rucker, M., 2006, Surface geophysics for characterizating existing bridge foundation and scour conditions: The Geophysics 2006 Conference.

Saarenketo, T., 1998, Electrical properties of water in clay and silty soils: Journal of Applied Geophysics, **40**, 73-88.

Samouëlian, A., Cousin, I., Tabbagh, A., Bruand, A., and Richard, G., 2005, Electrical resistivity survey in soil Science; a review: Soil and Tillage Research, **83**, 173-193.

_____, A., Isabelle, C., Richard, G., Tabbargh, A., and Bruand, A., 2003, Electrical

resistivity imaging for detecting soil cracks at the centimetric scale: Soil Science Society of America Journal, **67**, 1319-1326.

SCDOT, 2010, Geotechnical design manual: The South Carolina Department of Transportation, South Carolina.

Schoor, M., 2002, Detection of sinkholes using 2D electrical resistivity imaging: Journal of Applied Geophysics, **50**, 393-399.

Scollar, I., Tabbagh, A., Hesse, A., and Herzog, I., 1990, Archaeological prospecting and remote sensing: Cambridge University Press.

Sharma, V., 1997, Environmental and engineering Geophysics: Cambridge University Press.

Smith, C., and Vozoff, K., 1984, 2D dc resistivity inversion for dipole-dipole data: IEEE Transactions on Geoscience and Remote Sensing, **22**, 21-28.

Song, H.W., and Saraswathy1, V., 2007, Corrosion monitoring of reinforced concrete structures - a review: International Journal Electrochemical Science, **2**, 1-28.

Stein, S., and Sedmera, K., 2006, Risk based management guidelines for scour at bridges with unknown foundations: National Cooperative Highway Research Program.

Stolarczyk, G., and Peng, S., 2003, Advanced electromagnetic wave technologies for the detection of abandoned mine entries and delineation of barrier pillars: Mine Safety and Health Administration and Office of Surface Mining Reclamation and Enforcement, Kentucky.

Su, J.K., Yang, C.C., Wu, W.B., and Huang, R., 2002, Effect of moisture content on concrete resistivity measurement: Journal of the Chinese Institute of Engineers, **25**, 117-122.

Taylor, S., and Barker, R., 2006, Modeling the DC electrical response of fully and partially saturated Permo-Triassic sandstone: Geophysical Prospecting, **54**, 351-367.

Telford, W.M., Geldart, L.P., and Sheriff, R.E., 1990, Applied geophysics: Cambridge University Press.

Tuutti, K., 1982, Corrosion of steel in concrete. In: Polder R.B., 2001, Test methods for on site measurement of resistivity of concrete - a RILEM TC-154 technical recommendation: Construction and Building Materials, **15**, 125-131.

Udphuay, S., 2008, 3D electrical resistivity tomography for cliff stability assessment at Pointe du Hoc in Normandy, France: Ph.D. Dissertation, Texas A&M University.

Verma, R.K., and Bhuin, N.C., 1979, Use of Electrical resistivity methods for study of coal seams in parts of the Jharia coalfield, India: Geoexploration, **17**, 163-176.

Warren, L.P., 1993, Scour at bridges, what is it all about?; stream stability and scour assessment at bridges in Massachusetts: U.S. Geological Survey.

Wightman, W., and Jalinoos F., 2003, Application geophysical methods to highway related problem: Federal Highway Administration, U.S. Department of Transportation.

Yang, X., 1999, Stochastic inversion of 3D ERT data: Ph.D. Thesis, The University of Arizona.

Yang, X., and Lagmanson, M.B., 2003, Planning resistivity surveys using numerical simulations: Proceedings of the Symposium for the Application of Geophysics to Environmental and Engineering Problems, 488-501.

Zevenbergen, L.W., 2004, New AREMA bridge scour resources: 2004 Annual Conference & Exposition.

Zhou, B., and Dahlin, T., 2003, Properties and effects of measurement errors on 2D resistivity imaging surveying: Near Surface Geophysics, **1**, 105–117.

APPENDIX A

SUMMARY OF ERI DATA ACQUISITION

Profiles	Type of Foundation	Profile Length	Total of Electrode	Electrode Spacing	Date Acquired
BG14	Concrete piles	69.5	56 R-along	0.5	11-30-09
B15A	Concrete piles	33.5	56	0.61	01-27-10
B15B	Concrete piles	33.5	56	0.61	01-27-10
B15C	Concrete piles	33.5	56	0.61	01-27-10
BG15A	Concrete piles	55	56	1	01-29-10
BG15B	Concrete piles	55	56	1	01-29-10
BG15-1*	Concrete piles	55	56	1	01-29-10
BG15-2*	Concrete piles	55	56	1	01-29-10
BG15-A*	Concrete piles	27.5	56	0.5	01-30-10
BG15-B*	Concrete piles	27.5	56	0.5	01-30-10
NGES1	DS and SF	55	56	1	05-24-10
NGES2	DS and SF	55	56	1	05-24-10
NGES3	DS and SF	55	56	1	05-24-10
NGES4	DS and SF	55	56	1	05-24-10
NGES5	DS and SF	55	56	1	05-25-10
NGES6	DS and SF	55	56	1	05-25-10
NGES7	DS and SF	55	56	1	05-25-10
NGES8	DS and SF	55	56	1	05-25-10
NGES9	DS and SF	55	56	1	05-26-10
NGES10	DS and SF	55	56	1	05-26-10
NGES11	DS and SF	55	56	1	05-26-10
NGES12	DS and SF	55	56	1	05-26-10
NGES13	DS and SF	55	56	1	05-27-10
NGES14	DS and SF	55	56	1	05-27-10
NGES15	DS and SF	55	56	1	05-27-10
NGES16	DS and SF	55	56	1	05-28-10
NGES17	DS and SF	55	56	1	05-28-10
NGES18	DS and SF	55	56	1	05-28-10
NGES19	DS and SF	55	56	1	06-03-10
NGES20	DS and SF	55	56	1	06-03-10
NGES21	DS and SF	55	56	1	06-04-10
NGES22	DS and SF	55	56	1	06-04-10
NGES23	DS and SF	55	56	1	06-05-10

TS2A	Drilled Shaft	55	56	1	01-19-11

Profiles	Type of Foundation	Profile Length	Total of Electrode	Electrode Spacing	Date Acquired
TS2B	Drilled Shaft	55	56	1	01-19-11
TS2C	Drilled Shaft	55	56	1	01-19-11
SF1A	Spread Footing	13.5	28	0.5	01-24-11
SF1B	Spread Footing	13.5	28	0.5	01-24-11
SF1-3D	Spread Footing	6.5x4	56	0.5X, 1Y	01-25-11
UK1A	Drilled Shaft	55	56	1	02-15-11
UK1B	Drilled Shaft	55	56	1	02-15-11
TS4A	Drilled Shaft	55	56	1	02-28-11
TS4B	Drilled Shaft	55	56	1	02-28-11
RS5A	Drilled Shaft	55	56	1	02-28-11
F1	Spread Footing	55	56	1	01-30-11
SF3A	Spread Footing	27	28	1	01-25-11
SF3B	Spread Footing	27	28	1	01-25-11
SF3C	Spread Footing	27	28	1	01-25-11
SF3D	Spread Footing	27	28	1	01-25-11
SF3E	Spread Footing	27	28	1	01-25-11
SF3F	Spread Footing	27	28	1	01-25-11
BHW21A	Drilled Shaft	55	56	1	04-07-11
BHW21B	Drilled Shaft	55	56	1	04-26-11
RWB1	Spread Footing	54	28	2	07-06-11
RWB2	Spread Footing	54	28	2	07-06-11

* Inversion images are not included in this dissertation, DS is the drilled shaft, and SF is the spread footing.

APPENDIX B

RES2DINV INVERSION PARAMETERS

Lists of 2D inversion parameters for data of bridge foundation determination

Software: RES2DINV ver. 3.54

INVERSION DAMPING PARAMETERS

Damping factor
- Initial damping factor is 0.16, (larger for nosier data set).
- Minimum damping factor is 0.015, (larger for nosier data set).

Increase of damping factor with depth is 1.05.
Not attempt to optimize damping factor at each iteration.
Range of resistivity values are limited.
- Upper resistivity cutoff limit is 20.00.
- Lower resistivity cutoff limit is 0.05.
- Average resistivity used.

Vertical to horizontal flatness filter ratio is 2.0 for drilled shape and 1 for footing.

MESH PARAMETERS

4 nodes per unit electrode spacing.
Use finite-element method.
Use finer mesh.

INVERSION PROGRESS

Always use line search.
Minimum change in RMS error is 0.40.
Convergence limit is 1.00.
RMS convergence limit is 1.00.
Number of iterations is 10.

INVERSION METHODS

Not include smoothing model resistivity.
Not use combined inversion method.
Select robust inversion.
- Cutoff factor of data inversion constrain is 0.05.
- Cutoff factor of model inversion constrain is 0.001.

Use logarithms of apparent resistivity.
Recalculate the Jacobian matrix for all iterations.

No time lapse.

MODEL DISCRETIZATION

Layer thickness increase by 25%.
Not use extended model
Severely reduce the effect of the side blocks.
Use normal unit width model blocks.
Use model cells with widths of half the unit spacing.

TOPOGRAPHIC OPTIONS

Least-squares straight line is removed.
Distorted finite-element grid with uniform distortion.

APPENDIX C

2D INVERSION MODELS FOR QUASI 3D INVERSION MODEL

Inversion models along eighteen parallel profiles (NGES 1-18).

Inversion models along five perpendicular profiles (NGES 19-23), not include in 3D.

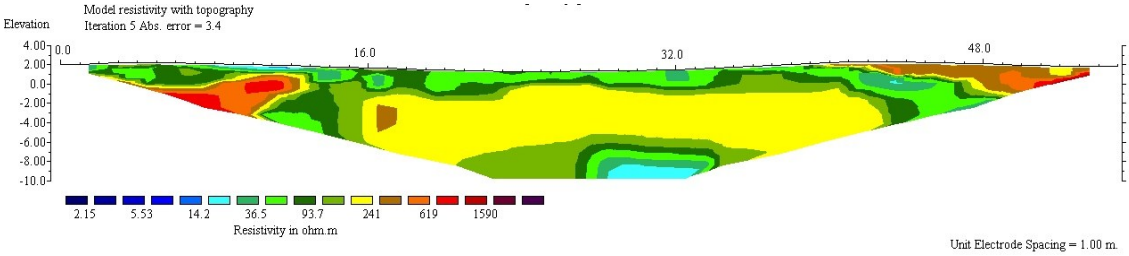

NGES 1

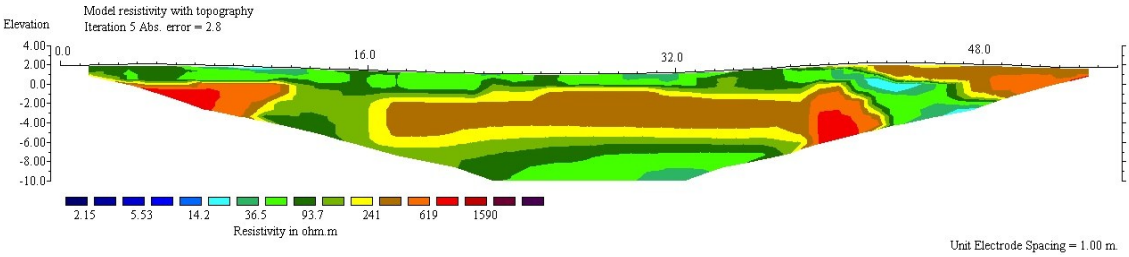

NGES 2

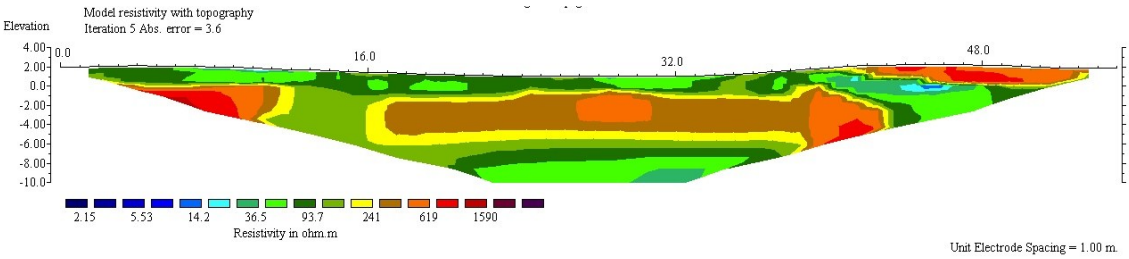

NGES 3

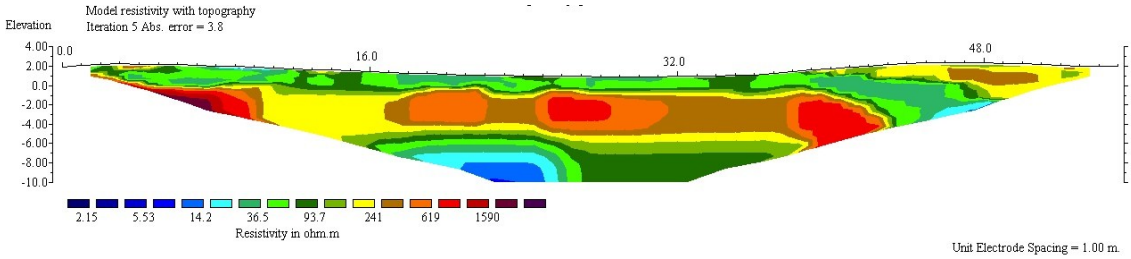

NGES 4

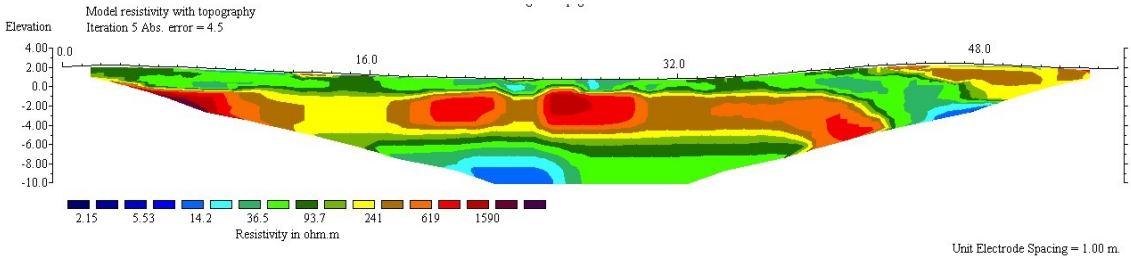

NGES 5

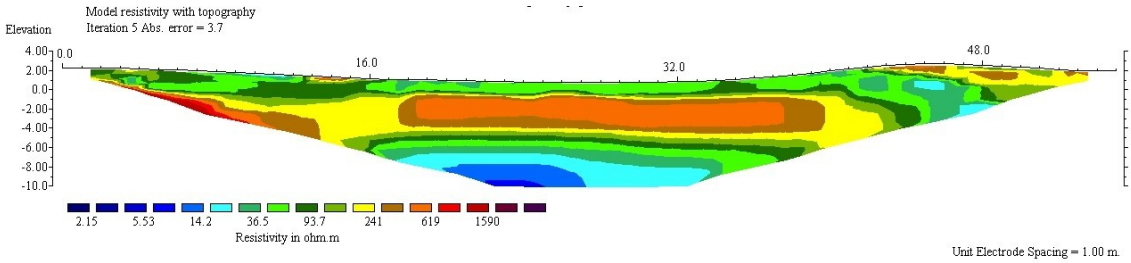

NGES 6

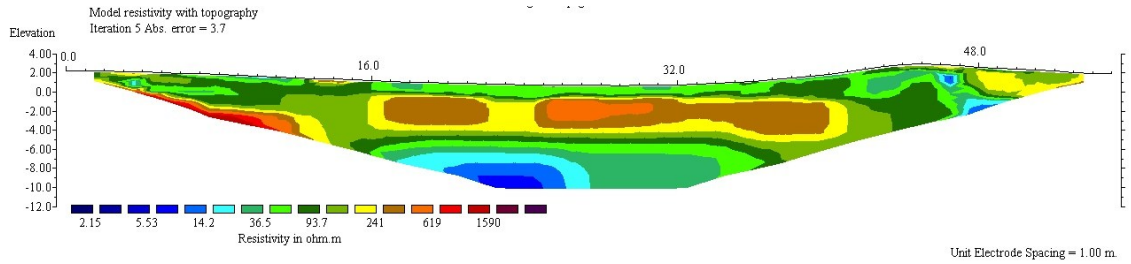

NGES 7

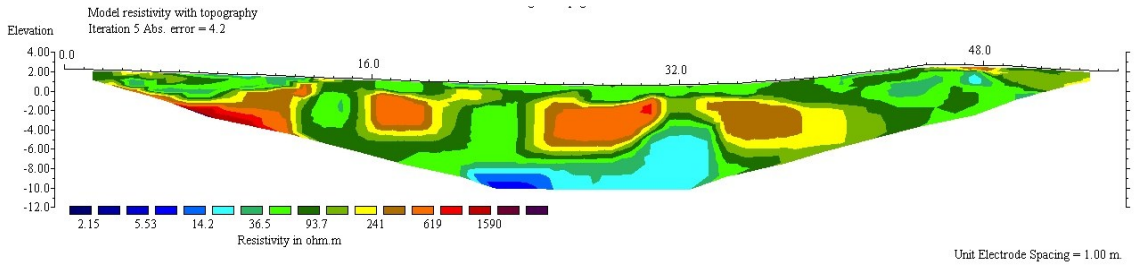

NGES 8

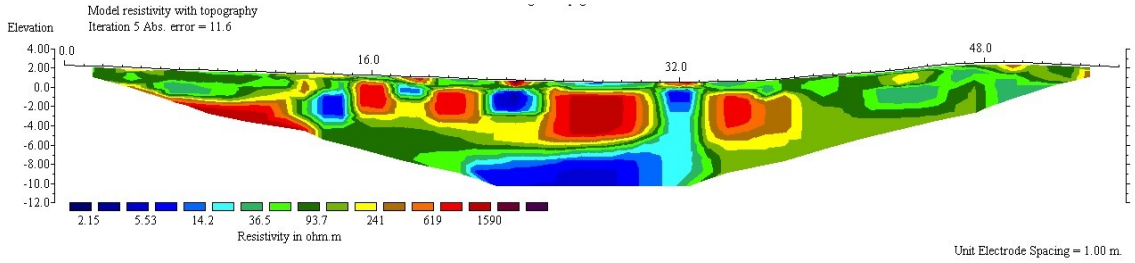

NGES 9

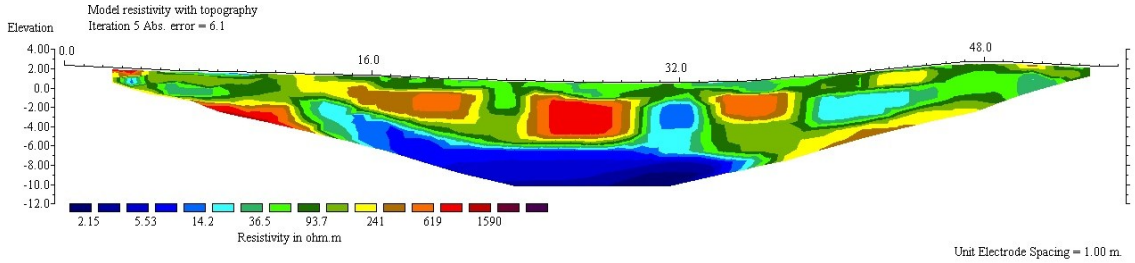

NGES 10

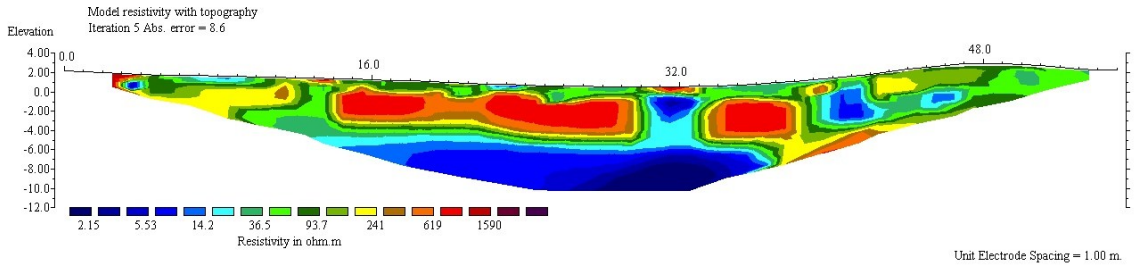

NGES 11

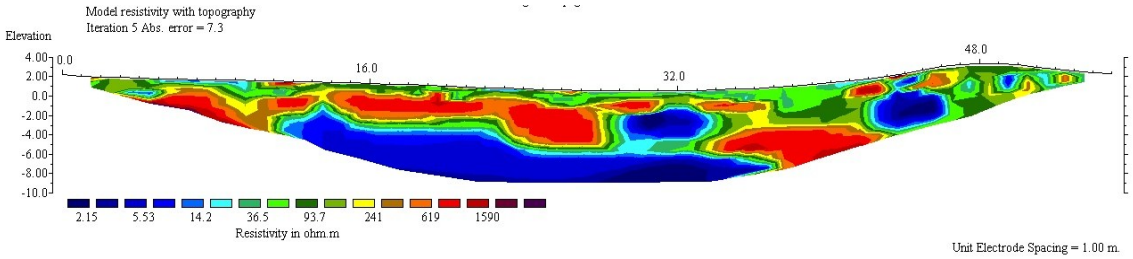

NGES 12

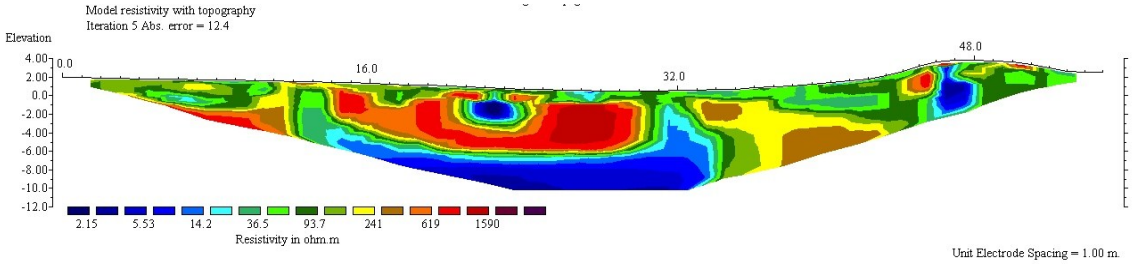

NGES 13

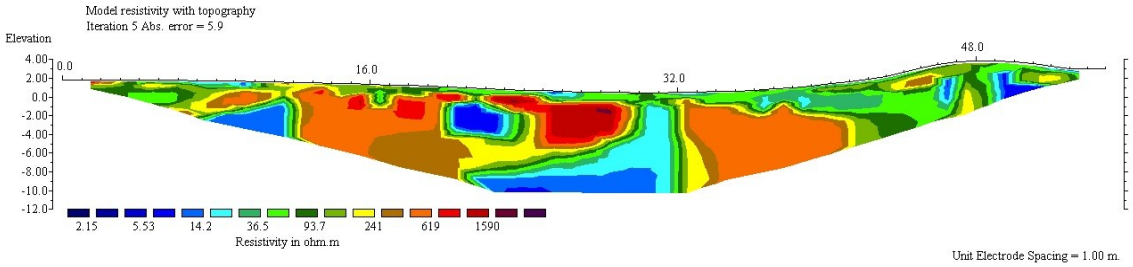

NGES 14

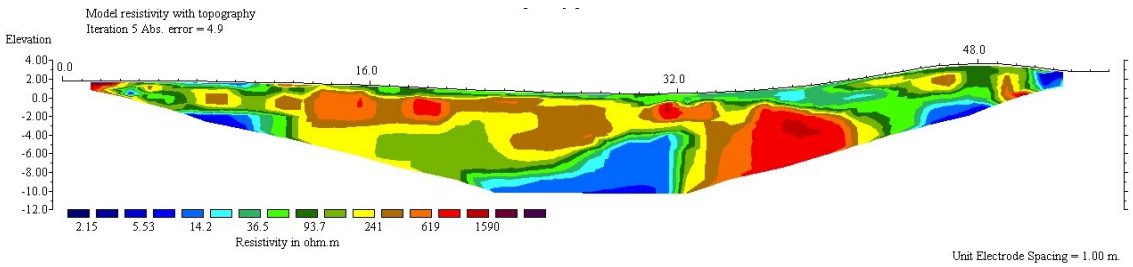

NGES 15

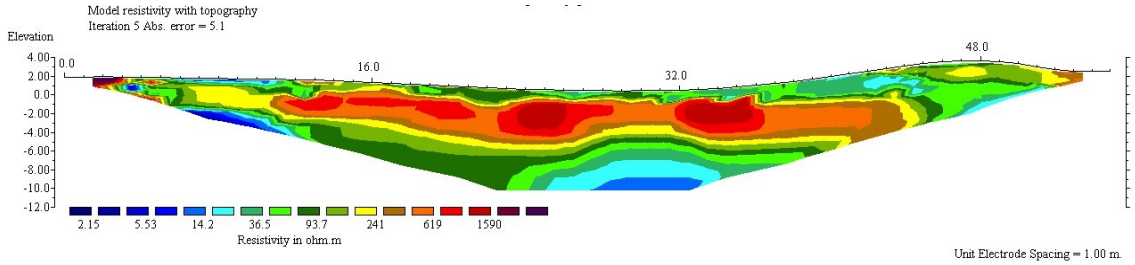

NGES 16

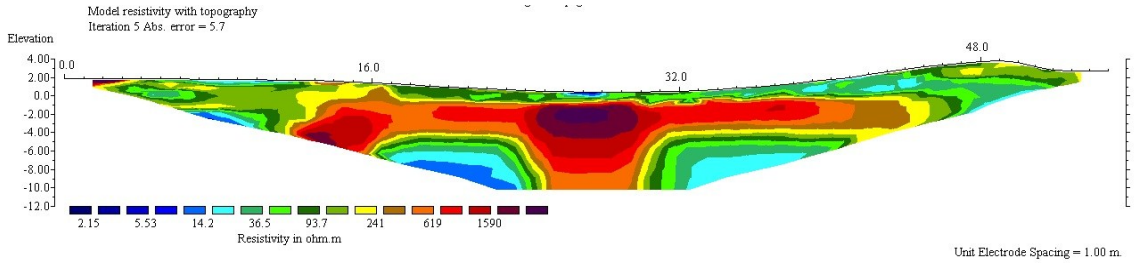

NGES 17

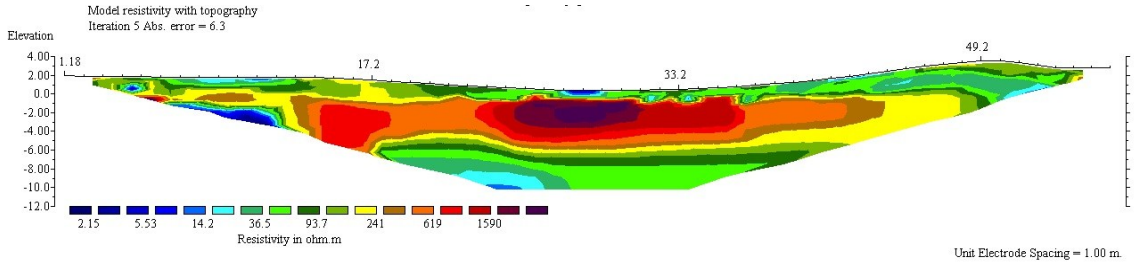

NGES 18

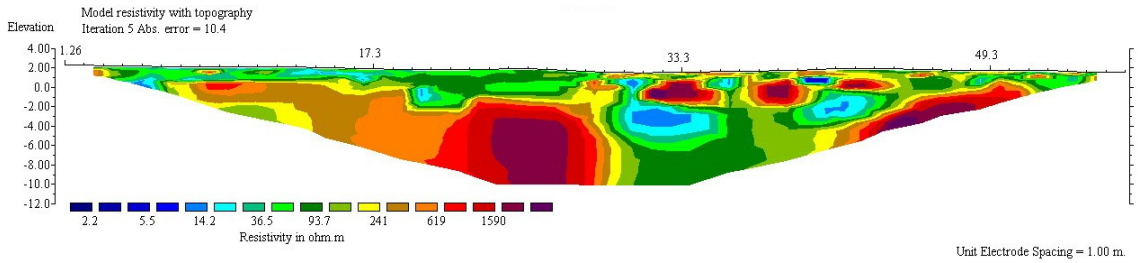

NGES 19

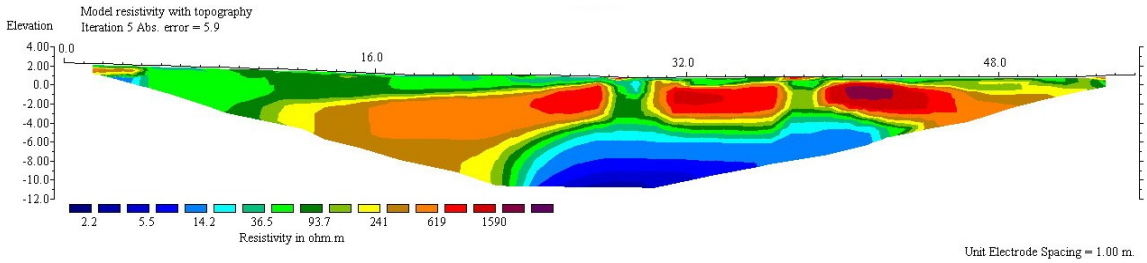

NGES 20

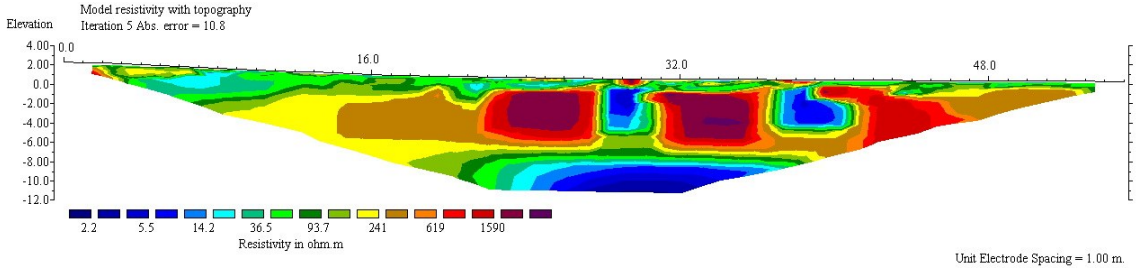

NGES 21

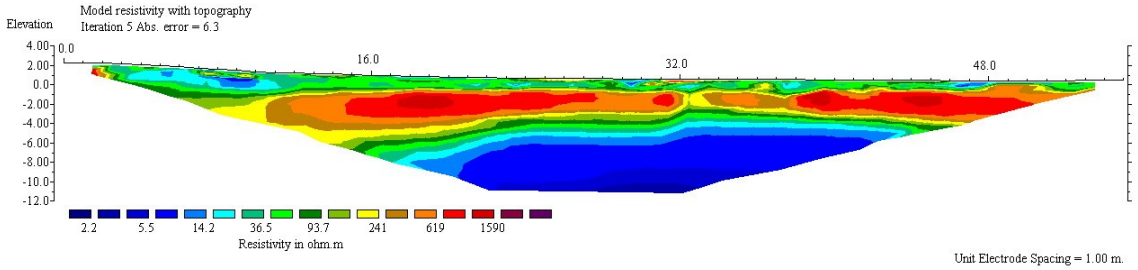

NGES 22

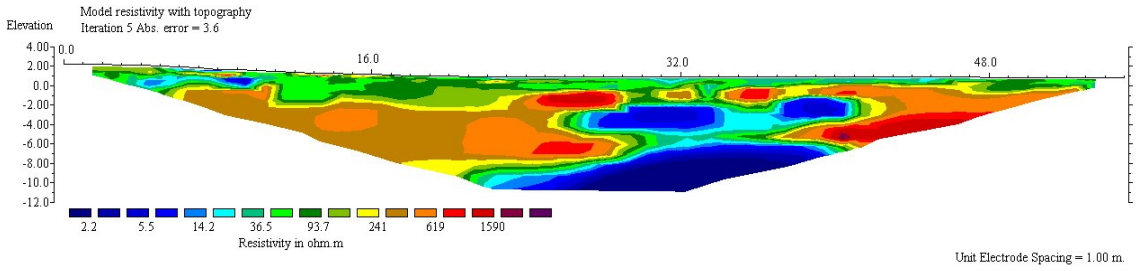

NGES 23

APPENDIX D

3D SYNTHETIC MODELS

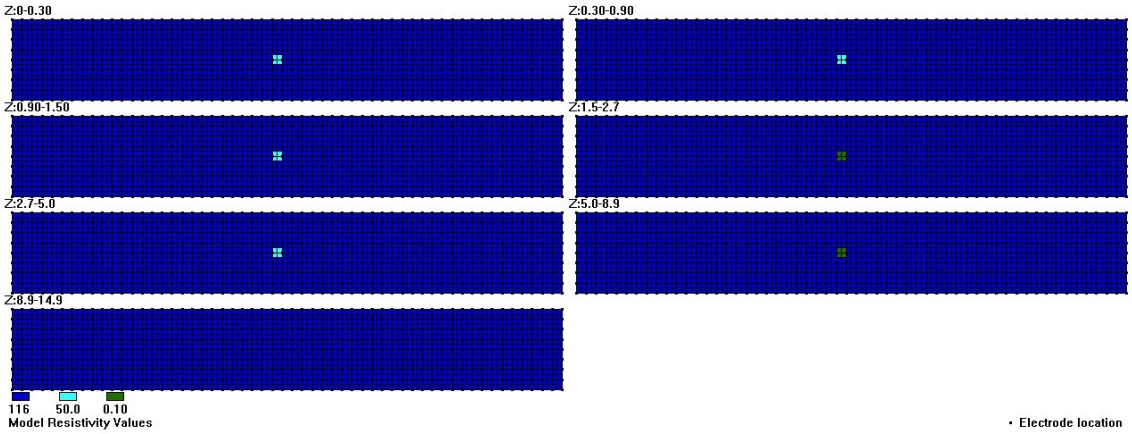

Synthetic model of 1x1x9 m foundation.

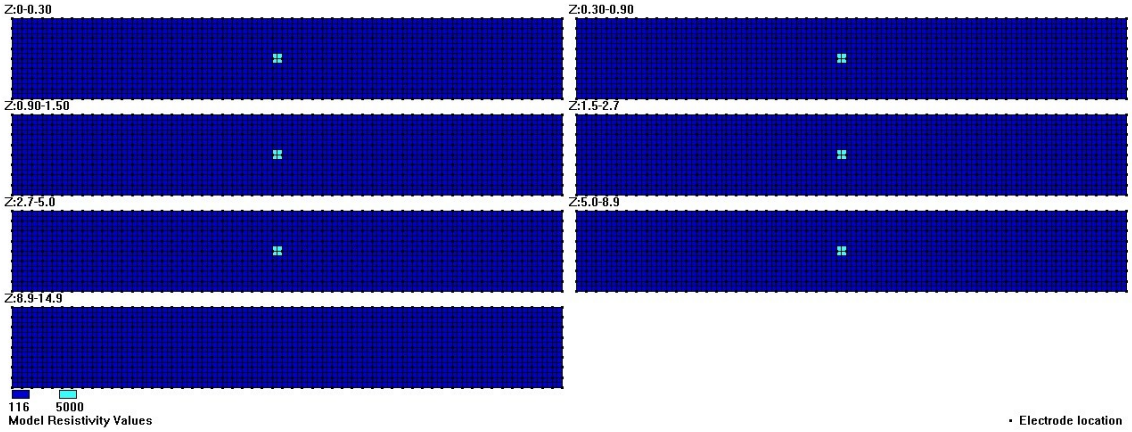

Synthetic model of 1x1x9 m foundation.

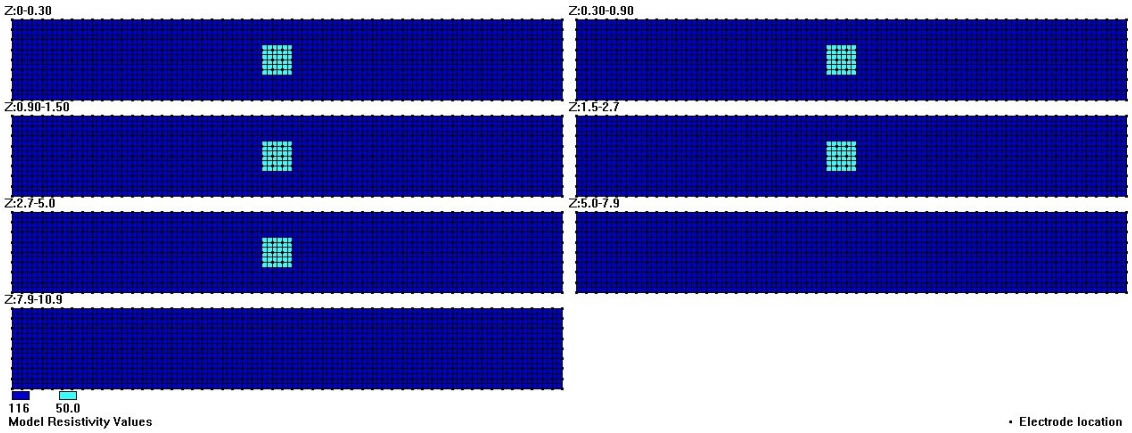

Synthetic model of 3x3x5 m foundation.

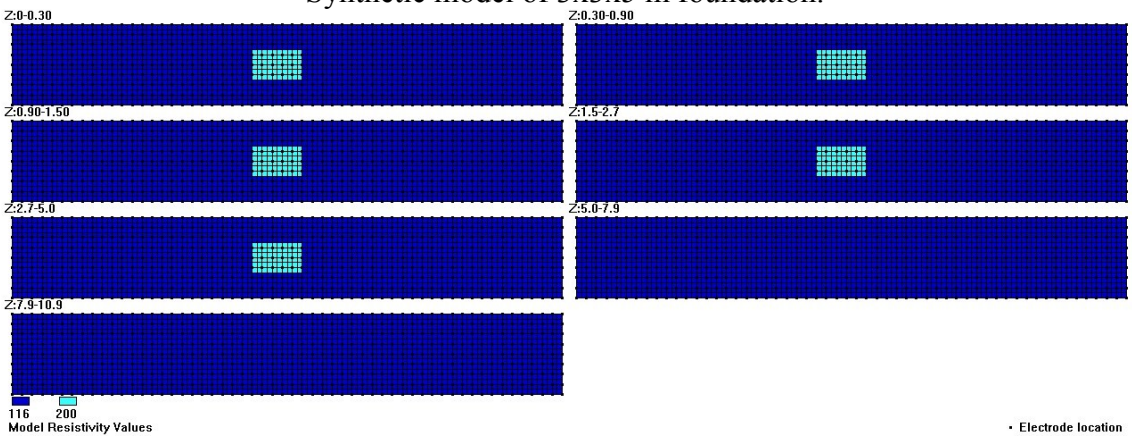

Synthetic model of 5x3x5 m foundation.

APPENDIX E

LAYOUTS OF KNOWN FOUNDATIONS

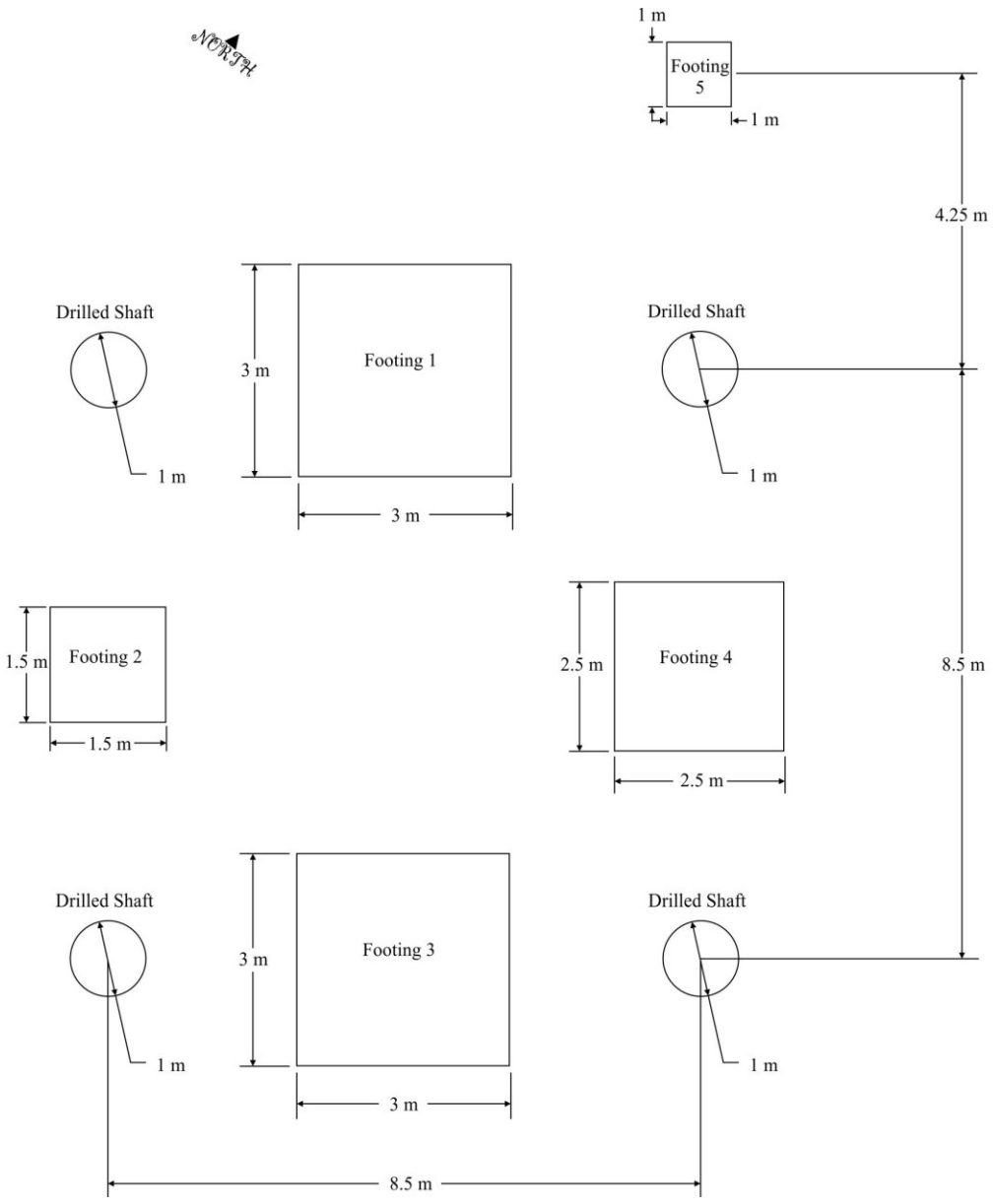

Footing and drilled shaft layout at the NGES (Gibbend, 1995).

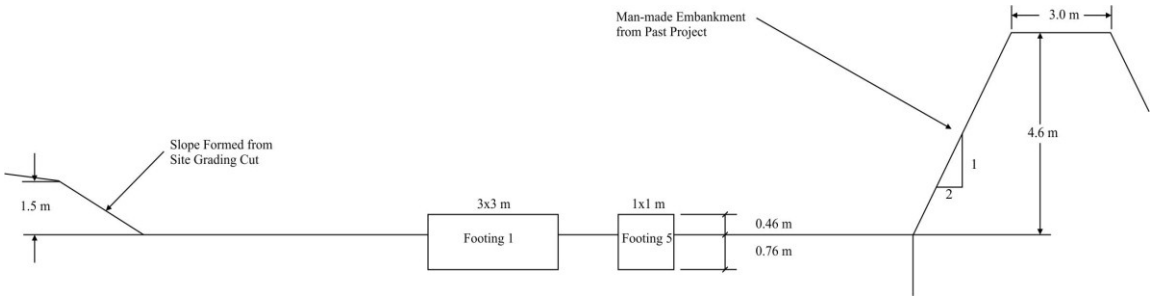

Site cross section of the layout over spread footings at the NGES (Gibbend, 1995).

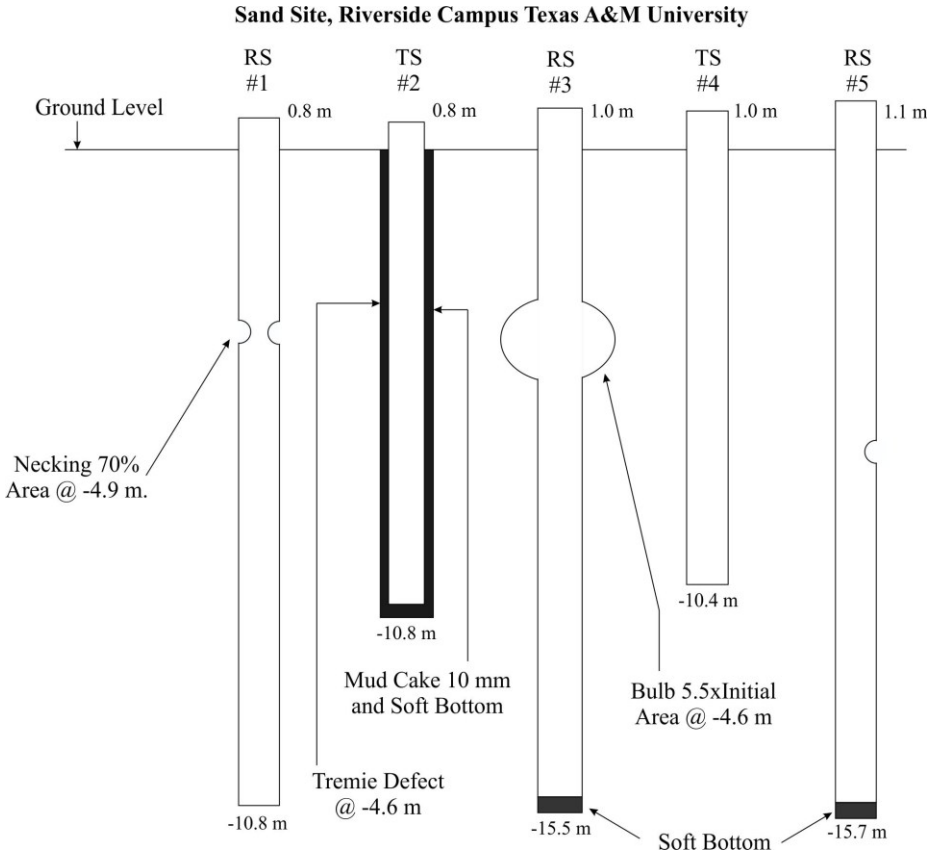

Cross-section of drilled shaft construction plan at the NGES (Ballouz et al. 1991).

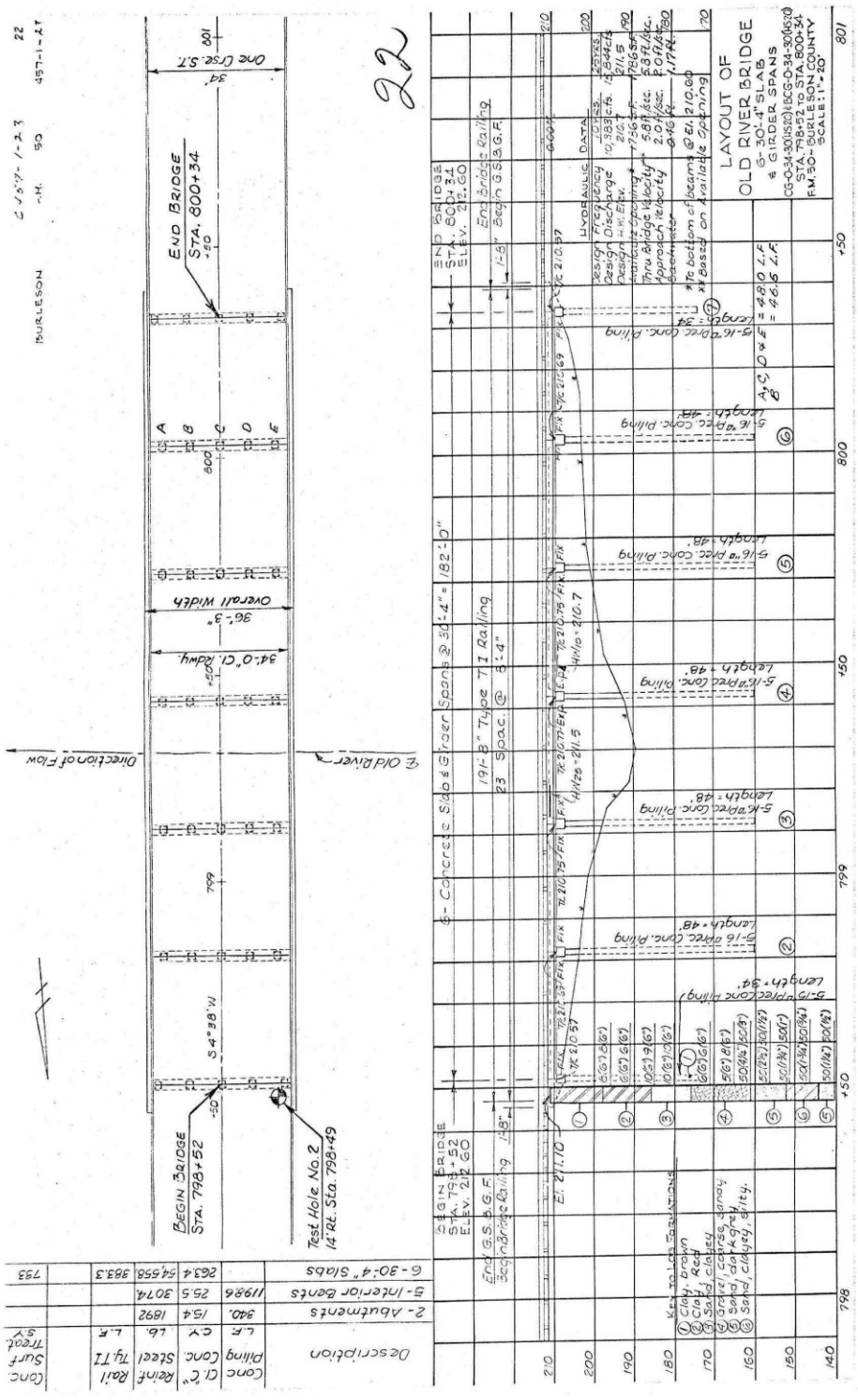

Lay out of Bridge 14 over Old River on FM Road 50

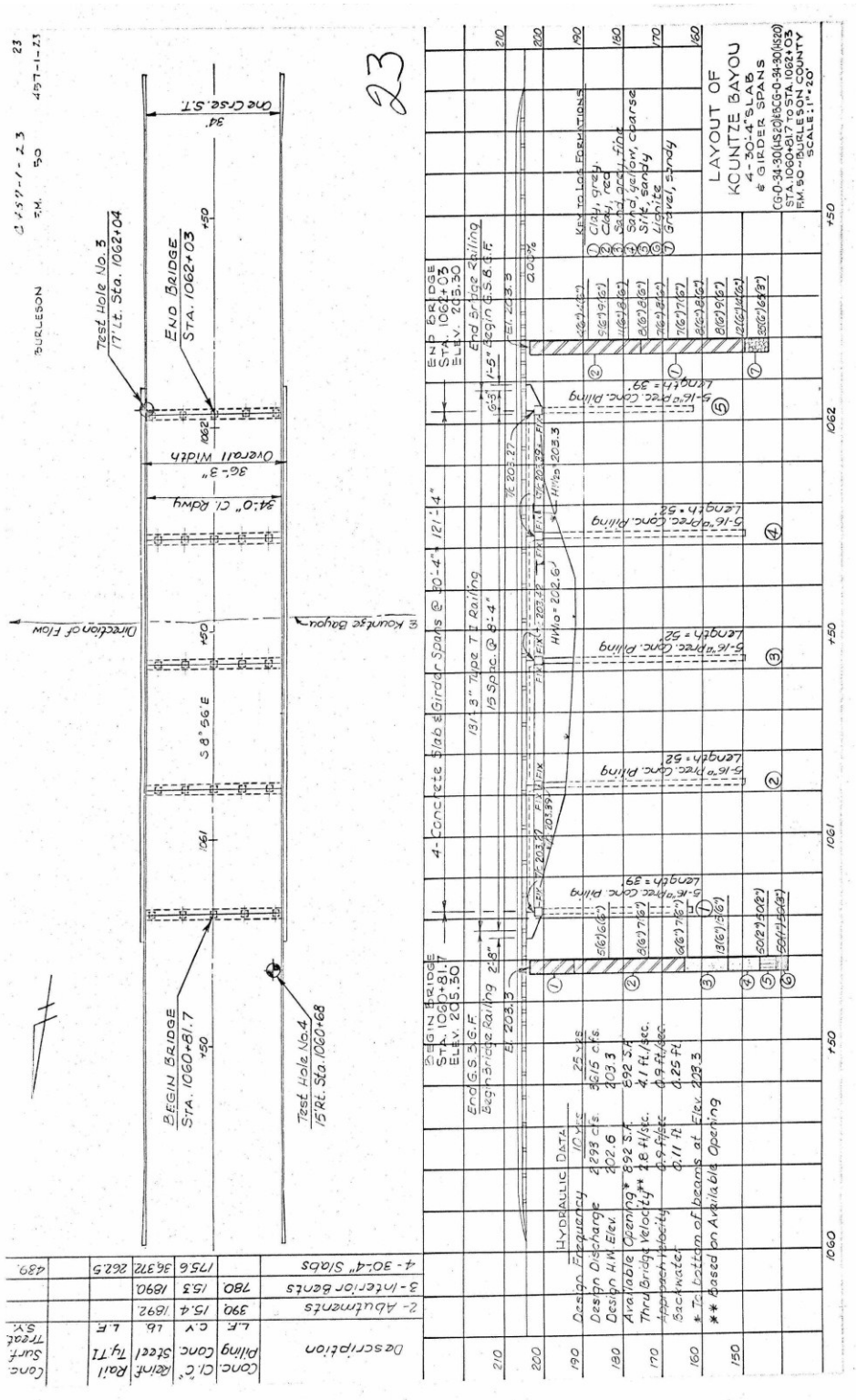

Lay out of Bridge 15 over Kountze Bayou creek on FM Road 50

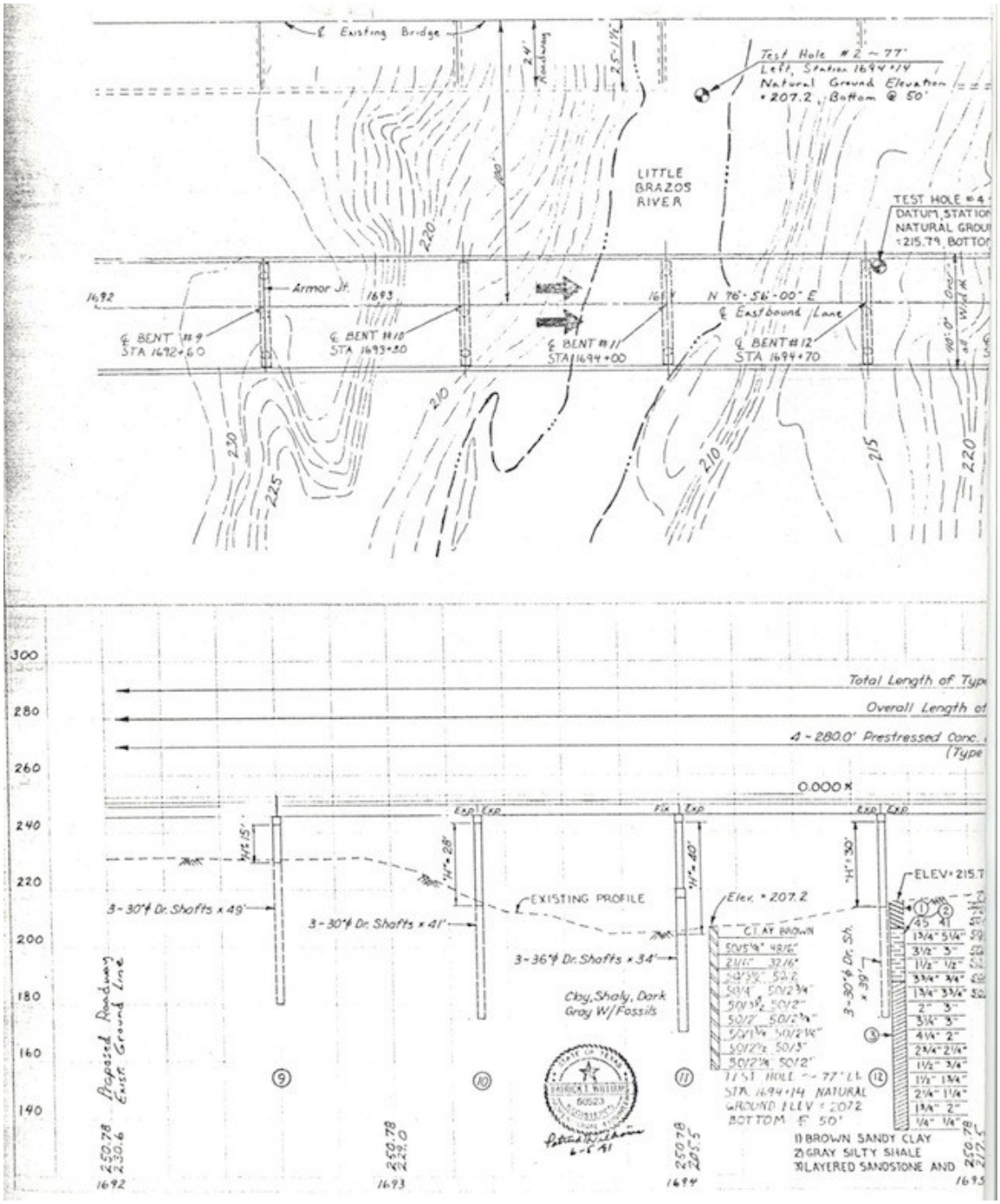

Lay out of a section of roadway bridge over the Little Brazos River on HW 21

VITA

Name: Rungroj Arjwech

Address: Department of Geotechnology, Faculty of Technology, Knon Kaen University, Khon Kaen, 40002, Thailand

Email Address: geohandsome23@hotmail.com

Education: B.A., Geotechnology, Khon Kaen University, 2003
M.S., Geotechnology, Khon Kaen University, 2006
Ph.D., Geophysics, Texas A&M University, 2011